INFORMATION TO USERS

This manuscript has been reproduced from the microfilm master. UMI films the text directly from the original or copy submitted. Thus, some thesis and dissertation copies are in typewriter face, while others may be from any type of computer printer.

The quality of this reproduction is dependent upon the quality of the copy submitted. Broken or indistinct print, colored or poor quality illustrations and photographs, print bleedthrough, substandard margins, and improper alignment can adversely affect reproduction.

In the unlikely event that the author did not send UMI a complete manuscript and there are missing pages, these will be noted. Also, if unauthorized copyright material had to be removed, a note will indicate the deletion.

Oversize materials (e.g., maps, drawings, charts) are reproduced by sectioning the original, beginning at the upper left-hand corner and continuing from left to right in equal sections with small overlaps.

Photographs included in the original manuscript have been reproduced xerographically in this copy. Higher quality 6" x 9" black and white photographic prints are available for any photographs or illustrations appearing in this copy for an additional charge. Contact UMI directly to order.

Bell & Howell Information and Learning
300 North Zeeb Road, Ann Arbor, MI 48106-1346 USA
800-521-0600

DESIGN, ANALYSIS AND TESTING OF HUMIDITY MICROSENSORS PRODUCED IN MITEL 1.5μm CMOS TECHNOLOGY

Lin Wang

A Thesis

in

the Department

of

Mechanical Engineering

Presented in Partial Fulfillment of the Requirements
for the Degree of Master of Applied Science at
Concordia University
Montreal, Quebec, Canada

January 2000

ABSTRACT

DESIGN, ANALYSIS AND TESTING OF HUMIDITY MICROSENSORS PRODUCED IN MITEL 1.5μm CMOS TECHNOLOGY

Lin Wang

The occupant comfort and working efficiency in confined spaces, such as buildings, aircrafts and mines, is strongly related to the air quality. Among many other factors, the humidity of air forms one of the most important parameters that need to be monitored and controlled. Low cost and reliable humidity monitors and controllers have not been realized due to complexities associated with the humidity measurement. The primary limitation of current designs of humidity microsensors is the high cost attributed to relatively complex post-processing techniques employed to integrate the humidity sensitive material within a structure of the humidity sensor.

The scope of this dissertation research is formulated to develop designs of fully integrated surface micromachined humidity sensors which can be realized using the standard CMOS process, and low cost and efficient post processing techniques.

The configurations of resistive and capacitive humidity sensors are designed, analyzed and optimized for miniaturization. The sensing properties of various humidity sensitive materials are reviewed in view of their potential application in microsensors. Polyaniline compound is proposed for fabrication of prototype micro humidity sensors. Analytical models of the resistive and

capacitive microsensors are developed to study the steady-state and transient performance characteristics of the sensor. The properties of the proposed compound are analyzed through fabrication and testing of an array of laboratory samples. Different designs of conditioning circuits are further presented for integration.

Different post-processings are analyzed, and low cost and efficient post-processing technique for fabrication of humidity sensors, based upon spincoating alone, is proposed. The influence of variations in spincoating on sensor performance, which include spin coating speed and viscosity of material, is investigated through the study of experimental results. The post-processing is also performed on the prototype sensors. The steady state and transient response characteristics of prototype sensors are evaluated through a series of laboratory tests. The validity of the analytical model of the sensor is examined using experiment results.

ACKNOWLEDGEMENTS

The author wishes to express her sincere thanks and appreciation to her supervisors, Dr. I. Stiharu and Dr. S. Rakheja, for their continued guidance and encouragement throughout the course of this research and during the preparation of this thesis.

The author also wishes to thank members of the faculty and staff of CONCAVE (Concordia Computer-Aided Vehicle Engineering) Research Center, Department of Mechanical Engineering, Department of Electrical Engineering, School of Graduate Studies and Concordia University, for their time and assistance during the progression of this work.

Financial and technical supports provided through CMC (Canadian Microelectronics Corporation) are gratefully acknowledged.

This thesis is dedicated to the author's parents, her sister for their love and encouragement. This thesis would not have been possible without their supports.

TABLE OF CONTENTS

LIST OF FIGURES

LIST OF TABLES

NOMENCLATURE

SYMBOL	DESCRIPTION
A	Surface area of the particle exposed to drag.
A_r	Relative area between two electrodes.
a, b	Coefficients.
C	Capacitance of transducer.
C_o	Basic capacitance.
C_r	Reference capacitance.
C_s	Sensor capacitance.
C_i (i=0, ...,n)	Constants or regression coefficients.
C_p	Parasite capacitance.
C_r	Reference capacitance.
C_x	Capacitance.
D	Diffusion coefficient.
d	Penetrating depth of water vapor into the humidity sensitive material.
d_r	Distance between two electrodes.
E	Free energy of absorption.
E_1, E_2	Measurement electrodes.
E_a	Activation energy.
F_c	Centrifugal force.
F_s	Clock frequency.
F_v	Viscosity force.

H	Absolute humidity level.
H	Thickness of sensitive material.
I_s	Supply current.
K	Coefficient.
k	Boltzmann constant.
M_A	Molecular weight of air.
M_w	Molecular weight of water vapor.
m	Mass of dispersion particle.
n	Empirical factor.
p	Partial pressure of air vapor.
p_A	Partial pressure of air.
p_S	Saturated air vapor pressure.
R	Bulk resistance of transducer.
R_1, $R_2 \ldots R_{10}$	Constant resistance.
R_{circle}	Resistance of circular cutout shape.
R_{sensor}	Resistance of transducer.
R_{square}	Resistance of square cutout shape.
R_{donuts}	Resistance of donut shape.
R_i	Resistance of each element on electrode.
R_L	Load resistor.
R_r	Reference resistance.
R_x	Resistance.
RA	Ratio of transient to steady state relative humidity.

$R\bar{A}(t)$	Average ratio of transient to steady state relative humidity over depth.
RH	Relative humidity level.
RH_1, RH_2	Specific humidity range.
RH(t)	Transient relative humidity.
r	Distance between rotation center and the center of particle.
T	Absolute temperature.
T_o	Reference temperature.
t	Time.
U	Instantaneous moisture content.
U_s	Surface moisture content.
$\bar{U}(t)$	Average moisture content over the depth.
V_i	Input voltage.
V_o	Output voltage.
V_{ref}	Reference voltage.
Z_x	Impedance.
α, β, γ, δ	Constants.
ρ	Resistivity of sensing material.
ε_o	Absolute dielectric constant.
ε_{1r}	Relative dielectric constant of polymer.
ε_{2r}	Relative dielectric constant of water.
ε_r	Relative dielectric constant.
ω	Angular velocity.

ν	Fractional volume of water absorbed.
ν_m^0	Maximum fractional volume of absorption.

CHAPTER 1

INTRODUCTION

1.1 GENERAL VIEW

The occupant comfort and working efficiency in confined spaces, such as buildings, aircrafts and mines, is strongly related to the air quality. Among many other factors, the humidity of air forms one of the most important parameters that need to be monitored and controlled. Low relative humidity (below 20%), either causes or aggravates the dryness of the mucus membranes of the nasal passages, throat, and eyes of the occupants. It has been reported that the occupants may become more susceptible to microbial infections under prolonged exposure to such environment [1]. Low relative humidity environment further encourages static electricity build up and increases airborne dust and spore levels leading to uncomfortable conditions. Higher levels of relative humidity, 70% and above yield considerable condensation on the cooler surfaces due to high moisture content. The occupants in such environment are more likely to breathe air with increased microbes, such as, molds, mildews, bacteria and fungi, which tend to multiply due to enhanced moisture content [2]. The relative humidity of air within a confined space thus directly affects the sensation of comfort.

The enhancement of air quality involves measurement and control of temperature and humidity. A large number of low cost and reliable temperature measurement and control devices have been developed for varied application in

heating, ventilation and air-conditioning (HVAC) and process industries. Low cost and reliable humidity monitors and controllers, however, have not been realized due to complexities associated with the humidity measurement, which serves as the primary sensing element for the humidity controllers. The design of humidity sensors has evolved from the simple natural hair to those based upon potentiometric ion selective, amperometric devices, surface acoustic wave or lamb acoustic wave [2]. The primary limitation of current designs of microsensors is perhaps the high cost attributed to relatively complex post-processing techniques employed to integrate the humidity sensitive material within a structure of the humidity sensor. The micro sensor technology presently employs different post-processing techniques, such as deposition, dipping, screen-printing and spin coating. A specific post-processing method is often selected based upon the properties of sensing material.

While many efforts have been mounted to design humidity sensors and sensing techniques, the need for realization of low cost and reliable humidity sensors has been emphasized. The current research efforts are directed towards miniaturization for application in confined spaces. The developments in such low cost micro-humidity sensors require systematic explorations in micro-electronic fabrication and processing techniques, humidity sensing materials with faster response time and design of integrated measuring circuits. The scope of this dissertation research is thus formulated to develop designs of fully integrated surface micromachined humidity sensors, which can be realized using the standard CMOS process, and low cost and efficient post processing techniques.

Concepts in capacitive and resistive humidity sensors are analyzed and optimal structures are proposed for miniaturization. The properties of different sensing materials are analyzed to select appropriate materials for humidity sensing. Analytical models of the sensing elements are derived and validated through limited measurements performed on the prototype elements.

1.2 SCOPE AND OBJECTIVES OF THE THESIS (CONTRIBUTIONS INDICATED AS UNDERLINE)

The overall objective of this thesis is to contribute to development of micromachined humidity capacitive and resistive sensors with integrated conditioning circuitry and post-processing, through systematic analysis and simulation of humidity microsensors. The specific objectives of the dissertation research are as follows:

- To design using CMOS MITEL 1.5μm technology electrode configurations for resistive and capacitive micro humidity transducers to realize optimal values of transducers resistance and capacitance, respectively.
- To study the absorption, desorption and sensing characteristics of selected humidity sensitive materials and select an appropriate material to provide a suitable sensitive thin film for humidity microsensors.
- To study different measuring and conditioning circuit designs and propose an efficient design for on-chip integration.
- To explore a new humidity sensitive material through testing on microsensors.

- To study different post-processing techniques and propose a low cost and efficient post-processing technique for fabrication of humidity sensors.
- To design a micro-humidity transducer and perform necessary post-processing on the prototype sensors obtained from the CMC.
- To develop an analytical model of the transducer.
- To perform laboratory tests to characterize the prototype sensors.
- To validate the analytical model of the transducer using the laboratory test data.

1.3 ROAD-MAP OF THE THESIS

The flow chart of the structure of the thesis (as shown in Figure1.1) shows how the contributions link together. In the flow chart, the contributions are indicated as underline.

1.4 ORGANIZATION OF THE THESIS

Chapter 2 discusses the literature background for design, modeling, fabrication, testing and conditioning of humidity sensors. The operating principles, application, developments of humidity microsensors, different types of humidity microsensors and humidity sensitive materials are investigated in detail. Fabrication and post-processing, design examples and conditioning circuitry are also studied in this chapter.

Chapter 3 describes design configuration of three different resistive humidity transducers. The electrode shapes are analyzed to derive near optimal

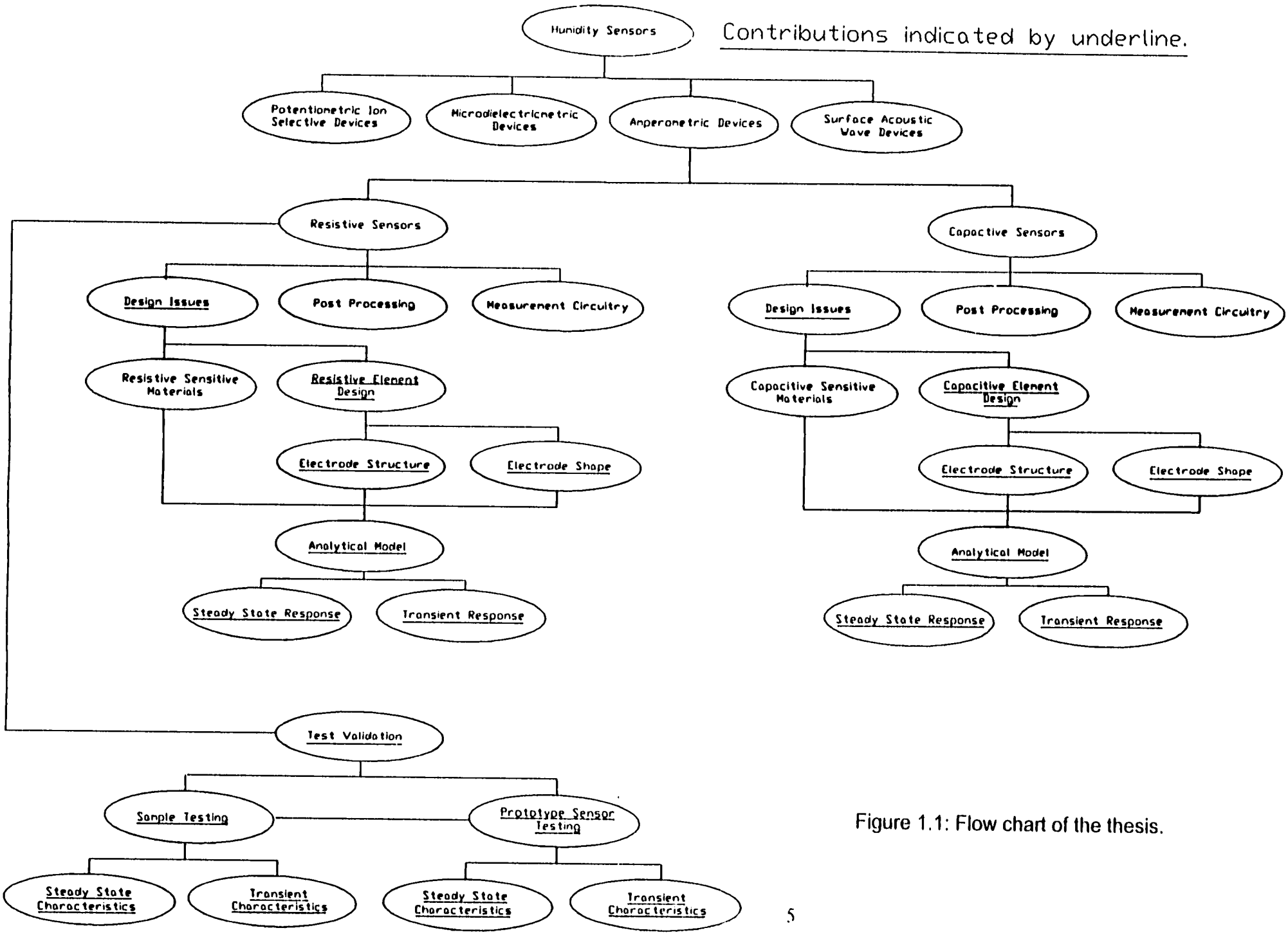

Figure 1.1: Flow chart of the thesis.

shapes for enhancement of transducer resistance. Various resistive type of humidity sensitive materials are reviewed in view of their relevant chemical and physical properties, and an appropriate material is proposed. Analytical models of the resistive transducers are further derived to study their steady and transient response characteristics. Finally, a design of the conditioning circuitry is proposed.

Chapter 4 presents the design configuration of capacitive humidity transducers, together with an analysis of the electrode shapes. Shape optimization is performed to enhance the capacitance of the humidity transducers. The selection of humidity sensitive material (capacitive type) is performed through study of physical and chemical properties of various materials. Analytical models of the capacitive transducers are derived to study their steady and transient response characteristics. The conditioning circuitry required for the capacitive sensors are further discussed.

The pose-processing performed on the transducer is described in Chapter 5. Efficient and low cost post-processing technique is proposed, which involved spin-coating under different speeds to obtain the optimal spin-coating speed. Full characterization of polyaniline as a resistive humidity sensitive was carried out. The diffusion coefficient according to Fick's law is determined. 1-methoxy-2-propanol ($CH_3CH(OH)CH_2OCH_3$) was used to thin polyaniline to reduce the thickness of the sensitive film. Laboratory tests performed on a prototype sensor to determine its static and transient properties are further described. The test data is used to examine the validity of the analytical model.

The major conclusions of the study and recommendation for future work are outlined in Chapter 6.

CHAPTER 2

BACKGROUND

2.1 INTRODUCTION

The development of a micro-humidity sensing system encompasses systematic efforts in various subjects, such as design of sensing elements, microfabrication techniques, post-processing, humidity sensitive materials, signal conditioning, and performance analyses. The reported studies in all the relevant areas are thus reviewed to enhance the knowledge and to formulate the scope of the dissertation. The reported studies, grouped under different relevant topics, are briefly summarized in the following sections.

2.2 OPERATING PRINCIPLES OF HUMIDITY SENSORS

Humidity is defined as the mass of water vapor contained within a unit mass of vapor-free gas. Using the Dalton's law, the partial pressure of each species in the mixture can be directly related to its molar fraction [4].

$$H = (M_w p_A) / (M_A(1 - p_A)) \quad (2.1)$$

Where H is humidity level; M_w and M_A are molecular weights of water vapor and air, respectively; p_A is the partial pressure of air.

The relative humidity (RH) of air is defined as the ratio of partial pressure of air vapor (p) to the saturated air vapor pressure (p_s) of the liquid at the gas temperature. Thus, the RH maybe expressed as [4]:

$$RH = p / p_s \quad (2.2)$$

The relative humidity is expressed in percentage of humidity level in the air and is most commonly used in applications involving human comfort and indoor air quality issues. Majority of the humidity measurement systems are thus based upon measurement of relative humidity.

Although the humidity sensors have been extensively used, majority of these sensors exhibit certain performance limitations in view of above mentioned requirements. Nearly all the commercial humidity sensors can be grouped into four classes, based upon their operating principle. The first group of such sensors, referred to as hygrometric sensors, provide measure of humidity due to change of a physical property of the material related to the absorption/desorption of the water vapors. Humidity sensors based on change in dimensions of natural or synthetic fibers, conductivity or electrical capacitance of a sensing material, oscillation frequency of a crystal covered by a humidity adsorbing layer, etc., fall within this class of sensors. The second group of humidity sensors utilizes the principle of psychrometry, where the sensor response is based on the implementation, in one way or another, of the classical 'wet and dry bulb' method. The third group of sensors is based upon the measurement of dew point, where the humidity content of a gaseous environment is deduced from the dew formation on a cooled surface. The fourth group comprises radiation absorption sensors, where the humidity content of a sample is deduced from the attenuation of the intensity of electromagnetic radiation in the microwave range.

2.3 APPLICATIONS OF HUMIDITY SENSORS

A wide range of humidity sensors have been developed to measure and monitor the relative humidity of air in confined spaces. The performance requirements of a humidity sensor are similar to those of any other measurement system, which include: high sensitivity over a wide input range, fast response, good reproducibility and low hysteresis, low temperature sensitivity, high resistance to contaminants and low cost. Such sensors are used in wide range of applications, such as domestic appliances, automobiles, medical sector, various process industries, agriculture and food industries [5]. Table 2.1 summarizes various applications of humidity sensors, together with the range of relative humidity (RH). Different applications require different types of humidity sensors, depending upon the range, desired accuracy, response time, etc.

2.4 DEVELOPMENTS IN HUMIDITY MICROSENSORS

While conventional humidity sensors are relatively expensive and require considerable signal conditioning circuits, the miniaturization of such sensors can offer many potential benefits. These include compact designs with fast response time of the thin moisture absorbing layers, low cost attributed to effective batch fabrication, and enhanced performance through integration of the sensor and signal processing circuitry on the same chip. The advances in micro-fabrication techniques and in the field of MEMS (Micro-Electro-Mechanical Systems) have facilitated the miniaturization of various sensors and devices.

Table 2.1: Applications of humidity sensors [5].

Area	Application	Operating Temperature (°C)	Humidity Range (%RH)
Domestic	Air conditioning and heating systems	5 to 40	40 to 70
	Clothes drier	80	0 to 40
	Microwave oven	5 to 100	2 to 100
Automobile	Car windows	-20 to 80	50 to 100
Medical service	Medical apparatus	10 to 40	80 to 100
	Incubator	10 to 30	50 to 80
Industrial	Textile mill (spinning)	10 to 30	50 to 100
	Drier for ceramic powder	5 to 100	0 to 50
	Dehydrated food	50 to 100	0 to 50
	Electric device manufacturing	5 to 40	0 to 50
Agriculture	Forcing culture	5 to 40	0 to 100
Measurement	Thermo-hygrostatic chamber	-5 to 100	0 to 100
	Radio-sonde	-50 to 40	0 to 100
	Hygrometer	-5 to 100	0 to 100
Prevention of dew condensation			

MEMS (Micro-Electro-Mechanical Systems) began as an outgrowth of expanding efforts to realize sensors and actuators using solid-state technology, and considerable strides have been made in this area during the past three decades [8,9]. Such efforts have evolved into image sensors in the mid-1960s, pressure sensors in the 1970s and an array of micro-sensors and devices in the 1980s and 1990s. Table 2.2 summarizes some of these developments in terms of the application. Most efforts to realize microsensors, however, have drawn extensively from the silicon-based and integrated circuit technology. While many of the devices listed in Table 2.2 maybe in relatively early stages of development, the efforts have clearly demonstrated the realization of various measurement and control systems in miniature, highly-integrated, and potentially low-cost forms.

Table 2.2: A list of some of the integrated sensors and micro devices reported as either developed or under development [8,9].

Visible Imagers	Linear Microdrives
Infrared Imagers	Microvalves
Tactile (Force) Arrays	Pressure Sensors
Accelerometers	Temperature Sensors
Humidity Sensors	Magnetic Sensors
Ion Concentration Sensors	Plasma Monitors
Ultrasonic Imagers	High-Energy Detectors
Acoustic Sensors	Neural Probes
Scanning Surface Probes	Gas Detectors
Mass Flowmeters	Gas Analysis Systems
Projection Displays	Gyroscopes
Prosthetic Systems	Mass Spectrometers
Microflow Controllers	DNA Analysis Systems
Cell Growth/Sorting Systems	Micropositioning Systems

MEMS (Micro-Electro-Mechanical Systems) fall broadly into two categories: microsensors and microactuators. Considerable research and development efforts have been expended to develop both effective microsensors and microactuators. The microsensors, in view of their varied application and significant benefits, have drawn majority of the efforts in the area. The major performance and cost benefits of such device include:

- The mass of the device is very small and therefore the inertial forces are negligible when compared to the electrostatic forces. These miniature mechanical structures can be operated with low level forces and thus low power.
- Batch technology for micro-fabrication and integrated circuitry for signal processing offers potential for enhancement of reliability and repeatability of the devices.
- The miniature size of sensors and devices is ideally suited for applications where size and weight are severely constrained, such as space crafts.

Initial attempts for fabrication of MEMS were made in 1960's using micromachining technology [10]. Micromachining refers to processes that enable precise three dimensional shapes to be formed on silicon. Presently, the technology allows control of dimensions ranging from less than a micron to a few millimeters with tolerances of less than one micron. The process of micromachining involves various steps, such as photolithography, three-dimensional silicon etching, thin film deposition and epitaxy. Some of the key features of micromachining which are still under investigation are:

- Ability to create precise three dimensional micro-structures.
- Repeatable dimensional stability.

- Ability of the process to yield micro-electronic circuits along with mechanical microstructures.
- Ability to vary the device dimensions without major changes in the fabrication process.

The concept of an integrated, surface-micromachined sensor was first outlined at Berkeley in 1984 [10]. A year later, the design of a relative humidity sensor was studied by Schubert et al [4], in which the principle of operation was based on the changes in the dielectric constant of a thin film of polyimide. Polymer films are well suited to standard IC processing techniques to fabricate a small, low cost sensor. The sensor comprised of two electrodes, where the top electrode was exposed to the environment and the bottom electrode was a planar metal film deposited on a silicon wafer. The post-processing was carried out by spinning the polyimide onto the wafer and three-stage curing. A similar polyimide-based capacitive humidity sensor was later designed by Ma et al. [11] for neonatal infant respiration monitoring. In 1991, Boltshauser et al. [12] developed a capacitive humidity microsensor using full industrial CMOS IC (complementary metal-oxide-semiconductor integrated circuit) processing. The post processing of the sensor structure included the deposition of the PI (polyimide) and maskless etching of the silicon substrate, which are both compatible with microfabrication. This facilitated the design and development of humidity sensors with on-chip circuitry.

Resistive humidity microsensors with Mg-Al thin films deposited on Si/SiO_2 substrate by the radiofrequency technique, using sintered $MgAl_2O_4$ powder, were investigated by Gusmano et al. [13]. The electrical behavior of the

resistive sensors was investigated with relative humidity ranging from 2% to 98%. The results showed significant changes in resistance with variation in relative humidity and good reversibility without the need for heat cleaning. A micromachined membrane based capacitive humidity sensor was developed in 1997 [14]. The porous material membrane realized using a standard anodisation technique served as the dielectric. The design employed a heating resistor underneath the membrane to reset the humidity sensor by driving out excess moisture [14]. The effectiveness of heating in order to reset the device to low humidity conditions was demonstrated through experimental data.

2.5 TYPES OF HUMIDITY MICROSENSORS

The performance characteristics of a humidity microsensor essentially depend on its design configuration. The design configurations of humidity sensors may be classified into potentiometric ion selective devices, microdielectrometric devices, amperometric devices such as capacitive sensors, resistive devices and surface acoustic wave or lamb acoustic wave devices.

2.5.1 Potentiometric Ion Selective Devices

The *potentiometric ion-selective devices* measure the potential variations in the properties of a conductive wire embedded in a perceptive material with variation in the humidity [5]. The gate of a MOSFET transistor can be omitted and the role of the wire is carried out by the function of the conductor, as shown in Figure 2.1. The sensitive material is chosen from a range of materials which

exhibit high sensitivity to variations in humidity [15]. In principle, the absorption of water molecule in the sensitive film results in the dissociation of ions, thus creating charged particles. The charged particles are transported by the electric field through the sensitive film, modifying the conductivity of the wire or junction. The sensitive material, however, must not chemically react with the water molecules.

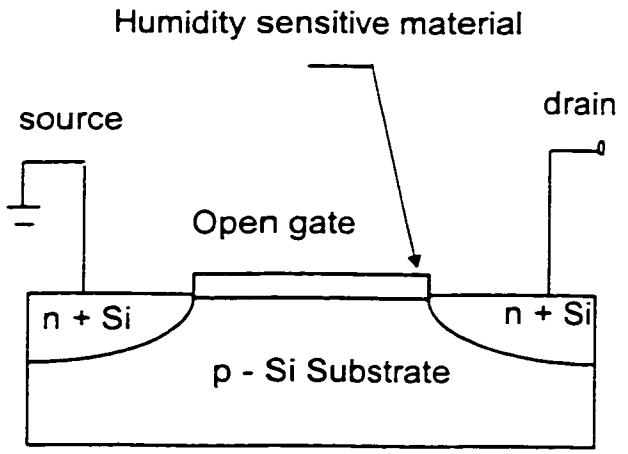

Figure 2.1: Structure of an open-gate field effect transistor.

2.5.2 Microdielectrometric Devices

A *microdielectrometric* device is based on the principle similar to that of a current flow transistor. The gate of a MOSFET transistor is partially removed, and filled by the humidity sensitive material. When a potential is applied across the two metallic electrodes of the gate, the dielectric permitivity of the humidity sensitive material influences the flow of charge through the non-conductive material, as shown in Figure 2.2. The collector current varies considerably with variations in the humidity sensitivity of the filling material. The response time to

achieve the full charge depends on the resistance of the film, the width of the gap and the thickness of the insulator.

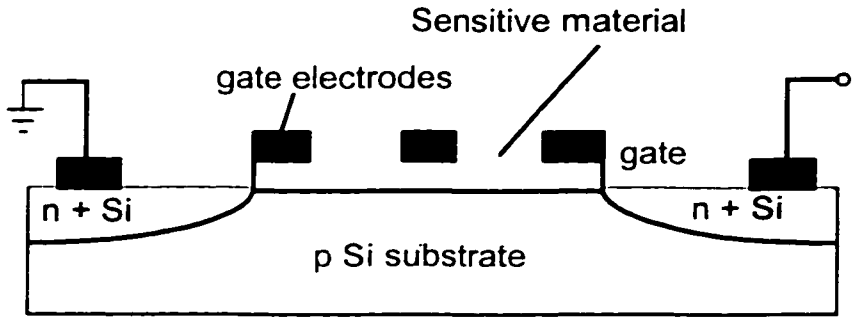

Figure 2.2: Schematics of a microdielectrometric device.

2.5.3 Amperometric Devices

The *amperometric devices* are based upon minimization of faradaic currents and thus the charging currents, leading to improved signal-to-noise ratio. They offer considerable potentials for miniaturization and for easier implementation in a standard IC processing. The capacitive sensors are one application of amperometric devices, which are simple to integrate and exhibit thermal sensitivity as the sensitive material exhibits through the relative permittivity variances. Figure 2.3 illustrates a typical structure of a capacitive sensor comprising two electrodes humidity sensitive dielectric material between the two capacitive surfaces and access to the ambient air or water vapors in the thin dielectric. The capacitive principle can easily be implemented on Si, and the measurement schemes become more and more reliable and sensitive with improved process.

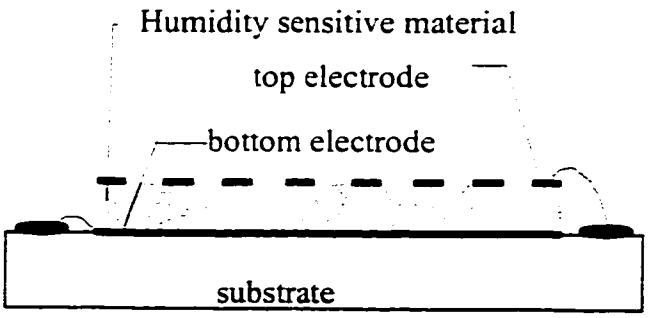

Figure 2.3: Schematic principle of a capacitive sensor.

Figure 2.4 illustrates a configuration of a typical resistive sensor. The resistive humidity sensitive material is deposited such that touches the measurement electrodes E1 and E2. Any change in the state of the humidity is translated into a change in the resistance of the contacting film.

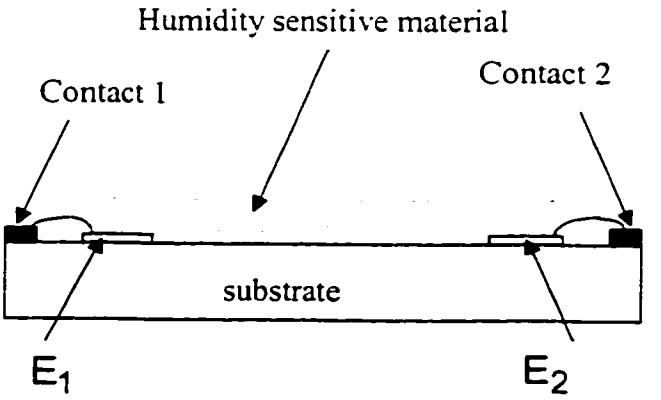

Figure 2.4: A schematic representation of the principle of a resistive sensor.

2.5.4 Surface Acoustic Wave Devices

The surface acoustic wave (SAW) sensors based on the propagation of surface acoustic waves have been successfully exploited in recent years. As the acoustic energy in surface waves is confined to a thin near-surface region of the propagation medium, these devices show high sensitivity to surface perturbations together with a reasonably fast response. Such sensors, however, pose considerable complexity associated with deposition of the piezoelectric substrate. The acoustic waves propagate through a material at the surface of the bulk for thick structures or within the entire thickness of the thin structure. SAW sensors have been used for detection of gases and liquids, and are based on the SAW sensitivity to mass loading, and the interactions between an analyte to be detected and the chemically sensitive layer deposited on the SAW propagation path [17,18]. The SAW devices, however, are also sensitive to temperature effects. The basic structure of a SAW humidity sensor is shown in Figure 2.5, which consists of a pair of metallic interdigital transducers (IDTs) deposited on an piezoelectric substrate forming a delay line of configuration. This delay line, with the sensitive material in the propagation path, serves as the active channel. SAW are launched on the active channel by the IDTs using the piezoelectric effect, which are then detected at the output IDT. The subtle changes in the wave velocity in the propagation path of the active channel, caused by the humidity sensitive film property changes, provide a measure of the relative humidity.

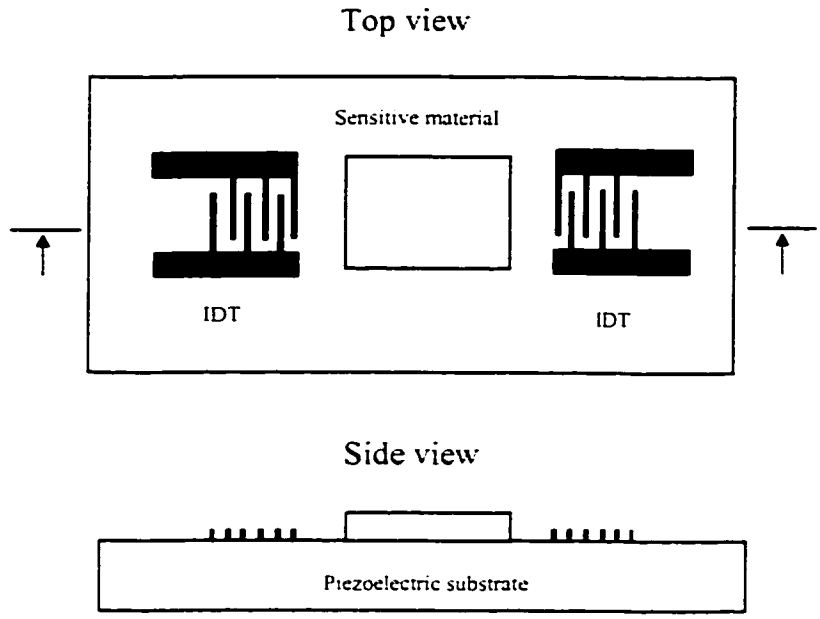

Figure 2.5: Basic structure of SAW sensor.

Among all configurations of humidity sensors, capacitive and resistive sensors have been the most popular ones for humidity measurement, due to their simple structure, adaptivity to large variety of sensitive materials, simple post processing, and ease of measurement. The basic measurement circuitry for capacitance and resistance are the simple R-C circuits, which are discussed in section 1.2.6. There are many technologies which can be used to achieve humidity microsensors, such as CMOS and Bi-CMOS. Mitel 1.5 CMOS technology was used to fabricate the microsensors with the support of Canadian Microelectronics Corporations (CMC) in this thesis.

2.6 HUMIDITY SENSITIVE MATERIALS

The sensing materials are the vital element in the design of humidity microsensors. The sensitivity, response time, stability, repeatability and durability of the humidity microsensors directly relates to various chemical properties of the material. A vast number of humidity sensing materials with different microstructures have been described in the literature. These sensing materials can be classified into three groups based upon their structure: calibrated salts, organic polymers and porous ceramics. In spite of various differences among the three groups of materials, all the materials exhibit variations in their properties with physical adsorption (or absorption) of water molecules, and thus can be effectively employed for humidity measurement. Although chemical adsorption of water can be also utilized, its application is still confined to very special cases [5].

2.6.1 Calibrated Salts

The sensitive salts, such as LiCl, $MgCl_2$, HgF_2, used in an electric hygrometer developed by Dunmore [15, 16, 19], operate on the principle that salt solution immersed in a porous binder changes its ionic conductivity depending on the relative humidity of the surrounding air. The humidity-resistance characteristics of salts, determined by the amount of impregnated salt, exhibit good linearity. Such sensors yield slow response to humidity with reasonably good stability, and have been widely used in radio-sonde circuits as well as in instruments for medical services [5]. Their use in very humid environments, however, is known to reduce their accuracy and life time [19].

2.6.2 Polymer Films

Although the performance of the polymer film humidity sensors still remain modest in practical applications compared with the ceramic based sensors, their use has been steadily growing, especially in the field of solid-state transducer technology. Polymer films are well suited for standard IC processing techniques to realize small size, low cost sensors. Most of the sensors making use of polymers as humidity sensitive materials are either resistive or capacitive type. A group of organic polymers having constituent ionic monomers such as sodium styrenesulphonate exhibit ionic conductivity and are called polymer electrolytes. Their ionic conductivity increases with an increase in water adsorption, due to increase in the ionic mobility and /or charge carrier concentration. Polymer electrolytes are generally hydrophilic and soluble in water, and thus exhibit poor durability against water or dew condensation [1, 16]. It should also be noted that the porosity of the humidity-sensitive polymer is extremely essential to obtain faster response.

Recent improvements [4, 12] in polyimide processing for integrated circuit (IC) and interlay dielectric applications have facilitated the design and fabrication of a humidity sensor on a Si chip. This fabrication technique can provide small size and low cost humidity sensors. The foremost advantage of such fabrication is perhaps the possibility to integrate the humidity sensor with other sensors or signal-handling circuitry on the same chip. Polyimides have been successfully applied on Si chips as humidity-sensitive dielectrics with high mechanical strength, high temperature capability, and high resistance to chemicals.

2.6.3 Porous Ceramics

From the viewpoints of mechanical strength, temperature sensitivity and resistance to chemical attack, ceramic materials appear to be the most suitable candidates for humidity sensors. A number of investigations have so far been carried out for humidity sensors utilizing porous ceramic elements. These sensors utilize either the resistance or the capacitance of the elements for humidity detection.

The resistive sensors consist of ionic and electronic types. The ionic resistive type ceramics, such as $MgCr_2O_4$-TiO_2, TiO_2-V_2O_5 and $ZnCr_2O_4$-$LiZnVO_4$ [21, 22, 23], make use of chemisorption on the surface of water molecules and capillary condensation of water vapor to detect the changes in relative humidity. The microstructure of an ionic ceramic determines the sensing characteristics of the material. The impedance-humidity properties of the ceramic can be enhanced through adequate distribution of different pore sizes. In case of electronic resistive type ceramics, such as $Sr_{1-x}La_xSnO_3$ and ZrO_2-MgO, the logarithm of the electronic resistance is linearly related with the logarithm of the water vapor concentration. The microstructure of an electronic resistive type ceramic, such as surface area and average particle size, has a less pronounced effect on its sensing characteristics when compared with that of an ionic resistive type ceramic.

The capacitive ceramics, such as alumina films, yield an increase in capacitance between two electrodes with an increase in relative humidity due to the large relative permittivity of the adsorbed water. The capacitance of an

aluminum film prepared by reactive ion plating, anodic oxidation and vapor deposition is known to be sensitive to variations in humidity, while sensing properties are directly related to its microstructure.

Table 2.3 summarizes properties of some of the reported sensing materials, such as operating temperature, range of humidity and response time of humidity sensors based on impedance or capacitive principle [20-30]. Most investigations have reported the properties of humidity sensitive materials based upon measurements performed on prototype sensors, while the properties associated with materials alone, such as their humidity sensitivity, absorption/desorption process, and specific post-processing requirements are neglected. This thesis aims to explore all those characteristics of sensing materials which have not been investigated. The best possible suited humidity sensitive materials must be sensitive to relative humidity level, exhibit fast response in absorption/desorption process, and be easy to be deposited on the surface of the sensor. These aspects will be discussed in Chapter 3 & 4.

2.7 MEMS FABRICATION AND POST PROCESSING

MEMS (Micro-Electro-Mechanical Systems) integrate mechanical elements, sensors, actuators, and microcircuits on a silicon substrate through the utilization of microfabrication technology. While the electronics are fabricated using integrated circuit (IC) process sequences (e.g., CMOS, Bipolar, or BICMOS processes), the micromechanical components are fabricated using compatible micromachining processes that selectively etch away parts of the

Table 2.3: Summary of application of sensing materials, their operating range and response time [20-30].

Type of material	Principle	Sensing element	Operating range		Response time (s) (4)
			Temp.(°C)	% RH	
Salts	Resistance	LiCl+polyvinyl acetate	-40 - 60	10 - 99	120-300
		LiCl+pith	-20 - 60	10 - 99	300-360
		LiCl+glass fibber sheet	-30 - 50	15 - 99	180-600
Polymer films	Resistance	(1)	0 - 40	0 - 100	120
		(2)	-20 - 80	0 - 100	5
		(3)	-10 - 60	94 - 100	10
	Capacitance	Cellulose acetate	-40 - 115	0 - 100	1
		Polyimide	0 - 50	0 - 100	60
		Cellulose acetate buthyrate	0 - 50	0 - 100	30
Porous ceramic	Resistance	$MgCr_2O_4$ - TiO_2	0 - 150	1 - 100	10
		$TiO_2 - V_2O_5$	0 - 150	15 - 100	10
		$ZnCr_2O_4 - LiZnVO_4$	0 - 150	30 - 90	180
		$Sr_{1-x}La_xSnO_3$	300 - 500	1 - 80	120
		$ZrO_2 - MgO$	400 - 700	10 - 90	10
	Capacitance	Al_2O_3	-10 - 40	1 - 100	10
		Ta_2O_5 - MnO_2	-10 - 55	1 - 100	60

(1) 2-hydroxy-3-methacryl-oxypropyl trimethyl ammonium chloride + methacrylic ester
(2) Polystyrene sulphonate + vinyl polymer + N, N- methylene-bis-acrylamide
(3) Crosslinked hydrophilic acrylic polymer + carbon particles
(4) Response time of sensor is gernerally defined as the time for which the variance of output reaches 63.2% of the difference between its final and initial value [25].

silicon wafer or add new structural layers to form the mechanical and electromechanical devices [31]. In micromachining, the fundamental fabrication processes are bulk micromachining and surface micromachining. Bulk micromachining is based on the principle of sculpturing mechanical structures out of a single-crystal silicon wafer. For the crystal-orientation dependent process (anisotropic), etchants, such as KOH, EDP and TMAH together with different etch-stop techniques are used. The final shape of micro structure can be predicated very accurately according to etching rate along various crystallographic planes [32]. Surface micromachining is the process of depositing and patterning of thin layers of structural and sacrificial material. At the end of processes, the sacrificial material is removed through post-processing, while the completely assembled micro mechanical devices remain on the chip [32]. A comparison of bulk micromachining with surface micromachining are illustrated in Table 2.4 [33]. While bulk micromachining can yield 3-D structures in a very convenient way based on the anisotropic etching properties of Si, microelectronic components cannot be achieved since the appropriate processes are not carried out. Further, the expensive step of coupling of microstructure with microcircuit through packaging is needed. Surface micromachining is based on using standard Si foundry processes to build and pattern the future structures, which will be further released by post-processing. As possibilities of practical applications and fabrication techniques using micromachining processes have been proved, many kinds of micromechanical systems have been proposed that could be developed using the silicon process [1-4, 31-34].

Table 2.4: A comparison of bulk micromachining with surface micromachining [33].

Bulk Micromachining	Surface Micromachining
Large features with substantial mass and thickness	Small features with low thickness and mass
Utilizes both sides of the wafer	Multiple deposition and etching required to build up structures
Vertical dimensions; one or more wafer thicknesses	Vertical dimensions are limited to the thickness of the deposited layers (~2 μm), leading to compliant suspended structures with the tendency to stick to support
Generally involves laminating Si wafer to Si or glass	Surface micromachined device has its built-in support and is more cost effective
Piezoresistive or capacitive sensing	Capacitive and resonant sensing mechanisms
Some mature products	Reduced number of commercial products
Not very compatible with IC technology	Natural but complicated integration with circuitry integration is often required due to the tiny capacitive signals

Post-processing is always done off-line the processing flow to avoid any possible contamination of the samples by not desired substances involved in the post-processing. However, post-processing might make use of similar types of process as those in the silicon foundry. The post-processing carried out in the bulk micromachining consists of the removal of bulk silicon from either side of

the wafer in a single maskless etch [31]. The dielectric layers (thermal and CVD oxides, nitrides) serve as natural etching masks during the post-processing etch. The post-processing carried out in the surface micromachining consists of the removal of thin sacrificial layers underlying an etch-resistant thin film, thus forming free standing microstructures. Besides the etching of Si (bulk etching) or polysilicon (sacrificial etching), selective etching of the sacrificial layers is used (as an example, in MUMPS, the sacrificial film SiO_2 is selectively etched releasing polysilicon structures [2]). Besides TMAH, EDP, HF, KOH which are used in wet etching, plasma etching or gaseous $XeFl_2$ isotropic are also used for etching. Selectivity is accomplished either through covering the specific areas that must be protected and leave those which need to be removed to the access of the etchant [31]. Thus, photolithography is usually necessary, However, since photolithography should be applied off-fabrication line, the costs involved in alignment are excessive. An alternative to avoid photolithography and masking is ablation with laser beam. These method present tremendous advantages but the drawback is that the method is not suitable with the bulk fabrication. Thus, post-processing in which photolithography is not necessary are more desirable than processes in which masking is a must. Besides, mainly in chemical sensor fabrication, besides the non-mandatory etching, high accuracy coating is necessary to build the active film. The definition of the sensing area can be easily accomplished through the standard CMOS. Depositions of various materials are feasible. There are a number of different techniques that facilitate the deposition or formation of thin films of different materials on a silicon wafer.

Metallic material could be deposited by vaporization or by sputtering. E-beam vaporization, laser vaporization, and selective reaction of gases with the active surfaces could deposit salts or ceramics. Low cost depositions consist of spin coating, spraying, dipping could yield very thin mono-atomic films. Such methods are used in large production for the very low cost involved. However, the deposition may sometimes require certain selectivity, which could be also accomplished by photolithography. Each photolithography step means exponential cost, mostly due to the nonplanar process, which requires extremely precise alignments.

The experience of researches with post-processing is usually related to specific CMOS technologies. Each reported work is specifically related to the internal stress in the structural layers, the thickness and the compactness of certain structural films or the selectivity accomplished through a certain etching process to the structural films versus the sacrificial layers [32]. Most of the reported work was carried out on small lots or individual components and the extrapolation to industrial environment is subjected to adjustment [35]. However, low cost post-processing steps require procedures that could be easily performed off fabrication line without any photolithography involved. Concerns related to the integrity of the structure after post-processing are risen. In particular, the problem of the protection of possible on-chip electronics against etchant still remain to be resolved, especially for a maskless post-process.

2.8 DESIGN EXAMPLES

The first humidity sensor was built in 1783 [5], making use of naturally curly hair and known as the hair hygrometer due to hair expanding with humidity. Many compact designs of low cost humidity sensors based upon change in the resistive or capacitive properties of sensitive materials have been developed during the past two decades [6].

2.8.1 Resistive Humidity Sensor

A typical resistive humidity sensor, developed by Nakaasa Instrument Co. Lt. in 1978, was referred to as "Humentt" [6]. The 8mm×13.5mm "Humentt", schematically shown in Figure 2.6, provided a resistance value of less than $10^7\Omega$ above 30-40% RH, which decreased exponentially within increase in the relative humidity. The sensor revealed a response time of approximately 2 minutes during absorption, which was slightly longer during desorption [1]. "Humentt" is large in size and exhibits long response time.

2.8.2 Capacitive Humidity Sensor

A typical capacitive humidity sensor "Humicape", developed by Vaisala [7], is now widely used in radio-sonde and many other humidity-measuring instruments. The configuration of the capacitive sensor is illustrated in Figure 2.7, which revealed nearly linear variation in the capacitance, ranging from 45 pF to 70 pF, with the ambient humidity in the 0 to 100% range. Such sensors exhibit rapid response time of approximately 1s. The structure of "Humicape" results

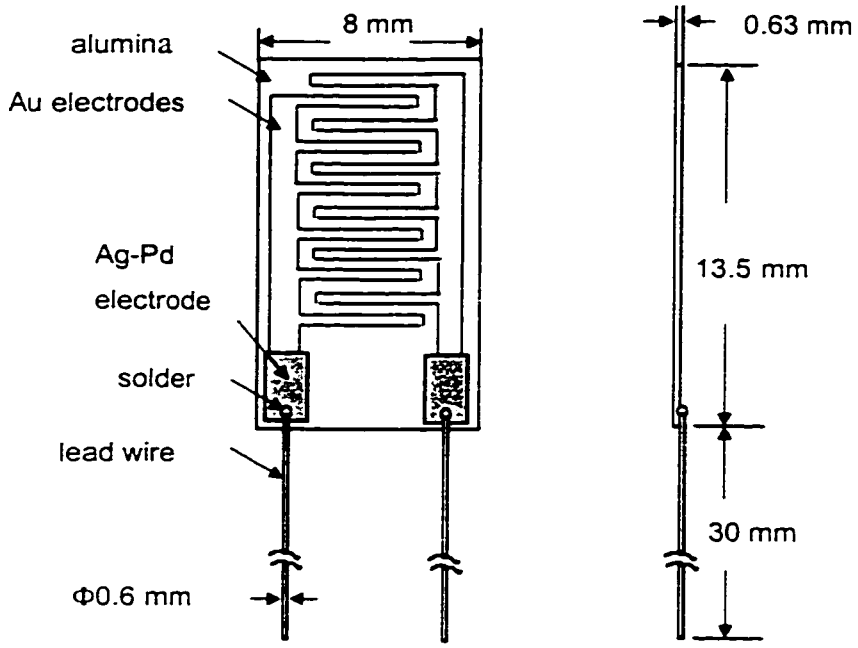

Figure 2.6: Schematic view of 'Humentt HPR' type humidity sensor [6].

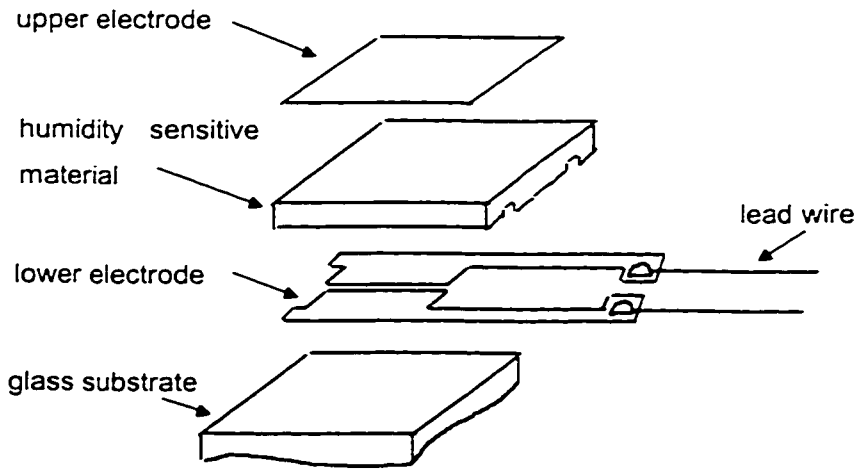

Figure 2.7: Configuration of a 'Humicape' humidity sensor [7].

complex fabrication process. An array of measurement circuits have also been developed for both resistive and capacitive sensors [7].

2.9 OUTPUT MEASUREMENT OF MICRO HUMIDITY SENSOR

The humidity sensors may be classified in three classes based upon the measurement principles, described below:

- Sensors based upon measurement of variations in a mechanical property of a film and filament.
- Sensors based upon variations in a electrical property of the material or film, such as resistance or capacitance.
- Sensors based upon psychrometric principles which compare the latent heat of evaporation of a saturated environment to the environment in question [4].

The developments and continued growth in automated systems have posed ever-increasing demands for various kinds of physical and chemical sensors. As humidity is a very common component in our environment, the measurement and control of humidity is important not only for human comfort but also for a broad spectrum of industrial processes. Among the different types of humidity sensors, those based on electrical properties such as resistance (or impedance) and capacitance are best suited for control of processes or systems. Such sensors can be conveniently integrated into the control loops, since they provide output in terms of voltage or frequency.

A large number of micro and conventional sensors thus utilize the measurement of resistance R_x, capacitance C_x or impedance Z_x, which are related to the physical quantity to be measured through either linear and

nonlinear calibration curves and signal conditioning circuitry. In humidity sensors, the physical quality (humidity) causes a variation in the electrical property, such as R_x, C_x or R_xC_x of the sensing element, which is manipulated to yield an output signal, using a conditioning circuit, such as an R-C bridge. In recent years, active RC circuits have been developed to simplify the design and enhance the performance. Figure 2.8 illustrates a typical RC circuit used for processing of the output of the sensing element signal. The circuit comprises two integrators and a differential amplifier, which compares the output of two amplifiers. In the conditioning circuit, C_r serves as the reference capacitor for capacitive humidity sensors, while R_r and R_x are held fixed. For resistive humidity sensors, R_r is taken as the reference resistor, while C_r and C_x are held fixed. Although such RC circuits offer simple and reliable means to manipulate the variation in electrical parameters of the sensing element, the accuracy of the measurement system strongly relies upon the accuracy of the reference values (R_r and C_r).

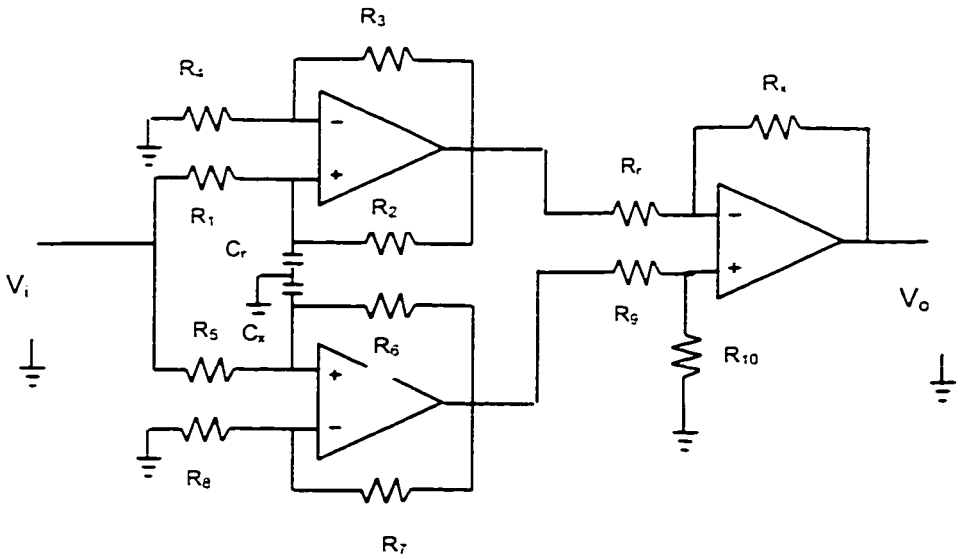

Figure 2.8: The basic scheme of RC circuit [36].

Figure 2.9 [37] illustrated a simple active RC circuit for the measurement of in-circuit, discrete, and incremental capacitance or resistance. The measurement circuit provides the measured value of capacitance or resistance directly in terms of the output voltage of the circuit. The circuit yields good accuracy of these measurements, while being independent of the signal frequency. For the measurement of in-circuit and discrete capacitance or resistance, the switch S remains open, and the output voltage is linearly related to the unknown capacitance C_x under constant values of V_i and R_x. The output can also to be linearly related to the unknown resistance R_x under constant values of V_i and C_x. The output voltage may be expressed as [37]:

$$V_o = (\frac{R_x C_x}{R_1 C_1})V_i \qquad (2.3)$$

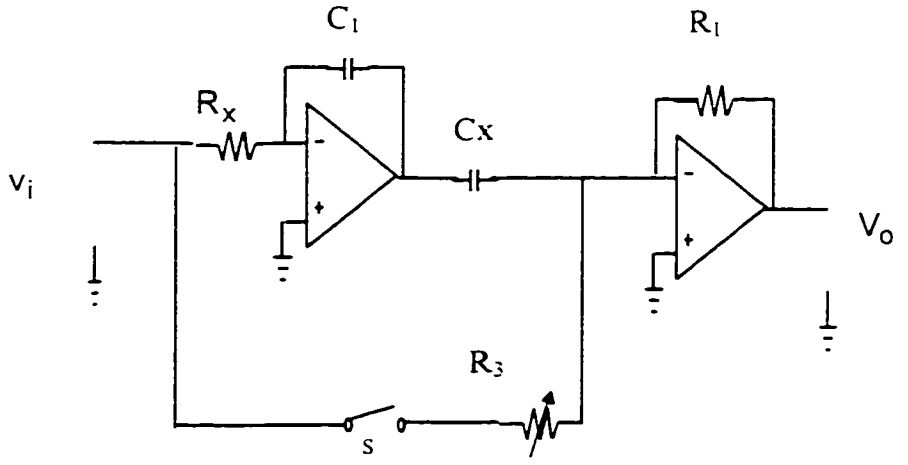

Figure 2.9: Capacitance or resistance measurement circuit [37].

For incremental measurement of C_x and R_x , the switch S is closed to yield output voltage as:

$$V_o = (\frac{R_x C_x}{R_1 C_1} - \frac{R_x}{R_3})V_i \qquad (2.4)$$

The output voltage is found to be linearly related to the unknown resistance R_x for known constant values of C_x and V_i. The output voltage is also linearly related to the capacitance C_x, while R_x and V_i are constant. The circuit may be conveniently balanced for null output voltage through the variable resistor, R_3. such that $R_1 / R_3 = C_x / C_1$. A small variation in capacitance yields a linear change in voltage variation, given by:

$$\Delta V_o = K\Delta C, \text{ where } K = \frac{R_x}{R_1 C_1} V_i \qquad (2.5)$$

This conditioning circuit offers an advantage to perform measurements over a wide range of parameter values by adjusting the sensitivity factor K through the ratio (R_1/R_x). The limitation of such low component active RC circuits is the same as that of the basic circuitry, which is the accuracy of the reference parameters [36,37].

A number of other conditioning circuits have also been developed for measurement of variations in capacitance and resistance, such as the use of a switch-capacitor interface in the measurement of capacitance. Microsensors, however, yield only minimal variations in output capacitance and resistance, which are very small compared to those treated by the conventional measurement circuitry. A growing need thus exists to develop a fabrication

process that will allow silicon machining and integrated circuit (IC) fabrication to be merged into a single process. The nominal capacitance of integrated humidity sensing devices may be well below 1 pF, while their full range variation may amount to only a fraction of the nominal value [38]. The characterization and calibration of such devices by an external capacitance meter is thus quite difficult in view of existence of large parasitic capacitances. The integration of the measurement circuit within the sensor chip can minimize such complexities associated with measurements [39]. The integrated design further offers considerable potential to enhance signal to noise ratio. Silicon micromachining techniques can be employed to integrate reference resistance or capacitance together with an operational amplifier to compare and amplify the measured unknown capacitance or resistance.

CHAPTER 3

DESIGN AND MODELING OF A RESISTIVE MICRO HUMIDITY TRANDUCER

3.1 INTRODUCTION

In response to the strong demands for low cost and reliable sensors for various monitoring and control application, a vast number of humidity sensors based on humidity-sensitive electrical properties have been commercially developed [16]. Among the different types of humidity sensors, those based on electrical properties, such as resistance and capacitance of the humidity sensitive materials, are considered to be best suited for process control applications. Micromachined humidity sensors offer significant potential benefits over the conventional sensors not only due to their small size and low power consumption but also due to their high sensitivity, high stability and low cost.

The design of resistive humidity transducers was initiated in the late 1930s [5], when humidity sensors with enhanced accuracy and reliability characteristics were required for balloon-carried meteorological radiosondes. Thereafter, several methods have been developed [6], and many different resistive humidity sensing concepts have been investigated using calibrated salts, ceramics and polymers. Some of these concepts have resulted in commercial sensor designs. In general, a resistive humidity sensor is designed to meet various performance requirements, such as wide sensing range, reasonable resistance output range, low hysteresis, short response time, low cost, high reliability and long life. Most conventional humidity sensors, however,

exhibit limited reliability and long-term stability, primarily attributed to complex interactions between the bare sensitive surfaces and the ambient gases [3]. Such sensors pose considerable challenge in selecting a humidity-sensitive material, which is suited for specific environments and which yields fast response time and adequate stability. Miniaturization of such designs may further reduce the output resistance variations and thus its sensitivity.

In this chapter, conceptual structure of the resistive humidity sensors is proposed in conjunction with the fabrication process. The fundamental properties, such as steady-state response, transient response, humidity sensitivity and response time are investigated through development and analysis of a simplified model. The post-processing and the conditioning circuitry for the resistive humidity sensors are also briefly discussed.

3.2 DESIGN ISSUES

The realization of micromachined transducers or devices involves many sequential steps, such as concept development, design and analysis, fabrication, post-processing and packaging. The design and analysis of a resistive humidity sensor involve consideration of its mechanical and electrical, static and dynamic performance characteristics. The mechanical characteristics of a sensor include sensor configuration, electrode shape and design dimension, which in case of miniaturization must be suitable for CMOS process followed by simple post-processing. The electrodes design relates to essential performance measures, such as nominal resistance, resistance range, power requirements and output

characteristics of the sensor. However, the electrode design is imposed by the design rules required by the CMOS process. The static performance characteristics of a humidity sensor, in general, include sensor input range, static sensitivity, linearity and accuracy. The dynamic performance characteristics relate to measurement, and are derived from the transient response behavior. However, performances such as response time, rise time and recovery time are typically different for increasing and decreasing humidity levels. The sensor performance may be also dependent upon the variations in the temperature of the environment.

The design concepts of micromachined devices utilize the principles developed for conventional sensors. Those principles have been implemented on various MEMS process and the performances of the resulting devices were optimized with respect to the processing and post-processing [8]. The studies on development of processes for sensor applications are extremely involving. They include investigations in thin-film materials and depositions, lithography and pattern-making technology, substrate bonding, etching technology, sacrificial layers and the integration of all these techniques with the conventional IC electronics [34]. Surface micromachining have been used for fabrication of many sensors due to its compatibility with IC fabrication techniques. The surface micromachining technology has generally involved the fabrication of polysilicon structures, usually by sequences of depositions and patterning of polysilicon, sacrificial layers of dielectrics and metallization on Si substrates, resulting in the sensing/control elements and devices [35]. Complementary metal-oxide-

semiconductor (CMOS) technology is one of the micromachining techniques, which has been widely used for developments in MEMS (Micro-Electro-Mechanical Systems). Microelectromechanical devices fabricated using a CMOS process offer considerable advantages due to their small size, light weight and low cost associated with the mature integrated circuit processing capabilities. A standard CMOS process includes two or three polysilicon layers P1, P2 or P3 and up to two metal layers M1 & M2. Insulating silicon dioxide layers between the conductive layers ensure adequate insulation between the conductors [38]. In this study, the designs of micromachined humidity sensors are realized based on a standard CMOS process, "MITEL 1.5μm", which comprises two polysilicon and two metal layers. These layers are integrated and patterned such that the post processing requirements are reduced to simple deposition of the humidity sensitive material on top of the Si foundry processed structure. The proposed design and post processing methodology can thus considerably reduce the fabrication costs.

3.3 HUMIDITY SENSITIVE MATERIALS

Resistive humidity sensors offer significant advantages in view of their simple structure and ease of measurement. The design of a humidity sensor is conceived based upon the variations in resistance of a humidity-sensitive material. The material selection plays an important role in the design of resistive humidity sensors. While majority of studies emphasized on certain sensing materials, only limited studies have investigated the relative merits or demerits of

different sensing materials in view of their applications in humidity sensors [15]. In this section, sensing characteristics of various humidity sensitive materials are reviewed based upon data reported in the published studies. The resistive sensing materials may be classified into three groups, i.e., organic polymers, porous ceramics and calibrated salts.

3.3.1 Organic Polymers

Synthetic polymers seem to be the most widely used materials of the 20th century [20], since they can be easily molded while conforming well with the CMOS MITEL15 technology. Such polymers can be easily deposited in thin film form. Depending on the type of charge carriers, such polymers may be grouped into two classes: (i) ionically conductive polymers, often called polyelectrolytes, and (ii) electronically conductive polymers. The fundamental properties of both classes of organic polymers are discussed below.

3.3.1.1 Ionic conduction type

A group of organic polymers with constituent ionic monomers, such as sodium styrenesulphonate, exhibit ionic conductivity and are called polymer electrolytes [16]. Their ionic conductivity increases with an increase in water absorption, due to increase in the ionic mobility and /or charge carrier concentrations. An important problem encountered in adopting these materials to humidity sensors is the water resistivity [20]. Some of the polymer electrolytes are hydrophilic and soluble in water, and thus exhibit poor durability under

exposure to water or dew condensation. The problem has been mitigated by crosslinking a hydrophilic polymer with an appropriate crosslinking reagent and/or copolymerizing hydrophilic monomers with hydrophobic monomers [43].

The polymeric films for applications in humidity sensors, however, must be designed to enhance their water resistivity, which may be realized by crosslinking or copolymerization. The sensitivity, stability and reliability of the polymer are mostly dependent upon its chemical structure. The properties of copolymers and copolymerization processes have been extensively investigated [27, 28, 44, 45]. Some of the examples include crosslinked copolymers prepared from styrenesulphonate, a vinyl polymer and N-methylene-bis-acrylamide (a crosslinking regent) [27,28], or from styrenesulphonate and polyvinyl chloride [45], a copolymer of sodium styrenesulphonate with 2-hydroxyethyl metacrylate [44], and a copolymer of tetrafluoroethylene with styrenesulphonate [41]. These investigations have provided considerable data concerning response time and sensing mechanisms. The response time is primarily determined by the time required for water vapors to diffuse into or out of a polymer film to the saturation or equilibrium state. The sensor response time can thus be enhanced by depositing polymer film as thin as possible. Apart from the film thickness, an increase in hydrophobicity of constituent ionic monomer appears to shorten the response time, while the mole fraction of the constituent ionic monomer to non-ionic monomer strongly affects the sensing characteristics [43, 51]. At a fixed relative humidity and temperature, the electrical resistance of the sensing material tends to decrease, when fraction of the constituent ionic monomer

increases. It has been further reported that the ion pairs of the polymer electrolytes are dissociated with water adsorption to liberate hydrated ions as dominant charge carriers [41].

3.3.1.2 Electronic conduction type

In the electronic conductive polymers, the current carrier function is performed by free electrons released from atoms in the structure of the polymer. The mechanisms through which the electrons are released in the structure of the polymer are known:

- A conductive filler is added to the polymer matrix, such that the capability of the polymer to conduct current is enhanced. Among the polymers used as matrices, one can enumerate: polyethylene, polymides, polyesters, poly (vinyl acetate) (PVAc), PTFE, polyurethane, poly (vinyl alcohol) (PVA), epoxies and acrylics, e.g. poly (methyl methacrylate).

- Doping the polymer with metallic materials increases the number of free electrons in the structure of the polymer. This type of polymers possess a very special structure containing one-dimensional organic backbones based upon the alteration of single and double bonds, and therefore are called electroconducting conjugated polymers. Composite films of polymer in liquid phase can be spin-casted.

Many recent studies deal with theoretical and experimental descriptions of ionic conductive polymers. However, the available models are still not matching experimental results with reasonably accuracy [49]. It is important to mention that the polymer conduction follows a pattern [1]: at low humidity, electronic conduction is dominant; at high humidity, ionic conduction plays the major role in the humidity-sensitive resistance change (with an increasing water content, the migration of hydrated ions is also possible).

3.3.2 Porous Ceramics

The ceramic materials are considered as most suited for chemical sensors due to their superior mechanical strength, temperature capability and resistance to chemical attack. Applications of porous ceramic elements in humidity sensors have been explored in number of studies [21-29]. Some of these sensors measure variations in impedance of the elements, which is used for humidity detection [21-24]. The conduction mechanisms in ceramics are similar to those in polymers.

The humidity-sensitivity of ionic type ceramic sensors is related to the electrical resistance of the bulk, which varies with the ambient humidity due to ionic conduction caused by water physisorption. The ceramic materials are usually ionic and apt to form a hydrophilic hydroxyl group on the sensitive surface when exposed to water vapor. Long exposure leads to water chemisorption resulting in degradation of the sensor [16]. In order to overcome this problem, it is necessary to refresh the sensitive area by heating the device up to around 500°C. Since the heating-type sensors can protect the sensitive surface from contamination, they exhibit better durability in various environments.

The microstructure of sensitive ceramic is another important element in deriving the sensing characteristics of the sensor [23]. The large porosities (the ratio of pore volume to the total volume of material) inherent in ceramic material, ranging from 25% to 50%, suggests the importance of capillary condensations,

which occur in addition to the above mentioned absorption [23]. Analyses performed by Nitta [23] demonstrate that larger porosities and wider pore size distributions give rise to a favorable resistance-humidity characteristics. Table 3.1 illustrates various examples of ionic-type ceramic humidity sensors with their resistivity, where majority of sensing elements possess large porosities and wide pore size distributions. The table illustrates that the large porosity and wide pore size distribution such as $MgAl_2O_4$ and $TiO_2 - V_2O_5$ result in wide resistivity range. These results indicate that the pore size distribution or porosity is decisively important for the sensing characteristics.

Ceramic materials in ion conduction type are only capable of using at a temperature ranging from 0 and 100°C, since the resistivity of materials are essentially depending upon the amount of phsisorbed or capillary condensed water molecules according to the change in relative humidity. However, there are still strong demands for humidity sensitive materials which are sensitive to humidity at temperature above 100°C. The electronic conduction type could satisfy this need. Water molecules act as electron donating gas on semiconductive oxides. In response to demands for operation at elevated temperatures, $Sr_{1-x}La_xSnO_3$ and $ZrO_2 - MgO$ ceramics proved to be among the most appropriate [23]. The microstructure of the elements, such as surface area and average particle size, has a less pronounced effect on the sensing characteristics than that observed in the ionic-type humidity sensors.

Table 3.1: Resistivity of ionic-type ceramic humidity sensor [23].

Material	Pore size distribution (μm)	Particle average size (μm)	Porosity (%)	Resistivity (Ωm) 10% RH	90%RH	Temp. (°C)
$MgCr_2O_4$ - TiO_2	+	0.3	33	40 M	190	20
TiO_2 – V_2O_5	0.4 - 1.0	0.7	45	121K	375	20
$MgAl_2O_4$	0.001 - 1.0	0.05	47	0.4M	395	20
$MgO-K_2O-Fe_2O_3$	0.1 - 0.4	0.2	41	80K	110	25
Silicone - SiO_2 – Na_2CO_3	1 – 10	+	+	25K	15	25
$ZnCr_2O_4$ – $LiZnVO_4$	0.1 - 0.4	0.3	12	300 K	4 K	25

AT 30% r.h.

+ not reported.

3.3.3 Calibrated Salts

The properties of a number of calibrated salts, such as lithium chloride and barium chloride, have been investigated for their application in humidity sensors. The measurement principle associated with lithium chloride salts as active material consists of a change in the ionic conductivity of the salt solution with variation in the relative humidity of the environment [30]. Partially hydrolysed polyvinyl acetate impregnated with lithium chloride has been proposed as a humidity-sensitive coating for the humidity sensor. Different amounts of impregnated lithium chloride can be applied to the humidity sensor to achieve different relative humidity range. Lithium chloride in sensors working in very humid environments, however, can result in poor accuracy of measurement and sensor durability. It has been reported that integration of lithium chloride within portable humidity transducers may pose certain difficulties because lithium chloride absorbs water, becomes liquid and leaks off the electrodes at high humidity level [30]. The lithium chloride is thus not considered suitable for applications in micro humidity transducers.

The use of barium chloride dihydrate as a humidity sensing material has also been reported by Yamazoe et al. [16]. Figure 3.1 illustrates a micrograph of the $BaCl_2 \bullet 2H_2O$ surface, where the salt crystals with needlelike structure reveal wide empty spaces. An analysis of the sensor based upon this salt, revealed that the crystals remain well oriented in certain direction and the structure does not undergo significant modifications even after exposure to an RH higher than 80%.

Figure 3.1: SEM (scanning electron microscopy) micrograph of the $BaCl_2 \cdot 2H_2O$ surfaces [42].

It has been further established that the changes in resistivity of $BaCl_2 \bullet 2H_2O$ with variation in RH follow an exponential law for temperatures, ranging from 280K to 320K, given by:

$$\rho = \frac{\delta}{\exp[\alpha RH - E_a / (kT)]} \tag{3.1}$$

Where $\delta = 2.22 \times 10^{15}$ and $\alpha = 1.3565$ are constants, E_a is the activation energy and k is the Boltzmann constant. The relation between the log of resistivity and the RH, as derived from Equation (3.1), is illustrated in Figure 3.2.

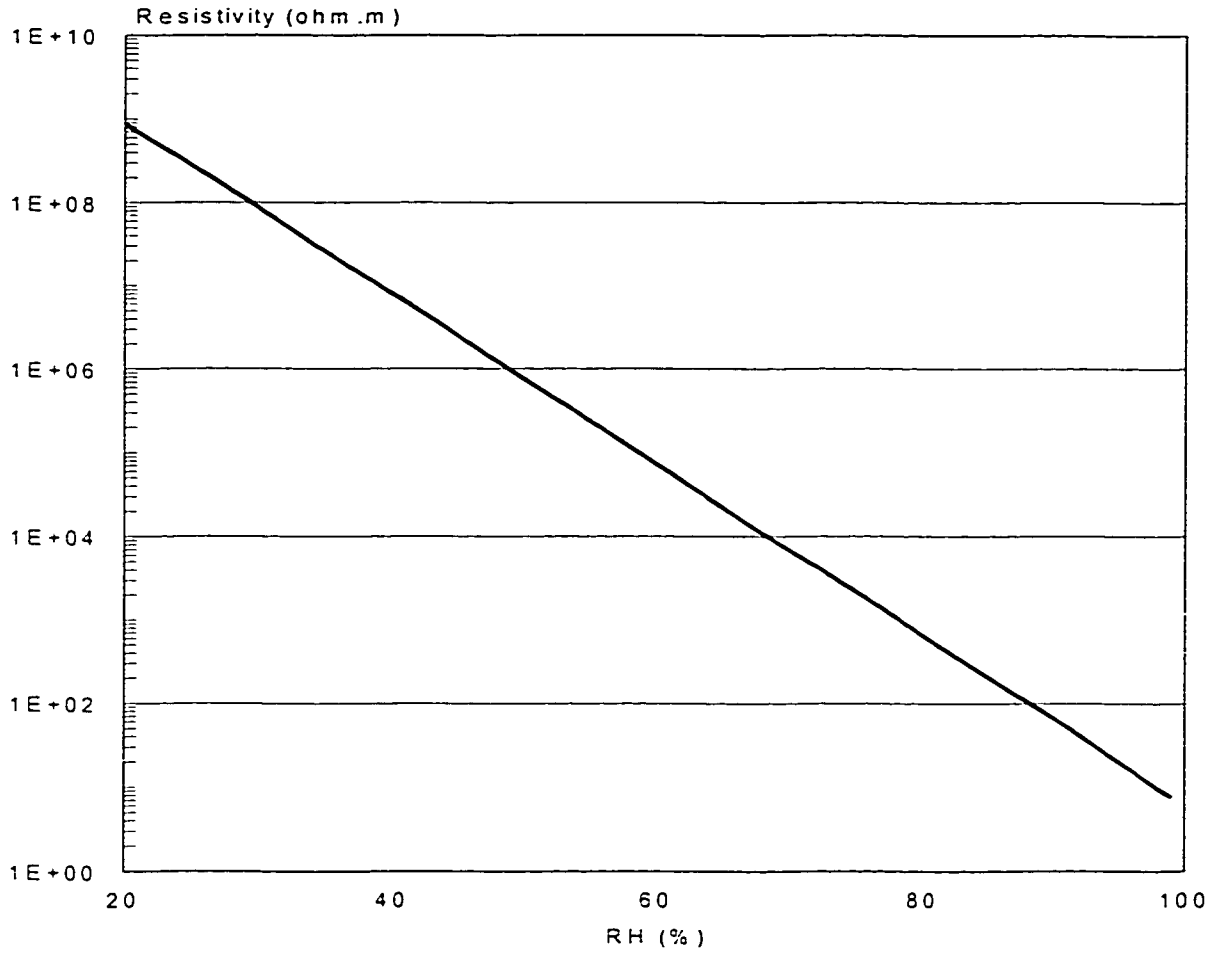

Figure 3.2: The relationship between resistivity of $BaCl_2 \bullet 2H_2O$ with the relative humidity level at room temperature (~300K).

A relationship between the activation energy and the relative humidity as shown in Figure 3.3 was further derived by Sbserveglieri et al. [46] through measurements. The measured data revealed a linear relationship, given by :

$$E_a \cong \beta + \gamma RH \qquad (3.2)$$

where β = -0.26 (eV) and γ = 0.029 (eV) are constants derived from measured data. Other studies have further established that $BaCl_2 \bullet 2H_2O$ is almost insensitive to interfering gases like CO_2, C_2H_5OH, H_2, hydrocarbons, NO_x and SO_2 [46].

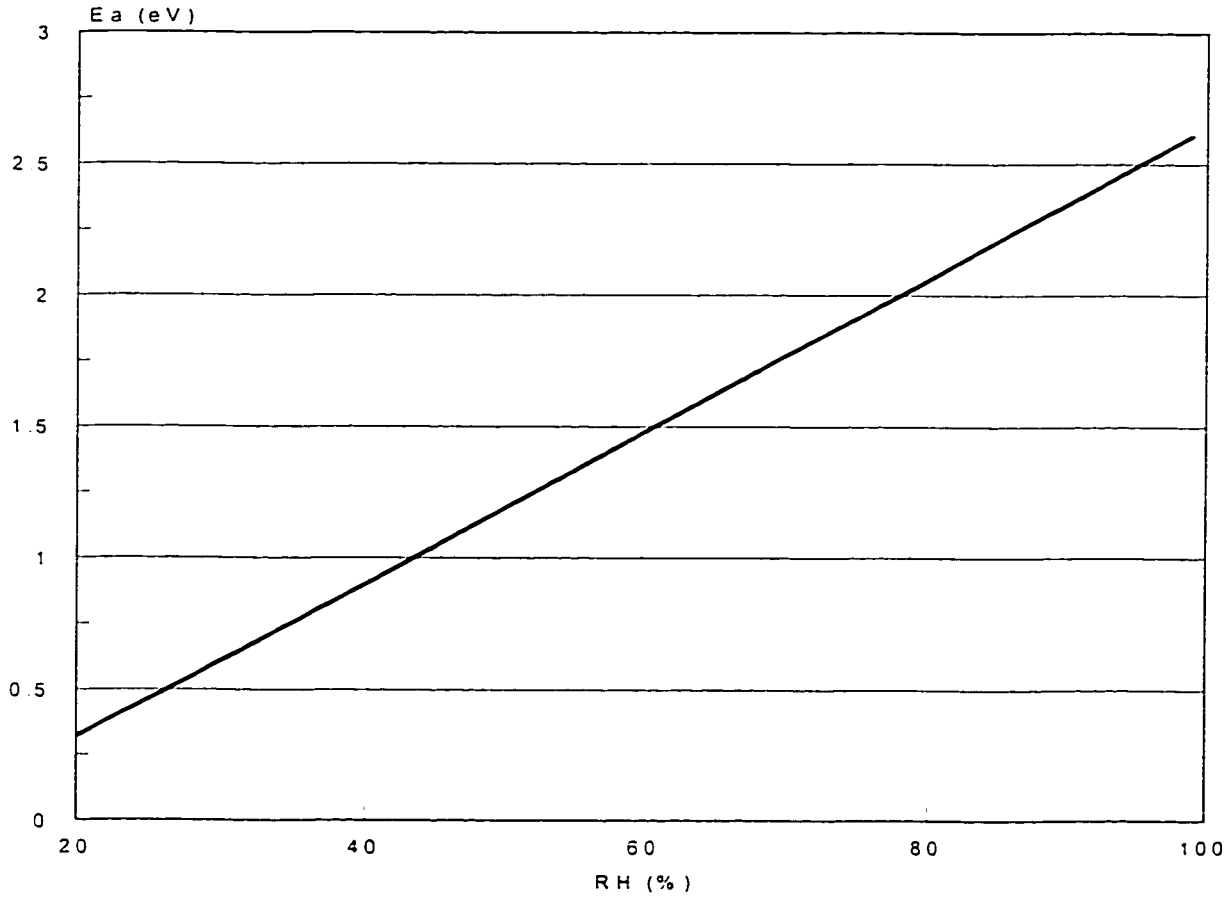

Figure 3.3: Activation energy E_a (eV) as a function of the RH (%). E_a exhibits insensitivity with temperature in the range of 278K to 320K.

3.4 RESISTIVE ELEMENT DESIGN

Apart from the obvious advantages of batch fabrication of resistive humidity transducers, such as low cost and miniature size, the use of thin film offers further potentials for enhancement of response time. Such potential benefits, however, can be exploited only if the substrate geometry and the sensing materials fulfill the structure requirements, which allows for efficient post-processing and integration of conditioning circuitry. Until now relatively few attempts have been made on possible micromachining structures for realization of integrated humidity sensors with desirable characteristics. The primary design considerations for resistive humidity sensors include the following:

- The electrode configuration to realize optimal nominal resistance and variation in resistance.
- The electrode shape to facilitate post-processing.
- The material selections for enhancement of static sensitivity and response time.
- The post-processing for integration of conditioning circuitry and cost reduction.
- The cost.

In order to optimize the design of resistive micro transducers, it is essential to design adequate electrode configurations and shapes to achieve reasonable values of nominal resistance and resistance variations within the constrains of the design rules. In following sections, three different electrode configurations are proposed and their characteristics are discussed in view of output resistance and issues related to fabrication.

3.4.1 Electrode Structure Configuration

The primary function of electrodes is to interface the electrical output with the active material. The contacting area between the electrodes and the active material must provide a reliable electrical contact. The shape and size of the electrodes are of primary concerns as well as the compatibility of the electrode materials with the humidity sensitive material. The relative position of the electrodes which directly affects resistance value is another important issue. Four different kinds of electrode configurations, as shown in Figure 3.4, were investigated by Pelino et al. [47] to derive the influence of their geometry on the output resistance, while identical sensitive material was used in all four electrode configurations.

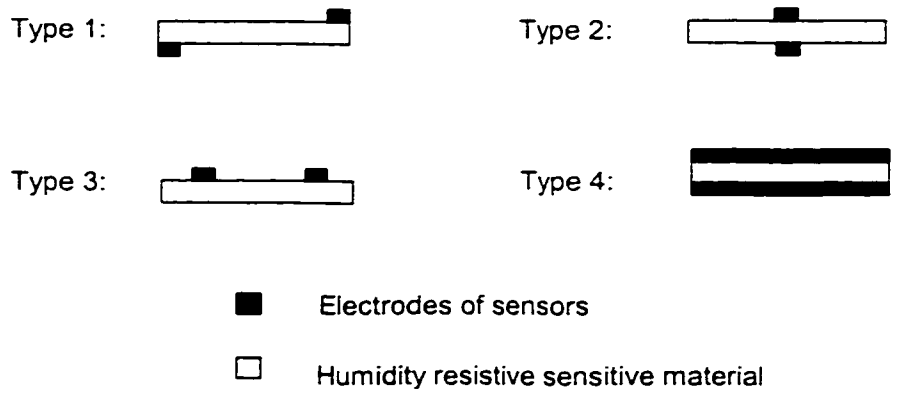

Figure 3.4: Schematic of different electrode configurations, studied by Pelino et al [43].

The study concludes that type 1 electrode yields highest impedance values as compared to the other configurations, since it enhances the bulk resistivity contribution with respect to the overall impedance of the material. The type 4 electrode results in lowest impedance value but a linear relationship with RH over the entire range. Type 2 electrode results in impedance value, which is midway between type 1 and type 4 due to existence of small capacitance. The type 3 electrode reveals insignificant impedance variation with RH higher than 70%. This is due to the fact that water condensation on the surface increases considerably at higher RH and the conduction mechanism is mostly electrolytic. The type 4 electrode further revealed more enhanced contributions due to the capacitance effect on the impedance magnitude variation, when compared to those observed for type 1 and type 2. All these four types of electrode geometry can be achieved through CMOS Mitel15 process. Type 2 and type 4 result in complex post-processing due to the electrode configuration. The top electrode for type 2 and type 4 has to be deposited after the formation of sensitive material. Comparing the above four types configurations, it is concluded that type 1 is a comparatively suitable electrode configuration due to applying bulk resistance of sensitive material with low capacitance effect and simple post-processing.

Taking into account the constraints of CMOS process (double-metal and double poly) and the results reported by Pelino et. al. [47], a structure of the electrodes for the resistive transducers is realized as shown in Figure 3.5. The passivation film is removed from the entire area of the transducer, while the top

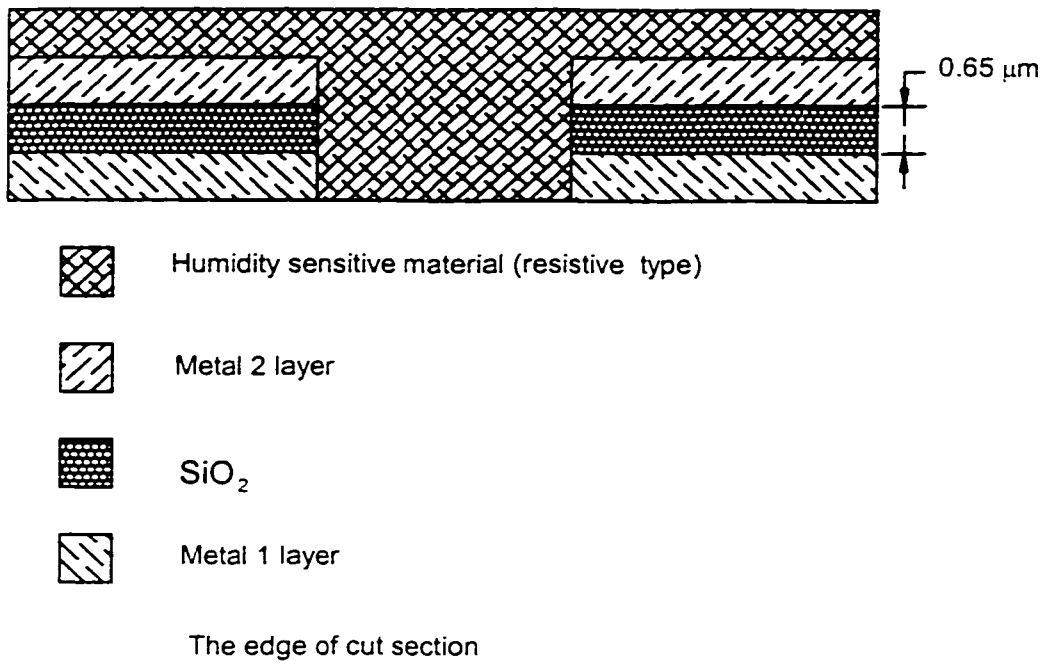

Figure 3.5: A cross section view of the electrode configured for resistive type sensors (not scaled).

electrode is patterned such that facilitates the penetration of water vapor into the sensing material. Bottom electrode is also patterned identical with top electrode. The sensing materials fill the gap between the two electrodes such that bulk resistance of sensing materials is accomplished. This kind of electrode configuration can be easily fabricated through the CMOS process. However, the fabrication imposes the omission of basic design rules. This design, similar to type 1 structure, makes use of bulk resistivity of the humidity sensitive material, while the post processing can be achieved by simple maskless spin-coating. It is desirable to deposit sensitive material as thin layer as possible in order to achieve fast time response of the sensor. The deposition of very thin layers rises challenges related to the compactness or to the integrity of the deposited films.

3.4.2 Electrode Shape Analysis

The realization of a reasonable value of the bulk resistance of a resistive sensor forms an important task in the design process. The bulk resistance of a sensor is strongly related to the electrode shape. The scope in investigating the shape of the electrodes is to ensure a configuration that could be accomplished through the proposed CMOS process and that would allow deposition of a controlled active thin film by simple post-processing. In addition, the configuration should yield desired values of the effective resistance of the transducer. Most of resistive humidity sensitive materials have large resistivity. The configuration of the electrodes may address this problem by providing a transducer with the reduced resistance. The effect of electrode shapes on the

bulk resistance is thus investigated in an effort to derive an optimal shape. The analysis is initially performed for square and circular shape cuts in the electrodes.

The square and circular cuts in the electrodes are fully feasible to be accomplished in CMOS process. One expects that the cut shapes in the electrodes would influence the performances of the transducers related to the post-processing. When the performances of the two cutouts are compared, a constant reference must be considered when referred to the sensitive materials. Thus, the volume of the humidity sensitive material filling the cutouts was imposed to remain constant. For the circular cutout, a convenient diameter of the circle was considered. To maintain the same volume for the square cutout, a non-even figure number resulted for the side of the square.

A square shape cut in the electrode is realized from small squares cut through Metals 1 and 2, and SiO_2 layers, as shown in Figure 3.6. These square openings are arranged in 99×112 array. The figure numbers were established based upon the limitation of chip size, while the size of square openings is selected as $5.76\times5.76\,\mu m^2$, as shown in Figure 3.7(a). This size and arrangement are considered suitable for spin-coating deposition of polymer. The duplication of these openings may further compensate for the non-perfect deposition or post-processing. The selected geometry of the structure yields an exact size of the transducer of $891\times1008\ \mu m^2$, which is in accordance with the permitted overall size of the transducer. The balance to $3008 \times 3008\ \mu m^2$ is

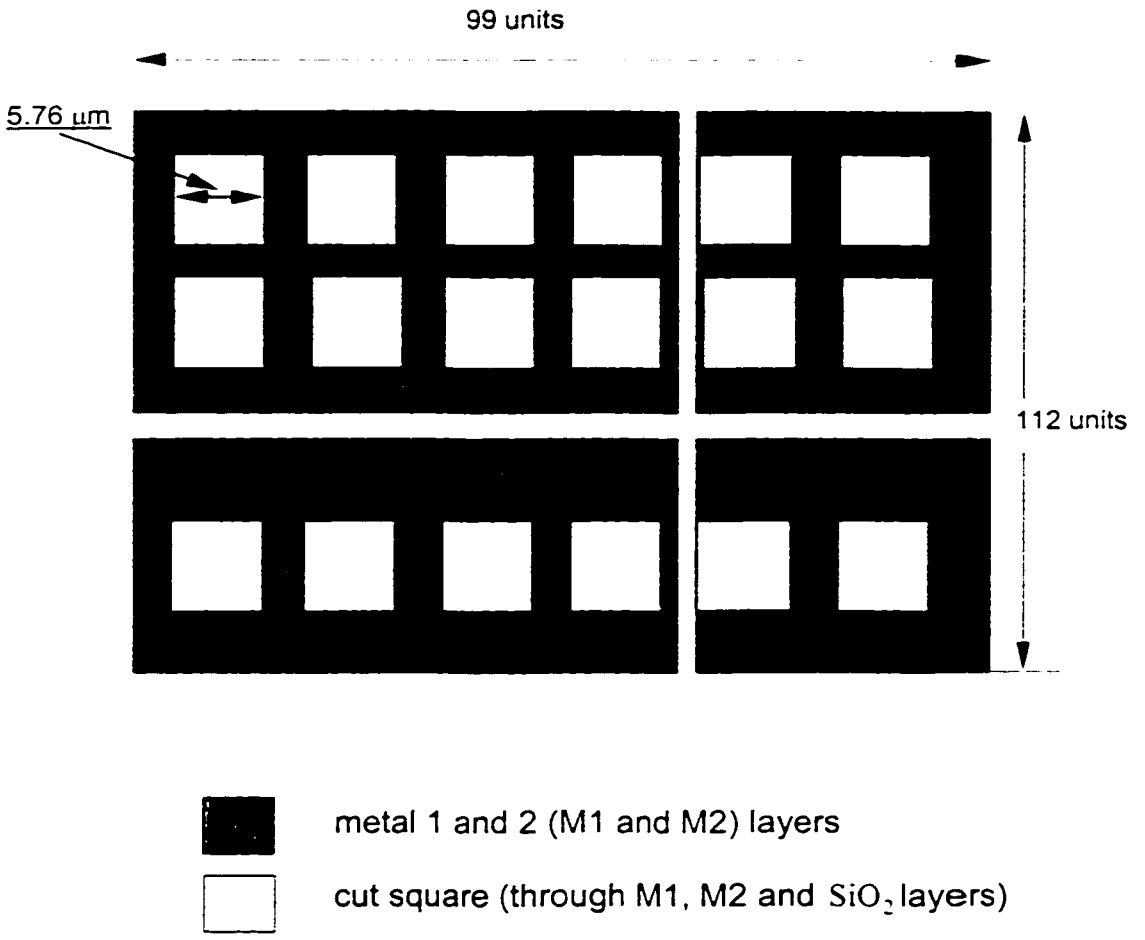

Figure 3.6: The schematics configuration of layout of square-cut shaped electrodes.

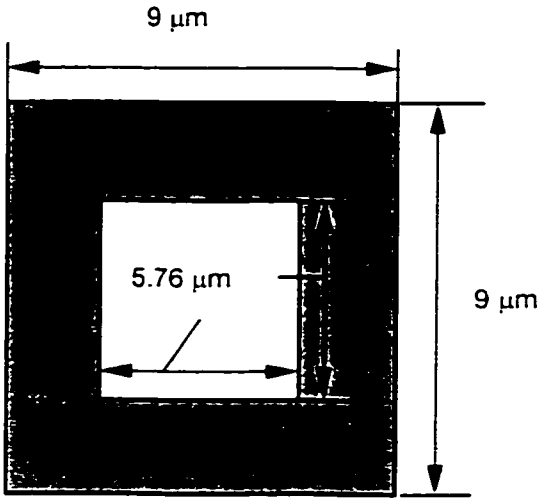

(a) square-cut shape in the electrodes.

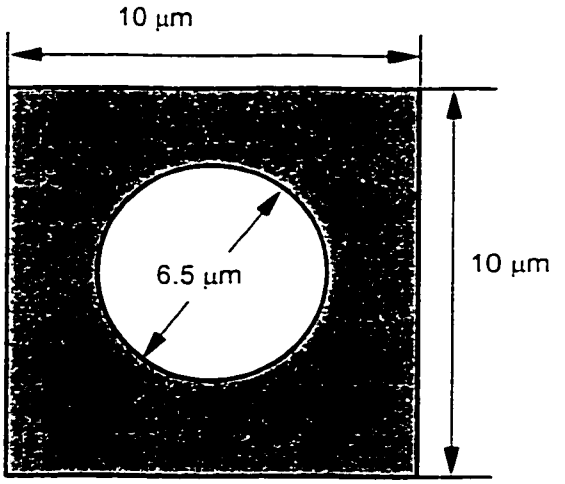

(b) circular cut shape in the electrodes.

Figure 3.7: Top view of one unit of square-cut and circular-cut shaped transducer electrodes.

reserved to the electronic circuitry including reference resistance and the contact pads.

A sensor with circular-cutout shaped electrode is illustrated in Figure 3.8. Similar to the square-cutout shaped electrodes, these circular openings are made through Metal 1, Metal 2 and via SiO_2 layers, and are arranged in 84×132 array which is the same as the number of cells in square-cutout shaped electrode configuration. This enables the two configurations to exhibit the same resistance. In comparison with the square-cutout shaped electrodes, the circular-cutout shaped designs facilitate the fabrication process by eliminating the occurrence of sharp corners. It should be noted that sharp corners of square-cutout shaped electrodes cannot be realized through etching. The diameter of each circle opening is selected as 6.5 μm, which yields the cross-section area identical to that of the square opening, as shown in Figure 3.7. The transducer size is thus achieved as 840×1320 μm^2. Since the cross-section area of squares and circles is identical, both electrode shapes are expected to yield comparable values of bulk resistance. Figure 3.9 illustrates an equivalent electric circuit for both circle-cutout and square-cutout shaped electrodes layout. The bulk resistance of the structure may be derived from:

$$\frac{1}{R} = \sum_{i}^{n} \frac{1}{R_i} \tag{3.3}$$

where R is the bulk resistance of the transducer, which may be referred as R_{circle} and R_{square} for circular-cutout and square-cutout shaped designs. R_i is the resistance due to each element or electrode.

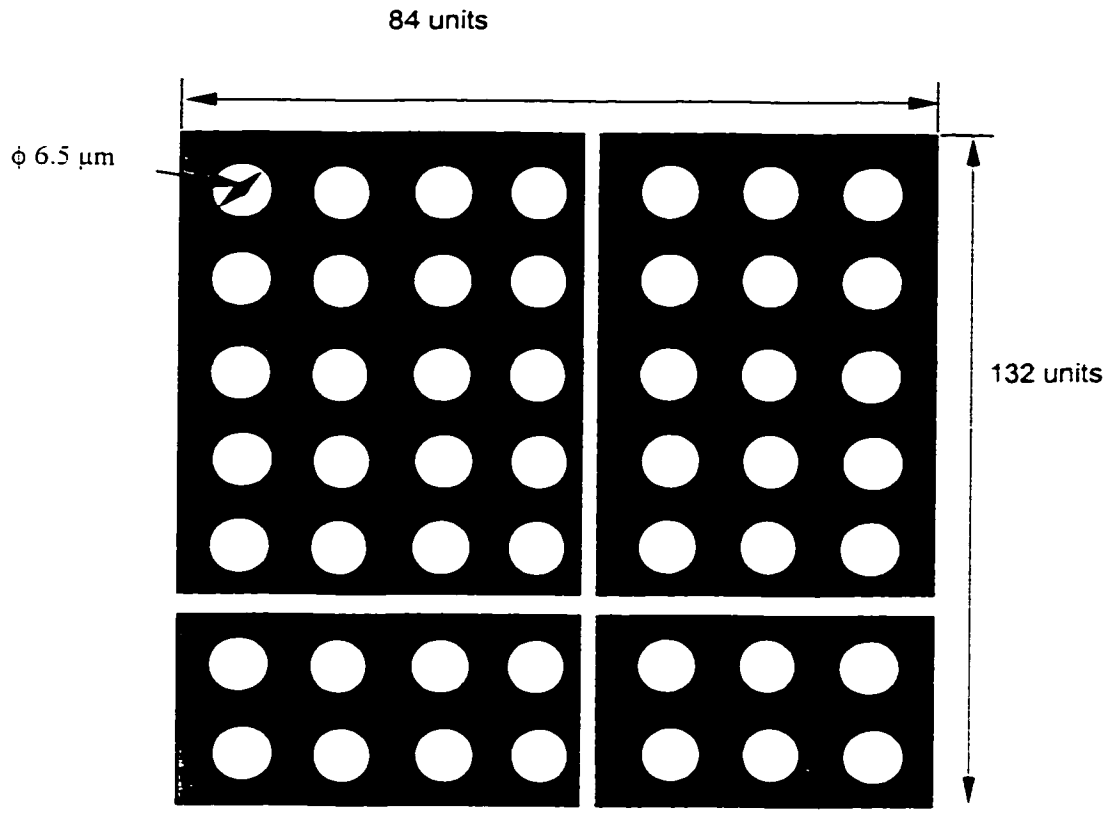

Figure 3.8: Schematic configuration of the humidity resistive sensor layout with circular cutout cells.

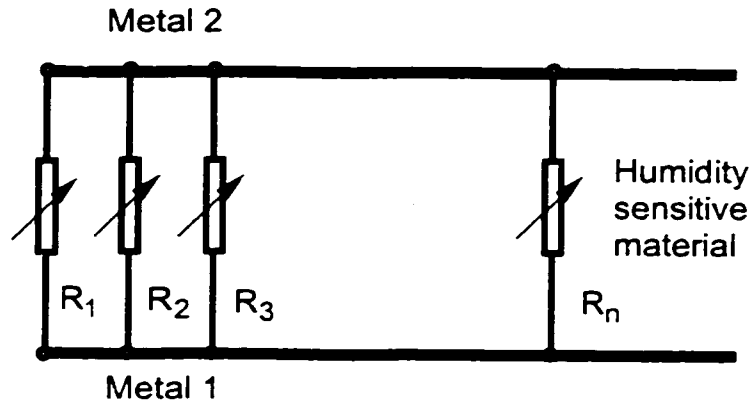

Figure 3.9: An equivalent electrical circuit of resistive sensor structure with circular-cut and square-cut shaped electrodes array.

The resistance of these two electrode shapes, however, are dependent on the resistivity of the active material, such that:

$$R_{circle} = R_{sqare} = 1.767\rho\ \Omega \qquad (3.4)$$

where ρ is the resistivity of sensing material.

An alternate electrode shape was further considered. An axisymmetric configuration which is based on the measurement principle that involved progressive increasing features is further proposed, as shown in Figure 3.10. The center of donut-shape is in the center of chip. During post-processing, the chip will be spun about its axis of symmetry. This will enable a uniform distribution of the humidity sensitive material over the electrodes. This observation does not stand anymore when spin coating is carried out on the entire wafer (bulk post-processing). This electrode shape also explores the results of sensitive material covering non-planar surface of chip. In actual design, more donut-shapes are used than Figure 3.10 shows. The two different types of metallic layers act as electrodes. The proposed configuration of the transducer

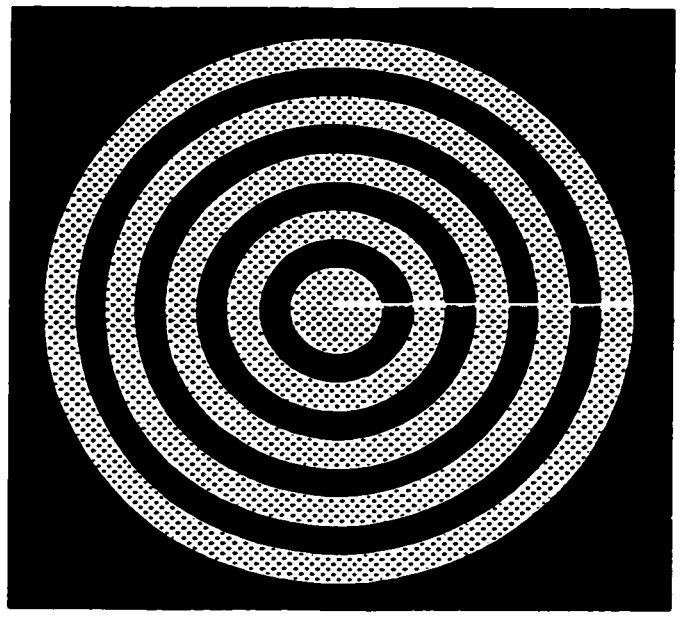

Metal 1 layer

Metal 2 layer

Under the second metal film, an insulating intermetallic SiO_2 film is interposed.

Figure 3.10: Top view of the concentric design of a resistive humidity sensor structure.

allows a good contact between metal 1 and metal 2 layers through the active material even if the active material is not uniformly spun. The electrode (Metal 2 layer), which is exposed to the environment, is made as a series of concentric rings with 3 μm wide traces spaced at a distance of 9 μm. The concentric rings are electrically connected by a trace. The bottom electrode (Metal 1 layer) is a planar metal film deposited on SiO_2 grown on Si wafer.

There are several reasons for the choice of this particular electrode geometry. First, the thin metal rings (3 μm wide) permit rapid absorption and desorption of water vapor within the film. Secondly, the circular geometry provides uniform absorption for each region of the sensor surface [11]. Thirdly, the proposed design eliminates the existence of sharp corners and thus permits a uniform deposition of sensing material. The proposed configuration realized through photolithographic techniques is quite producible.

The size of Metal 1 layer is 1605 μm × 1605 μm, while the outside diameter of the largest ring of metal 2 layer is 1602 μm due to limitation of chip size. The radius of center circle of the design is also 6 μm, as shown in Figure 3.11. The area of the trace is made from Metal 2 which connects different rings and is considered negligible since it is very small. The trace is insulated by Metal1 through the intermetallic SiO_2.The resistance of the concentric shape sensor is dependent on the resistivity of the active material (ρ), and can be expressed as:

$$R_{donuts} = 0.54\rho\Omega \tag{3.5}$$

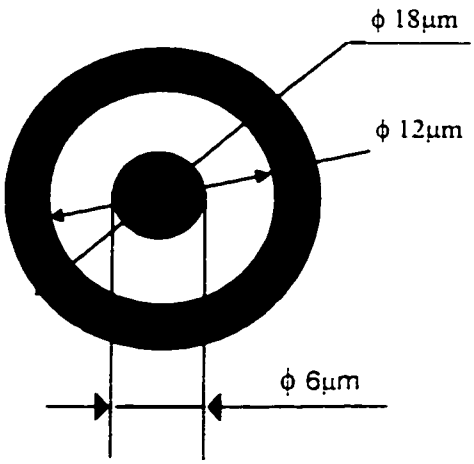

Figure 3.11: Top view of center part of metal 2 layer of the concentric design.

Through comparison, the donut-shape configuration results less than one third of resistance output of circle shape and square shape. However, the area of the donut configuration is almost three times larger than that of the array of square cutouts. Overall, the performance of resistance over the area is almost similar for these three configurations. After performing the calculations of the resistance versus area, the best index is shown by the donut shape followed by square-cut shape and circular-cut shape. However, the differences are small. Most resistive sensitive material exhibit very high resistivity. So it is necessary to use the proper electrode configuration to reduce output resistance. So the donut shape configuration is the best suited electrode configuration of the above three. Donut shape configuration is also convenient to manufacturing processing due to no sharp corner involved in the design. Donut shape configuration exhibits the important advantages in the post-processing.

3.4.3 Analytical Model Development

The static and dynamic characteristics of a transducer can be conveniently evaluated through systematic static and dynamic calibration tests. Alternatively, analytical models may be developed and analyzed to derive the transducer's steady and transient response behavior. Such models for humidity sensors, however, involve complex characterization of thin film humidity sensitive materials. The models, when validated, may serve as reliable design tool for steady and transient response characterization of the transducer.

3.4.3.1 Humidity sensitive material selection

In this study, a typical humidity sensitive material ($BaCl_2 \bullet 2H_2O$) is considered to develop the analytical model. Calibrated salt ($BaCl_2 \bullet 2H_2O$)is a well investigated and fully characterized humidity sensitive material [46, 47, 48]. The model of $BaCl_2 \bullet 2H_2O$ available in the literature [46] is coupled to the studied transducer. The preparation and processing of $BaCl_2 \bullet 2H_2O$ have been discussed in some reports [47, 48, 49]. The transducer could be prepared by dipping the substrate containing the electrodes in a saturated aqueous solution of $BaCl_2 \bullet 2H_2O$, kept at a constant temperature of about 350K, followed by curing at about 1100k for 20 min [47]. The resistivity of the $BaCl_2 \bullet 2H_2O$ material was established by Sberveglieri [46] over the RH range of 20% to 100%. A semi-empirical relationship was proposed, which is described in equation (3.1). Relationship between the RH and the resistivity is further illustrated in Figure 3.2.

3.4.3.2 Steady response of the transducer

Steady response of a transducer describes its performance at a certain steady input of a physical quantity under controlled conditions, such as temperature and pressure [25]. The steady response of a humidity transducer is directly determined by the properties of the sensing material applied on the transducer. For donut-shape electrodes, the resistance of the transducer can be derived by substituting equation (3.1) to equation (3.5), and expressed as following:

$$R = \frac{1.20 \times 10^{15}}{\exp[\alpha RH - E_a / (kT)]} \Omega \qquad (3.6)$$

The relationship between the RH and the resistance of the sensor, described in equation (3.6), is further illustrated in Figure 3.12. As shown, the logarithm of output resistance is linearly dependent on the relative humidity level. Resistance of the transducer decreases considerably with increase in the relative humidity level. When the relative humidity level is low, the variance in resistance is more pronounced than that attained under high relative humidity levels. The high resistance of transducer under low relative humidity, however, poses certain measurement challenges.

The resistance of the transducer is strongly affected by the ambient temperature. Figure 3.13 illustrates the influence of temperature variations in the 280K-320K range on the resistance of humidity sensitive material. The results show that the variance of output resistance of the transducer within the range of temperature variations is lower, when the RH level is below 50%, and grows

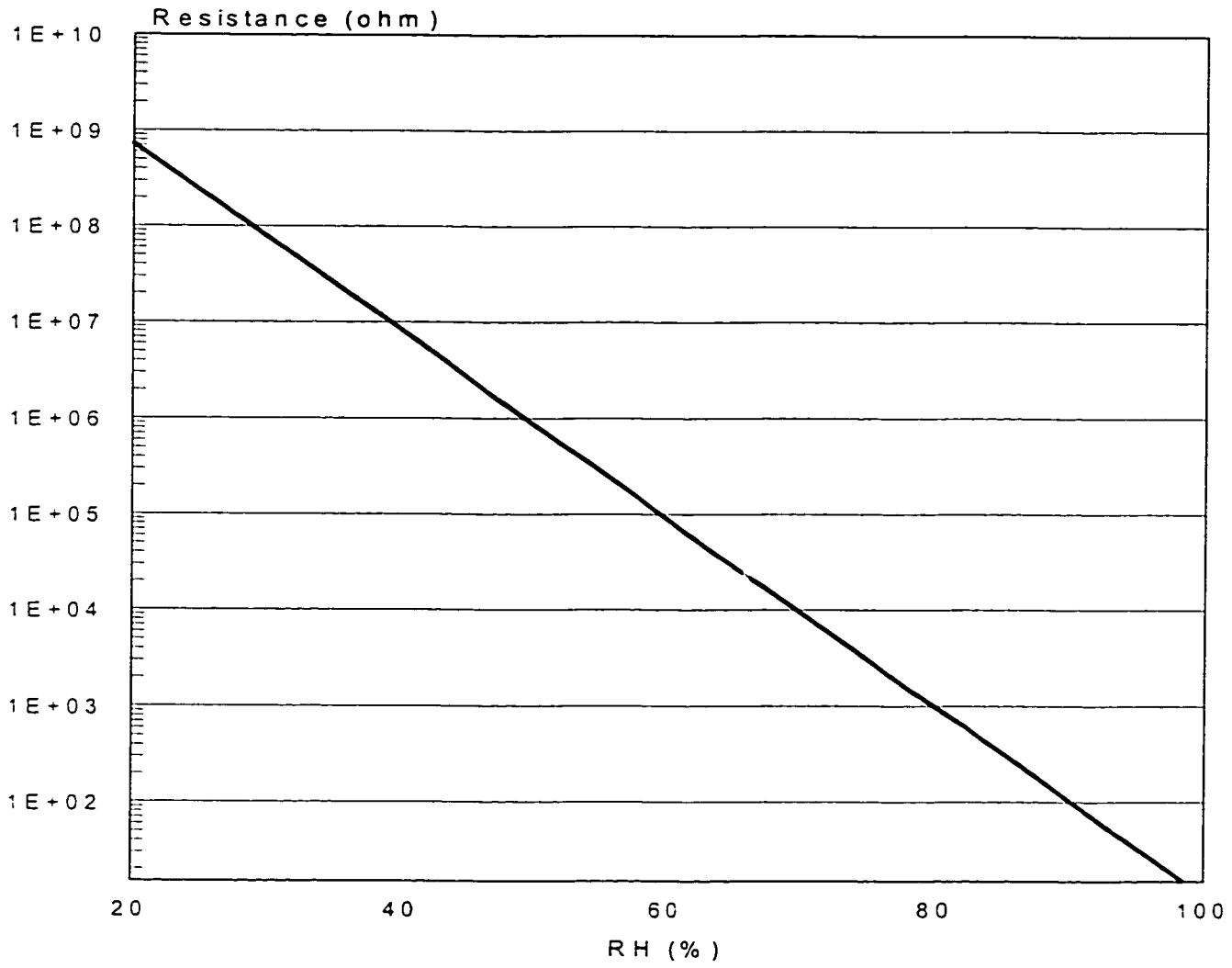

Figure 3.12: Relationship between the RH and the resistance of the donut shape transducer model (T=300°K).

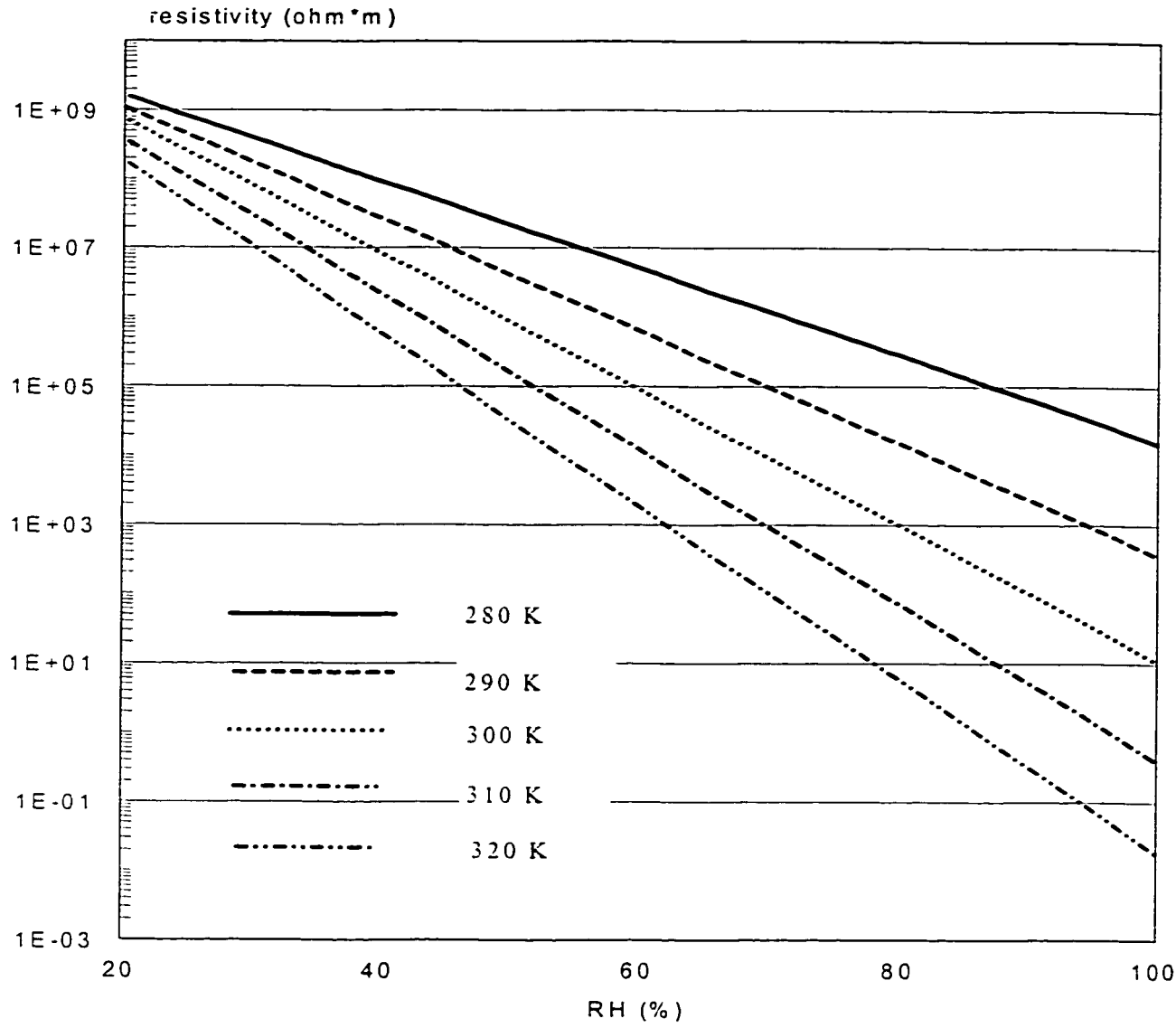

Figure 3.13: Influence of temperature variations on the resistivity of the humidity sensitive material $BaCl_2 \bullet 2H_2O$ [42].

significantly when RH approaches 100%. Thus, one can conclude that the influence of temperature is more significant to high humidity levels.

3.4.3.3 Sensitivity of the transducer

Steady sensitivity of a transducer is the ratio of change in transducer output to the change in the input physical quantity. For a resistive humidity transducer, the output refers to the change in resistance, while the input refers to relative humidity level of the environment. The sensitivity of the transducer over a given input range can thus be expressed as:

$$K = \frac{\Delta(\text{output})}{\Delta(\text{input})} = \left|\frac{dR}{dRH}\right| \tag{3.7}$$

where K is steady sensitivity of the transducer. The sensitivity will depend on the temperature. However, the value of sensitivity will be established at the room temperature and further we will assume no variation in temperature. Equation (3.7) is solved using equation (3.6) to derive the expression for steady sensitivity which is given by:

$$K = 2.82 \times 10^{14} \exp[-\alpha RH + \frac{E_a}{kT}] \tag{3.8}$$

The steady sensitivity for the resistive transducer is shown in Figure 3.14. Sensitivity of the transducer is established from the slope of the calibration curve. It is apparent that steady sensitivity of the transducer is nonlinearly related to the relative humidity. The transducer further yields high bulk resistance and high steady sensitivity for low values RH variations.

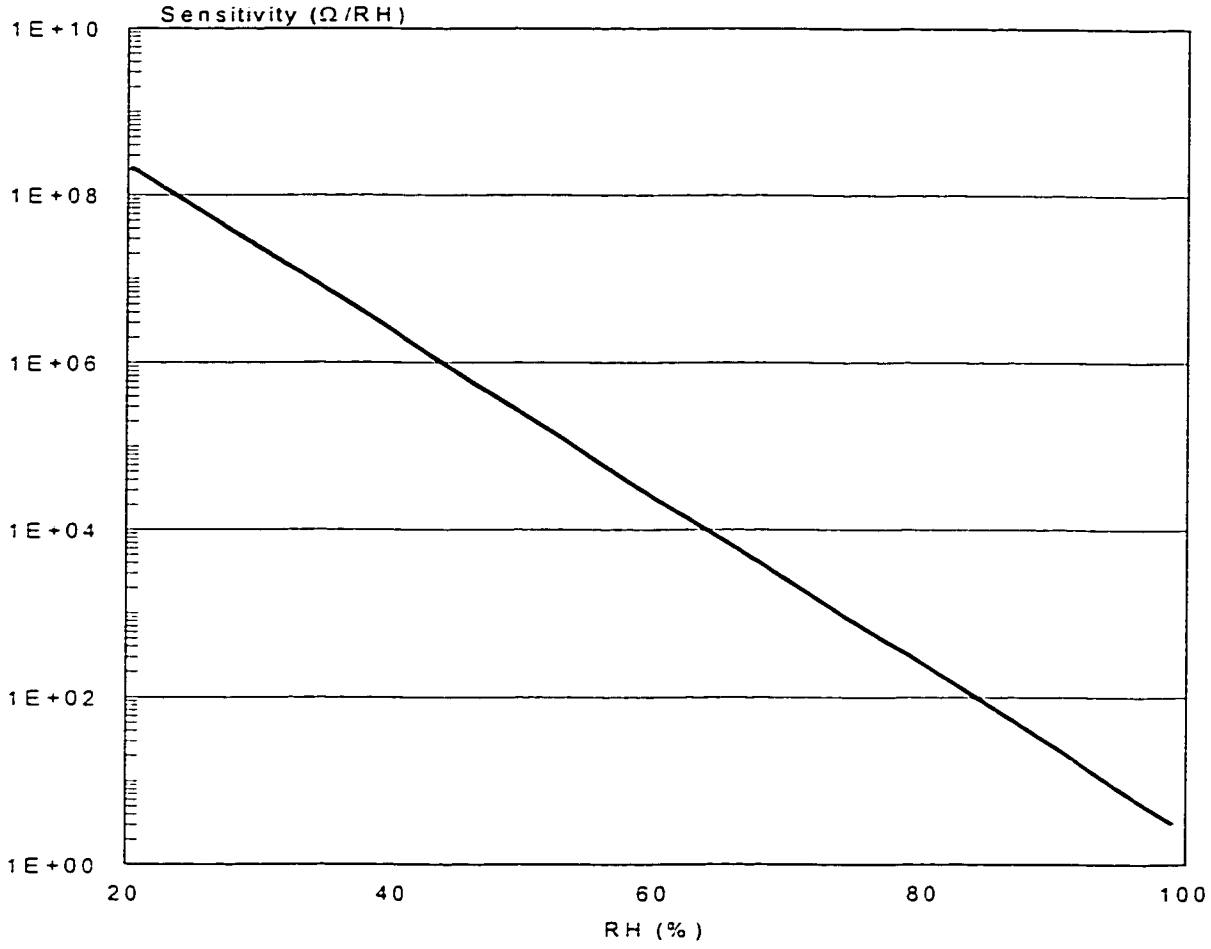

Figure 3.14: Steady sensitivity of a resistive humidity transducer (T=300K).

3.4.3.4 Transient model of sensitive material

When the water vapors are absorbed into the humidity sensitive film, water molecules are diffused inside from surface. Assuming uniform concentration of water molecules in the air at the interface, the moisture content is considered to be homogeneously distributed along the exposed sensing surface. During the adsorption process, however, the humidity or moisture content distribution is not homogeneous over depth until the material gets saturated. The uniformity of water vapors distribution across the thickness of the material film is related to its saturation, this is, when the material does not accept any further water contents from the air. Figure 3.15 presents the diffusion process into the sensitive material. Initially, the absorbed water vapors are nonuniformly distributed across the sensitive materials, as shown in Figure 3.15 (a). The sensor surface thus exhibits humidity level identical to that of the environment. Upon saturation, the sensitive material exhibits more homogeneous distribution of absorbed water vapors, as shown in Figure 3.15(b).

The water diffusion into the material could be described by the Fick's equation [24], which is based upon the following assumptions: vapor pressure is the only driving force, the process is one-dimensional; the process is isothermal (i.e. heat generated by moisture absorption at the surface is assumed negligible); the process exhibits negligible hysteresis. The isotherm absorption is used to model the water absorption capacity of the material, while the water diffusion coefficient is assumed to remain constant during the absorption process. The

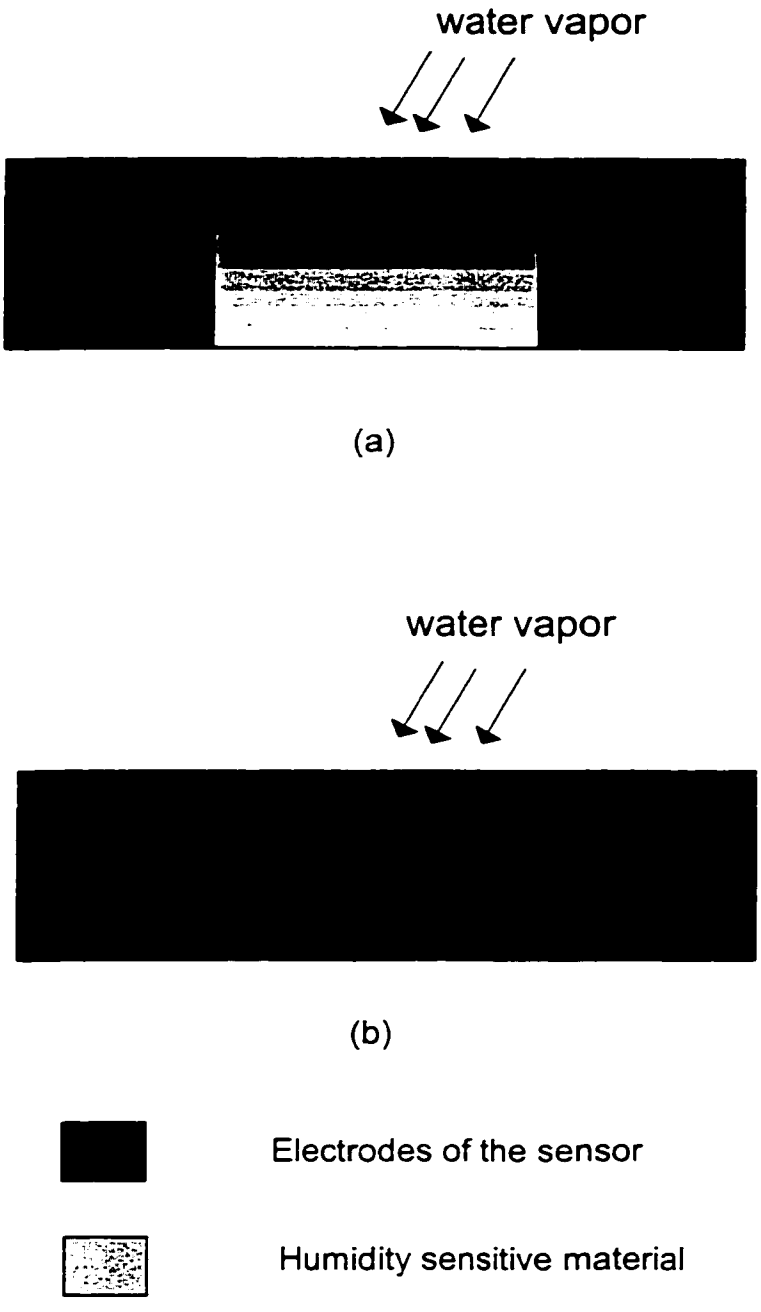

Figure 3.15:Diffusion of water vapors into the depth of sensitive material.

Fick's equation of one-dimensional diffusion is expressed as:

$$\frac{\partial U}{\partial t} = D\frac{\partial^2 U}{\partial d^2} \tag{3.9}$$

Where U is the instantaneous moisture content, D is the diffusion coefficient for water vapor in humidity sensitive material; and d is the penetrating depth of water vapor into the humidity sensitive material. Under steady humidity level of the environment, the moisture content of the surface of the sensitive material approaches the same value as that of the surrounding environment. One of the boundary conditions can thus be expressed in the following manner:

$$U_s = U(0,t) \tag{3.10}$$

Where U_S is the surface moisture content, which is same as the moisture content in surrounding environment. U(0,t) is the surface moisture content (d=0) at any time instant t.

The moisture content of material layer, far away from the surface when assuming infinite thickness of the absorption material, is zero, such that

$$U(\infty,t) = 0 \tag{3.11}$$

Assuming that a dry sensing surface is exposed to environment with certain humidity level, the initial moisture content of material at any depth, remains zero, such that

$$U(d,0)=0 \tag{3.12}$$

The Fick's equation can be solved using the initial and boundary conditions described in Equation (3.10) to (3.12), to yield [24]:

$$U(d,t) = U_S \operatorname{erfc}\left(\frac{d}{2\sqrt{Dt}}\right) \tag{3.13}$$

The complementary error function, erf(z), is derived from:

$$\text{erfc}(z) = 1 - \text{erf}(z) = 1 - \frac{2}{\sqrt{\pi}} \int_0^z e^{-u^2} du \qquad (3.14)$$

The water vapor diffusion coefficient D for different humidity sensitive materials is, in general, evaluated from the experimental data. A regression model describing the variation in the vapor diffusion coefficient in terms of the relative humidity for a particular range (RH_1, RH_2) is given by the following equation[44]:

$$D(RH) = C_0 + C_1RH + C_2RH^2 + \ldots\ldots + C_nRH^n \qquad RH_1 < RH \leq RH_2 \qquad (3.15)$$

Where D(RH) is the vapor diffusion coefficient, chosen as a polynomial function of the relative humidity level RH. C_i (i=0, ...,n) are constants or regression coefficients, considered valid over a specific range of RH and derived from the measured data. Table 3.2 summarizes the coefficients for some of the materials [44].

The diffusion coefficient in this study is assumed as a constant C, for 0%≤RH≤100%. Different materials have different diffusion coefficients. However, the diffusion coefficient can be identified from the properties of the material versus humidity. Thus the response time at certain thickness of the given material yields a specific value for the diffusion coefficient. The ratio of the transient to steady state relative humidity is expressed by:

$$RA(t) = \frac{RH(t)}{RH} \qquad (3.16)$$

Table 3.2: Regression constants model of the diffusion coefficient materials [44].

Material	Range of relative humidity	$C_0\times10^{-12}$	$C_1\times10^{-12}$	$C_2\times10^{-12}$
Gypsum	0%≤RH≤100%	42	0	0
Fiber Insulation	0%≤RH≤100%	78	0	0
Cellulose Insulation	0%≤RH≤100%	60	0	0
Wood	0%≤RH≤50%	1.82	9.69	2.86
	50%<RH≤70%	-58.2	201.6	-140.0
	70%<RH≤85%	-480.0	1197.0	-700.0
	85%<RH≤95%	-15.7	57.3	-9.45
	95%<RH≤100%	-727.0	840.0	0

Where RH(t) is the transient relative humidity. RH is the steady state of relative humidity. The equilibrium of moisture content (U) can be approximately expressed in terms of the relative humidity (RH) by linear function.

$$U = aRH \tag{3.17}$$

Where a is linear coefficient. Thus, the ratio of the transient to steady state relative humidity RA can be further derived as following:

$$RA(d,t) = \frac{RH(t)}{RH} = \frac{U(d,t)}{U_s} \tag{3.18}$$

Where d is the current depth at which the amount of water vapor into the humidity sensitive material is assessed, t is time, U_S is the surface moisture content. If an average moisture content $\bar{U}(t)$ over the depth is used in equation

(3.18), then the average ratio of the transient relative humidity and steady state of relative humidity $\overline{RA}(t)$ could be expressed as:

$$\overline{RA}(t) = \frac{RH(t)}{RH} = \frac{\bar{U}(t)}{U_s} \tag{3.19}$$

Where $\bar{U}(t)$, the average of transient moisture content in thickness of material, can be expressed as:

$$\bar{U}(t) = \frac{1}{h}\int_0^h U(d,t)dd \tag{3.20}$$

Where h is the thickness of the sensitive material, $0 \le d \le h$. Therefore, the average ratio of the transient to steady state relative humidity $\overline{RA}(t)$ can be derived as:

$$\overline{RA}(t) = \frac{\bar{U}(t)}{U_s} = \frac{\frac{1}{h}\int_0^h U(d,t)dd}{U_s} = \frac{\frac{1}{h}\int_0^h U_s \operatorname{erfc}\left(\frac{d}{2\sqrt{Dt}}\right)dd}{U_s} = \frac{1}{h}\int_0^h \operatorname{erfc}\left(\frac{d}{2\sqrt{Dt}}\right)dd \tag{3.21}$$

When a step input in relative humidity is applied, the output will change non-linearly toward the final value (100% output range) over a period of time. The length of time required for the output to rise to a specified percentage of its final value (as a result of a step input) is the response time. A special term and symbol have been assigned to 63.2% of the time response: time constant which is also called the response time of sensor [20]. The necessary time to reach 63.2% of the steady state value when a step input in applied is the response time of the sensor. Therefore, the average ratio of transient to steady state of relative humidity $\overline{RA}(t)$ is 63.2%, when t equals to time constant. From the

equation (3.21), the relationship between the response time and diffusion coefficient can be derived, as shown in Figure 3.16 for an assumed thickness 3.4μm of sensitive material.

From Figure 3.16, it is concluded that the diffusion coefficient is directly related to time constant. The larger time constant is, the smaller is the diffusion coefficient. Lower diffusion coefficient is associated with slower travel speed of water vapor within the thickness of the active material. Thus, longer travel time in the sensing film is expected. The response time approaches zero, when the diffusion coefficient approaches infinite. Since the response time reported in literature for $BaCl_2 \bullet 2H_2O$ humidity sensitive material is around 7 seconds, it can be derived from Figure 3.16 that the diffusion coefficient for water vapor in $BaCl_2 \bullet 2H_2O$ is about 4×10^{-13} m^2 s^{-1}.

3.4.3.5 Transient response of the transducer

Dynamic characteristics of a transducer are related to its response to dynamic variations in the physical quantity or measurand. Shorter rise time and settling time are considered as most desirable dynamic properties of a transducer, which are primarily determined from its transient response characteristics under a step change in the measurand. Such transient response characteristics of transducers are mostly influenced by the energy storage type elements of the transducer. In case of humidity sensors, the transient response behavior is directly related to the water vapor absorption and desorption rates of

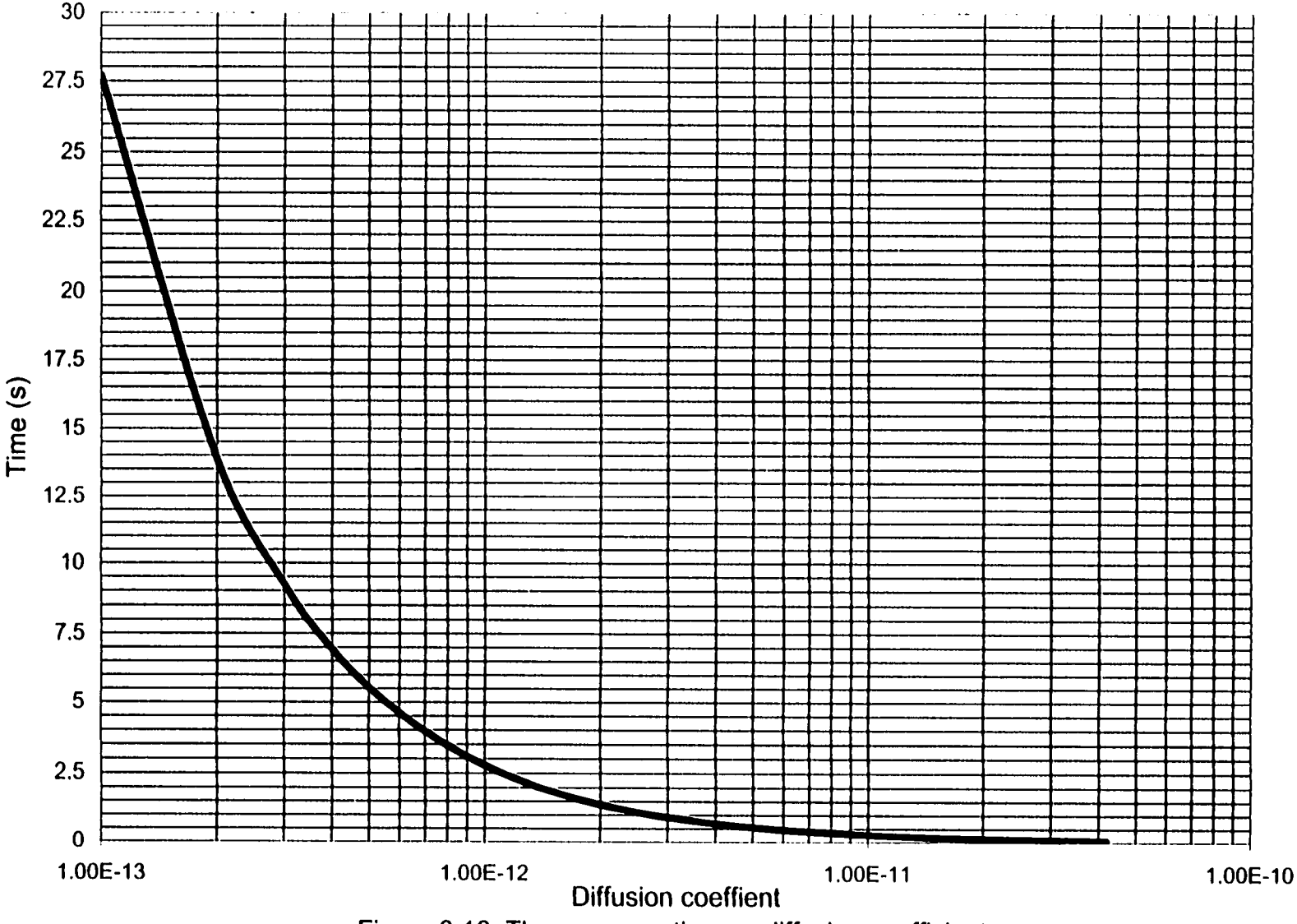

Figure 3.16: The response time vs.diffusion coefficient.

the sensitive materials, which may further depend upon the thickness of the material film.

The relationship between the ratio of the transient to steady state of relative humidity RA(d,t)can be obtained by substituting equation (3.13) into equation (3.18), as shown in equation (3.22).

$$RA(d,t) = \frac{U(d,t)}{U_s} = \frac{U_s \operatorname{erfc}\left(\frac{d}{2\sqrt{Dt}}\right)}{U_s} = \operatorname{erfc}\left(\frac{d}{2\sqrt{Dt}}\right) \qquad (3.22)$$

Where $D = 4\times10^{-13}\ m^2\ s^{-1}$ for the sensing material $BaCl_2 \bullet 2H_2O$.

Figure 3.17 illustrates the relationship between RA(t) with the penetrating depth of water vapor at certain time t after exposure to step humidity input. When exposure time is constant, the ratio of the transient to steady state of relative humidity approaches to one as the penetrating depth decreases. It is shown that the transient humidity is almost the same as the steady humidity level of environment near the surface of the sensing film. Figure 3.17 also shows that the slope of the curve decreases as the time increases. This shows that the rate of absorption decreases when the amount of absorbed water increases in the sensitive film. The RA(t) is going to achieve 100%, not affected by depth or time, when material is saturated.

Further, the transient response of the sensor with donut configuration for the electrodes and $BaCl_2 \bullet 2H_2O$ as active material will be evaluated. For a resistive sensor using $BaCl_2 \bullet 2H_2O$ as sensitive material, the steady response (the relationship between the relative humidity and the output resistance) is shown in equation (3.6). The transient response of the transducer can be

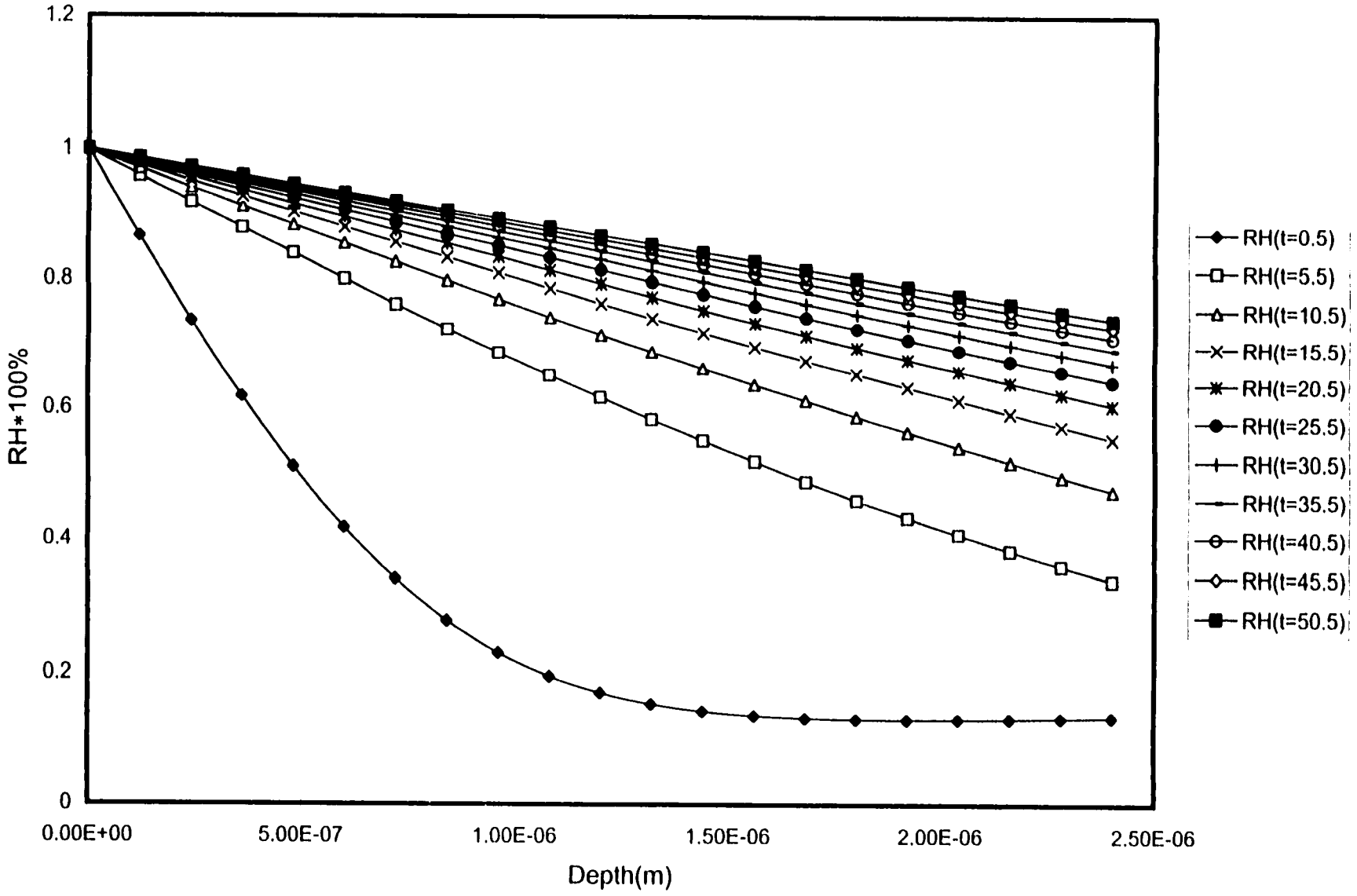

Figure 3.17: The relationship between RA(t) with the penertrating depth of water vapor at certain time t after exposure to step humidity input.

derived by multiplying the steady resistance R with the ratio of the transient relative humidity and steady state of relative humidity RA(t), which is shown as Figure 3.18. For different step input levels of relative humidity, all the curves describing the transient response of the sensing configuration exhibit the same trend. This is, the resistance of transducer decreases with time increasing. When humidity level increases, the resistance decreases. When time is less than 50 seconds, the resistance changes more dramatic than the time after 50 seconds, which attributes to the short response time of the transducer with $BaCl_2 \bullet 2H_2O$ as sensitive material. It is also shown in the figure the resistance of transducer approaches stable value which is the steady resistance of the transducer as time passing by.

3.5 POST-PROCESSING

CMOS (Complementary Metal-Oxide Semiconductor) technology, is a well developed, low-cost process flow with high availability, capability in microelectronic circuits. However, it has been demonstrated that a standard CMOS yields limited capabilities for micromachined mechanical microstructures. The general pathway that should be followed when a microstructure is fabricated consists of [32]:

- Design of the non-conventional layout for a specific CMOS process.
- Access the specific CMOS industrial process.
- Perform the post-processing.

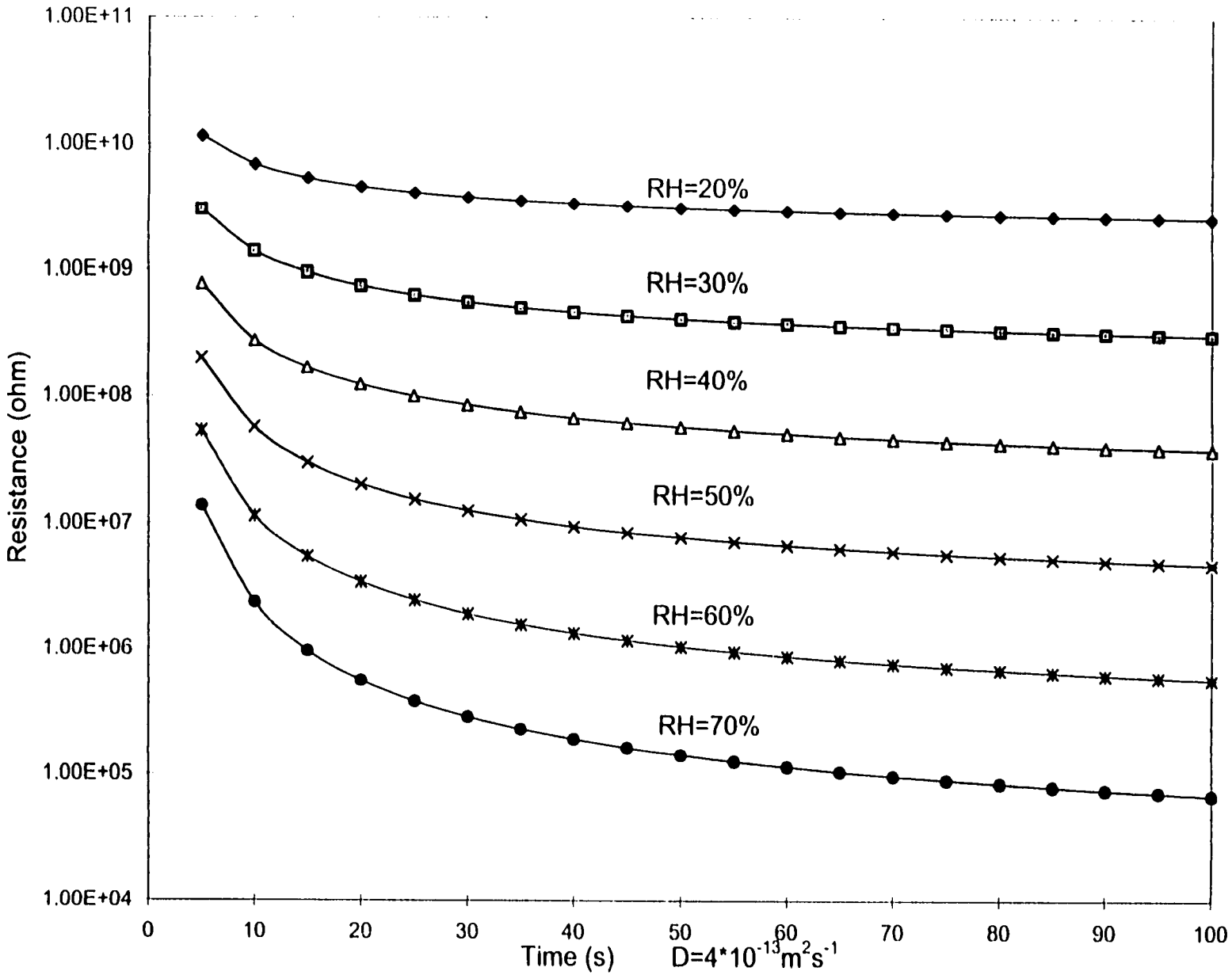

Fgiure 3.18: The transient response for resistive sensor.

In most of situations, post-processing is carried out in a post-processing module where either a thin film is deposited or etching is performed, with or without previous protection through photolithography. Each additional step in post-processing requires implementation of resources which increase the cost exponentially with the number of carried out steps. Thus, the minimization of the number steps that one should carry out during processing could substantially reduce the cost of the product. Besides, if the post-processing requires very little preparation, the costs associated with post-processing could be insignificant if compared with processing on packaging, as an example. The active material coating a structure of electrodes represents a basic configuration for humidity sensors. The area of sensitive material should be exposed to attain water vapor from the environment.

In terms of coating material, by far the majority employed in humidity sensor applications are polymeric materials chosen primarily on the basis of analyte solubility. Metal oxide films have also been used, largely on the basis of previously known sorption interactions with water vapor[32]. The choice of coating method will be dictated largely by the type of the coating material. However, the main deposition methods are: vapor deposition from solid state; coating from liquid state followed by the evaporation of the solvent. The appropriate methods for active materials used in humidity measurements are illustrated in table 3.3.

Table 3.3: Coating materials and deposition methods for thin film depositions.

Coating	Method
Calibrated salts	Spray or spin coating, solvent evaporation
Ceramics	Thermal or plasma deposition
Polymeric film	Spray or spin coating, solvent evaporation

Deposition of materials in liquid phase presents an important advantage against the deposition from solid phase. They include: spin coating, painting, dip coating, spraying etc. Each of the above methods can be used in conjunction with photolithography process. The only constraint of the method is related to the chemical reactivity of the solvent with the substrate. Concerns related to the uniformity of the film thickness and homogeneity are risen where depositions are carried out of dispersions of micro-particles in volatile liquid phase. Dilute or dispersed solutions are prepared in volatile solvents such as methanol, chloroform, acetone, or toluene and coated onto the device surface. The criteria of selection of the liquid phase is in connection with the property of wetability of the fluid on the substrate. It is essential to provide a clean and uncontaminated substrate to ensure a good quality adhesion of the film in intimate contact with the substrate. When the chips are out of the foundry, they are already clean. One should make sure that they remain clean.

The coating method may well leave specific morphological features in the film. Spin-coating can also yield morphological consequences. The required coating material is dissolved in a suitable solvent, which is then spun over the

surface at speeds up to 4000 rpm to spread the coating across the device surface. The success of this technique depends on the viscosity of the coating solution and the volatility of the solvent and the spin time.

3.6 MEASUREMENT CIRCUITRY

There are many measurement methods available for determination of electrical resistance, such as ammeter-voltmeter method, potentiometer method, differential galvanometer method, bridge methods and so on. Ammeter-voltmeter method is the most common method. Here, a measured current is passed through the resistor under test, and the potential difference across its terminals is also measured. The resistance in ohms is the ratio of the voltmeter reading in volts to the ammeter reading in amperes, in accordance with Ohm's law. The accuracy that may be attained by the ammeter-voltmeter method depends upon the accuracy of the two instruments. Potentiometer method requires the replacement of the ammeter with a standard resistor, and the measurement of the potential difference across the standard resistor yields the value of the current if this potential difference is divided by the value of the resistance of the standard. The method is especially good in cases where an accuracy of 0.1 percent or better is required. The differential galvanometer method is used rather extensively for the comparison of equal resistances. By far the largest proportion of measurements of electrical resistance are made by means of bridge methods. All these methods above rise one common problem, that is, they cannot be integrated on chip.

To overcome this problem, a resistance measurement circuitry is developed through one operational amplifier and a reference resistor. The OPAMP is included in the standard library of circuit for Mitel15 design kit. The schematic view of the measurement circuitry is shown as Figure 3.19. The operational amplifier and a reference resistor can be achieved by CMOS techniques. The principle for measurement is as the following. Through the comparison the reference resistance and the resistance of transducer, the value of resistance of the transducer can be derived from the output voltage, as shown in equation (3.23). The accuracy of R_3 is crucial in the design. R_3 directly determines the accuracy of R_{sensor}.

$$R_{sensor} = \frac{R_3}{\frac{R_1 + R_2}{R_1} \cdot \frac{U_i}{U_o} - 1} \tag{3.23}$$

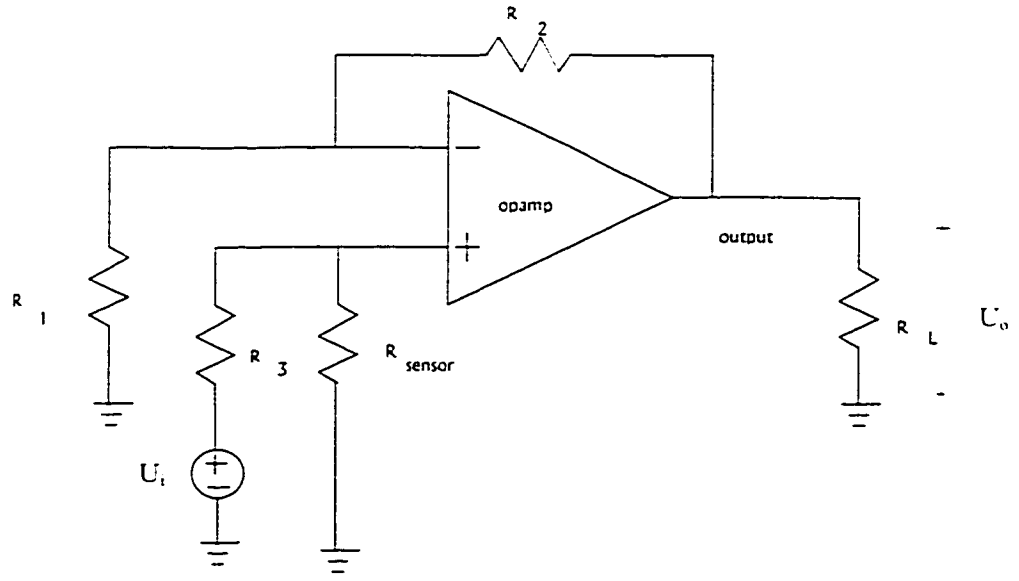

Figure 3.19: The bridge measurement method conditioning circuitry for the resistive sensor.

3.7 SUMMARY (CONTRIBUTIONS INDICATED AS UNDERLINE)

Resistive humidity sensors offer significant advantages in view of simple structure and operation principle and easy measurement. The summary of this chapter is outlined as following:

- The realization of micromachined transducer or devices involves many sequential steps, such as concept development, design and analysis, fabrication, post-processing and packaging. The design and analysis of a resistive humidity sensor involve consideration of its mechanical and electrical, static and dynamic performance characteristics.
- The designs of micromachined humidity resistive sensors are realized based on standard CMOS process MITEL 1.5μm, which comprises two polysilicon and two metal layers.
- The design of a humidity resistive sensor is conceived based upon the variations in resistance of a humidity-sensitive material. The resistive sensing materials is classified into three groups: organic polymers, porous ceramics and calibrated salts.
- The primary design considerations for resistive humidity sensors include electrode configuration, electrode shape, material selections, post-processing and cost.
- A structure of the electrodes for the resistive transducers is proposed as shown in Figure 3.5. The passivation film is removed from the entire area of the transducer, while the top electrode is patterned such that facilitates the penetration of water vapor into the sensing material. Bottom electrode

is also patterned idential with top electrode. The sensing materials fill the gap between the two electrodes such that bulk resistance of sensing materials is accomplished. The kind of electrode configuration can be easily fabricated through the CMOS process, while the post processing can be achieved by simple maskless spin-coating.

- Three different electrode shapes (square-cut, circle-cut, donut) are proposed and their characteristics are discussed in view of output resistance and issues related to fabrication. The donut shape is the best suited electrode of the three proposed. Donut shape exhibits the advantages in the post-processing.
- Barium chloride dihydrate ($BaCl_2 \bullet 2H_2O$) is chosen as the humidity sensing material in the simulation of sensor, which is because the relationship between RH and resistivity of $BaCl_2$ is available in the literature.
- An analytical model of the humidity transducer with thin film is developed to study its steady-state and transient response characteristics.
- Fick's equation is used to derive transient model of humidity sensitive material, which is the relationship between the response time and diffusion coefficient.
- Different post-processing method are discussed and compared.
- The resistive measurement circuitry which consists of one operational amplifier and a reference resistor is proposed.

CHAPTER 4

DESIGN AND MODELING OF A CAPACITIVE MICRO HUMIDITY TRANSDUCER

4.1 INTRODUCTION

Capacitive sensing presents certain advantages versus the resistive measurement. Low power consumption associated with improved thermal characteristics are the most important advantages of capacitive measurement. Capacitive humidity sensors have been widely used in the building, automation and factory fields because of their wide range, high accuracy and long term stability [4]. These advantages are due to the properties of the largely selected humidity sensitive materials. In miniature sensors, however, capacitance measurement poses various problems related to the reduced size of the sensors, such as the very low effective value of the capacitance, the difficulty in integration of conditioning circuitry, etc.

Some reports were published on capacitive humidity micro-sensors [12,14,16,47], such as the integrated capacitive humidity sensors fabricated with the industrial SACMOS (self-aligned contact CMOS) technology [12], the improved IC compatible capacitive moisture sensors [47], the bulk micromachined humidity sensor based on porous silicon [14] and etc. The above studies demonstrate sensor realizations, some of which are now commercially available. The majority of these examples use the well-established technology of bulk silicon micromachining for the fabrication of the sensor chip [16]. However, progress on surface micromachining of capacitive sensors was made as well.

The surface micromachining approach is more amenable to a monolithic integration of the sensor and its electronic interface. The motivation of this study on surface micromachined sensors is to propose a design associated with the low cost post-processing that could yield reliable capacitive microsensors, which could be further implemented with a measurement circuit.

In this chapter, structure and fabrication process of the capacitive humidity sensors based on Mitel 1.5μm process are presented. The designs of capacitive microsensors are partially optimized due to design constraints. The characteristics of fundamental properties, such as steady response, transient response, humidity sensitivity and response time are investigated. The post-processing and the conditioning circuitry of capacitive humidity sensors are also briefly discussed.

4.2 DESIGN ISSUES

Generally, there are two principal aspects that should be followed in the design of humidity transducers. First is to select and/or design a material for the sensor's humidity-sensitive film. Humidity measurement of capacitive sensors is usually based on the modification of the relative dielectric permititivity of the active material. Proper material selection can make sensors exhibit good sensitivity over a wide humidity range, good stability, repeatability and minimal hysteresis. Second is to optimize the sensor configuration and measurement method. The sensor configuration is strongly related to the fabrication process. During layout, all design constraints shall be considered. Some of design rules

were ignored, while some essential rules were carefully followed. Proper design can lead to easy process and post-processing, easy measurement, high sensitivity and, where possible, high degree of linearity.

The primary concerns in design of capacitive sensors include: measured capacitance and parasite capacitance[15]. It is desirable to maximize the sensor capacitance and variation with humidity, while minimize the parasite capacitance. On-chip measurement can be applied to reduce the parasite capacitance and reduce the resistance between the transducer and measurement circuitry. Parasite capacitance, however, cannot be eliminated. Thus the sensor capacitance variation should be at least one order of magnitude large than parasite capacitance, as the rule of thumb. There are also concerns for miniature sensors, where the overall size constraint reflects directly on the sensor capacitance and thus the performance [7]. The sensor capacitance can be increased considerably through judicious design of electrodes with large relative surface area between the electrodes, by decreasing the distance between electrodes and by selecting materials with higher dielectric constant [4,12]. Increased capacitance output could further ease the measurement method.

4.3 CAPACITIVE HUMIDITY SENSITIVE MATERIAL

The design of a humidity sensor is conceived based upon the variation in the dielectric constant, which further changes the capacitance of sensing configuration. Therefore, material selection plays an important role in the design of capacitive humidity sensors. There are many materials which can be used as

capacitive humidity sensitive materials. Ceramics and polymers are widely used, due to the larger change of their characteristics with water absorption.

Theoretically dielectrics do not contain movable electrical charges. However, the gravities of electrically charged particles can be shifted under certain conditions. The permittivity describes most comprehensively the dielectric property of a material. Permittivity changes may be detected due to the absorption of molecules with high dipole moments such as H_2O. Thus, the humidity change can be detected by the change of the relative permittivity which is directly reflected in the change of capacitance of a structure.

4.3.1 Porous Ceramics

Ceramic materials are known to be sensitive to humidity in capacitive measurement. Ceramic material is an insulating oxide or a mixed oxide prepared so that it is permeated by fine pores, on the walls of which water can be absorbed. The water vapor existing within the surrounding air collects in those pores inside ceramic materials. The existence of water molecules will modify the dielectric characteristics of ceramic materials. Usually ceramics have high relative dielectric constant, which is much higher than the dielectric constant of water. When ceramic absorbs water, the mixture of ceramic and water is expected to have a lower dielectric constant than ceramic itself. Therefore, the capacitance of the ceramic film decreases with an increase in relative humidity due to the low relative permittivity of the adsorbed water. Control of

microstructure of ceramic materials is very important for sensing characteristics, and the preparation conditions should be carefully chosen.

4.3.2 Polymer Films

Polymeric materials have conquered a large part of sensing materials. Nowadays, almost half of the promising chemical sensors are based on polymers. The great variety of properties that can be altered and controlled with different additives in polymers is the basis of their application for various chemical purposes [4]. Their potentiality is still growing, especially in the field of integrated microsensors [16]. Polymer films are well suited to standard IC processing techniques to fabricate small low cost sensors [6]. The relative permittivities of humidity sensitive polymers such as polyimides (PI) and cellulose acetates are known to range from 3 to 6, whereas pure water has a far larger value of 80 at 25°C [48]. It follows that the capacitance of polymers changes with the absorption of water, and thus if the polymer is known to absorb water, this can be considered as a desirably humidity-sensitive property. The porosity of the humidity-sensitive polymer is important to obtain quick response. The stress-induced fracture technique proposed by Delapierre [49] appears to be useful in this respect. A porous chromium electrode has been evaporated under conditions such that the humidity sensitive film is tensile stressed. The stresses cause a lot of pores in the polymer, resulting in an increase in the penetration rate of water vapor by several orders of magnitude.

Recent improvements in polyimide (PI) processing for the integrated circuit (IC) and interlay dielectric applications developed the idea that PI could be used to fabricate humidity microsensors on one single chip. This technique yields small, low cost humidity sensors. Most important, it becomes possible to integrate humidity sensors with other sensors or signal-conditioning circuitry on the same chip [50,51]. The sensitivity and response of polymer sensor also depend on the sensor geometry, including the shape of the electrodes. Polyimide is a normally infusible, colored (often amber) high performance polymer with predominantly aromatic molecules of high thermal stability. It has linear response to humidity changes, good absorption of water, resistance against chemical attack, mechanical strength and compatibility with IC fabrication. The photosensitive polyimide also can reduce the number of post-processing steps, since standard lithography and etching techniques are not required for pattern definition. Polymerization directly on sensor surfaces is the commonly used technique for post-processing of thin polymer layers. The synthesis and shaping occur on the sensor structure itself. Therefore, the compatibility of polymer with inorganic sensor parts shall be considered.

4.4 CAPACITANCE ELEMENT DESIGN

Capacitance-based sensors are extremely popular for a large variety of process measurements because they can be made reasonably rugged, simple, and inexpensive. However, it is important to investigate the electrode configuration and electrode shape such that to optimize the performances of the

transducers. This section provides a detailed study on capacitance element design, followed by a development of an analytical model of a capacitive humidity sensor. This study will help to improve the post-processing and conditioning circuitry of capacitive humidity transducers accomplished in a standard CMOS process followed by a simple low cost post-processing.

In order to optimize the design of capacitive micro transducer, it is essential to design the proper electrode configuration and electrode shapes suited to design constraints and low cost post-processing. In following sections, different electrode configurations are discussed. Three different electrode shapes are proposed and compared.

4.4.1 Electrode Configuration

The most widely used thin-film type humidity sensor, such as "humicape" in humidity measuring instrument was developed by Vaisala in 1975 [7]. Figure 4.1 illustrates the electrode configuration of the sensor. The lower twin electrodes are deposited onto a glass substrate by iridium evaporation. Cellulose acetate was dissolved in ethylene dichloride and then applied to the surface to form thin humidity-sensitive dielectric. On top of this, gold is evaporated as the upper electrode, which is thin and porous enough to permit quick transversal moisture transport. The upper electrode acts as a common counter armature to the lower twin electrodes. Most of electrode configuration designs are based upon "humicape", in which the upper and the lower electrodes are designed to consist the capacitor.

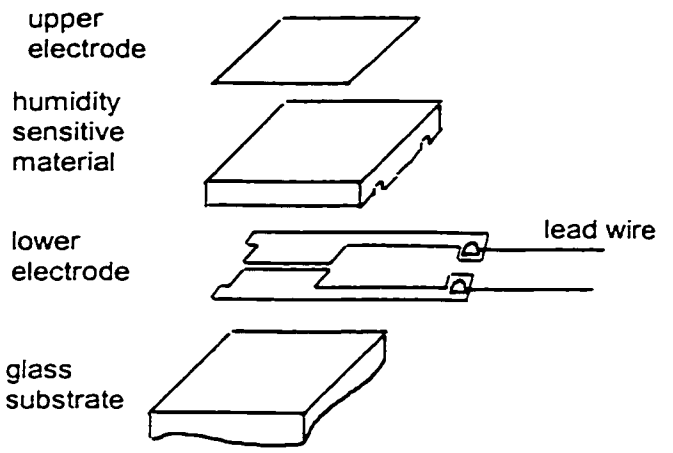

Equivalent Circuit

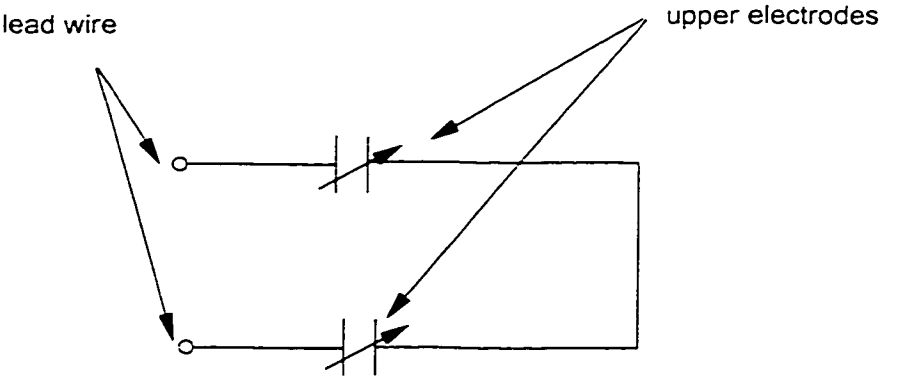

Figure 4.1: Configuration and equivalent circuit of 'humicape' humidity sensor [7].

The limitation of upper and lower electrode configuration poses a difficulty in post-processing. Due to this configuration, the upper electrode must be deposited after the deposition of sensing material, which will arise the problem of pattering of top electrode. The patterning process may alter the sensing properties of the active material. There is another concern of this design, which is the access of water vapor to the humidity sensitive material since sensing film is covered by top electrode. Thus a new electrode configuration which uses CMOS MITEL 1.5μm technology is developed as shown in Figure 4.2. CMOS MITEL 1.5μm technology is provided for custom design to the universities involved in MEMS research by the CMC, which established that this CMOS technology is most appropriate to be used for MEMS. The minimum feature size of this technology is 1.5 μm. Thus, the minimum distance between two electrodes and the width of electrodes cannot be less than 1.5 μm. The electrodes consist of three layers: Poly 2, Metal 1 and Metal 2. Poly 1 is also available, but is not used for electrode configuration in the design. The constraints imposed by the fabrication technique yield the overall thickness of each electrode as 1.875μm. The advantage of this design is related to the position of the electrodes in the same plane, which provide high sensitivity, and low cost through simple post processing. The parallel electrodes also enable an easy access of water vapor absorption into humidity sensitive material due to the humidity sensing material exposure to the surrounding environment.

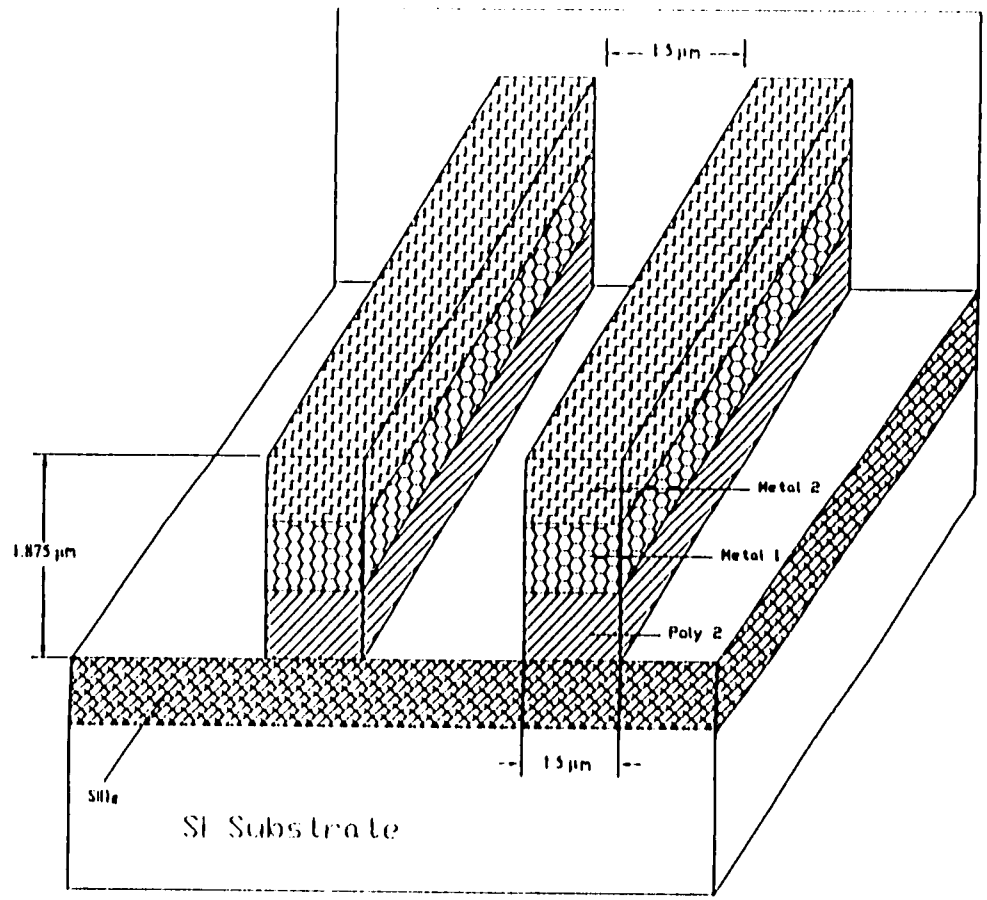

The thickness of the layers:

------ Poly2 (Poly deposition) 2500±250 Å
------ Metal1 (Metallization 1) 8000±800 Å of Al, 250 Å of SiCr
------ Metal2 (Metallization 2) 8000±800 Å

Figure 4.2: Configuration and structure of two electrodes.

4.4.2 Electrode Shape

The miniature sensors yield low value capacitance output which produce a serious challenge in the design of measurement circuitry. The maximization of the transducer capacitance is essential in the electrode shape design. If ignoring nonlinearities such as the fields at the edge of the parallel capacitor electrodes, the capacitance of transducer with basic structure can be shown in Figure 4.3. The capacitance of the planar capacitor can be expressed as equation (4.1).

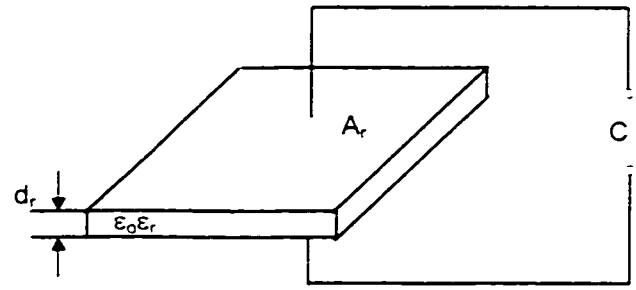

Figure 4.3: Capacitance between the two electrodes of a basic structure.

$$C = \varepsilon_0 \times \varepsilon_r \times \frac{A_r}{d_r} \tag{4.1}$$

where ε_0 is absolute dielectric constant; ε_r is relative dielectric constant; A_r is the relative area between the two electrodes; d_r is the distance between the two electrodes; C is the capacitance of transducer. In the following analysis, the selected humidity sensitive material is assumed to be fully filled between the two electrodes which is ideal configuration to ease the post-processing. In reality, the sensing material polymer might remain on the top or partially fill the gap. Therefore, post-processing plays a crucial role in securing most uniform

distribution of the polymer on the structure of electrodes. The relative dielectric constant ε_r is changed with the change in relative humidity level of the surrounding environment. For the same sensing material, since the distance between electrodes is fixed to 1.5 μm, capacitance of transducer is determined by the relative area between two electrodes. Three different designs of electrodes are realized in an attempt to maximize the relative area between two electrodes and further the capacitance. In the following study, analysis of geometric shapes that can be manufactured in CMOS Mitel15 technologies are analyzed and the best of considered shape is further implemented in the design.

There are many ways to maximize relative area between the electrodes of the sensor. The followings are some feasible design methods. For easy calculation, the size of the humidity sensor is assumed to be $1000\,\mu m \times 1500\,\mu m$, and the distance between two electrodes is assumed to be $1.5\,\mu m$. The basic structure as shown in Figure 4.3 consists of upper and lower electrodes with 1.5 μm gap between them. Therefore, the basic capacitance C_0 is as followed:

$$C_0 = \frac{\varepsilon_0 \varepsilon_r 1000 \times 1500}{1.5} (\mu F) \qquad (4.2)$$

Where ε_0 is basic dielectric constant; ε_r is relative dielectric constant. C_0 is used as the reference capacitance for other electrode shapes.

- **Shape 1**

The structure of shape 1 as shown in Figure 4.4, consists of two comb-like 1.5 μm-wide electrodes with 1.5 μm gap (the minimum feature size of MITEL15

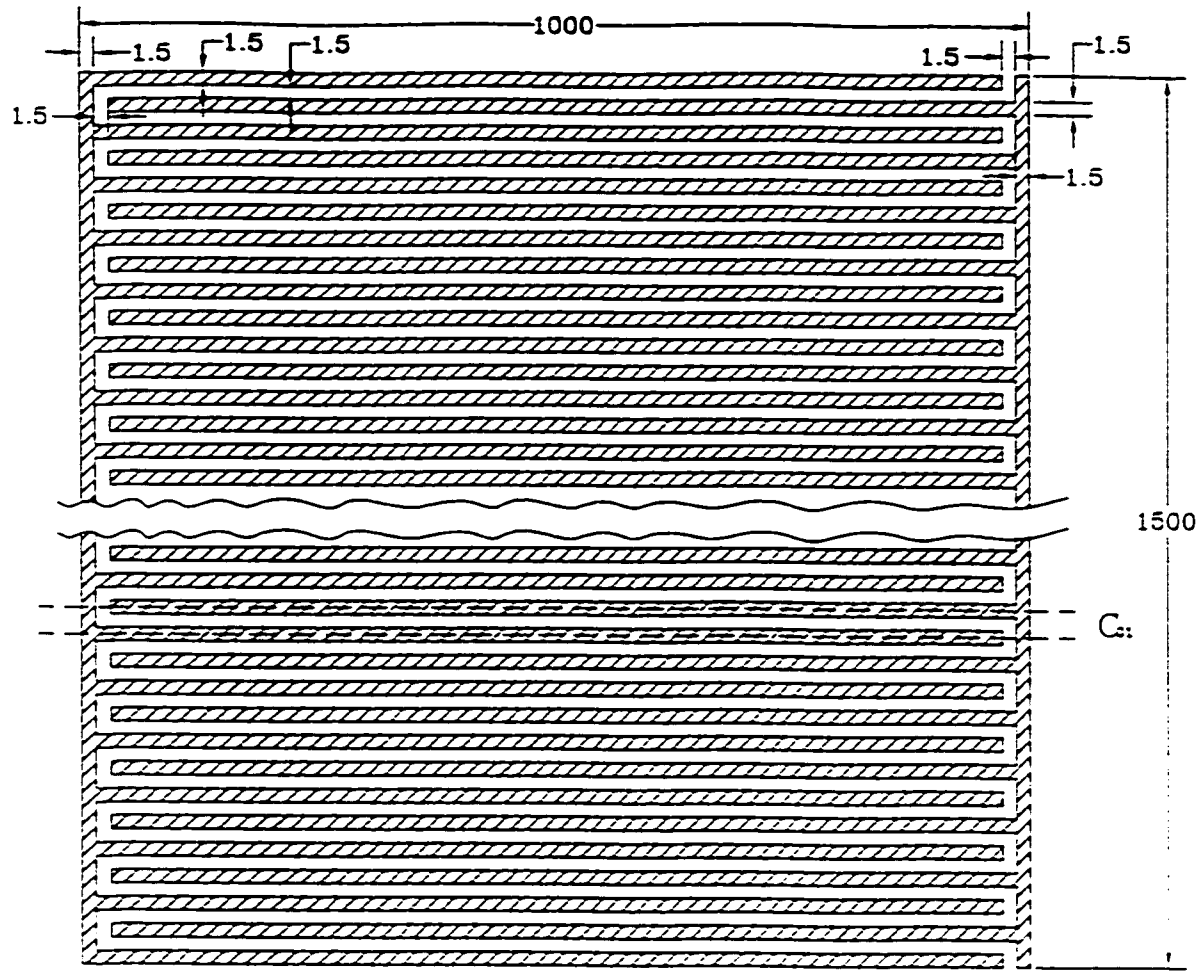

detail for C_{01}

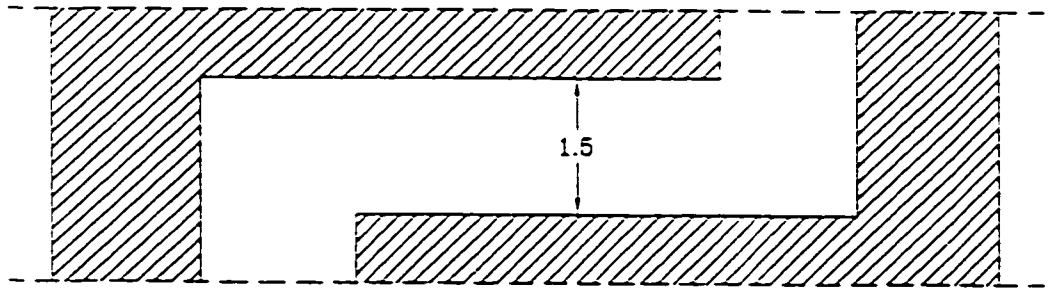

electrodes

unit: μm

gaps between the electrodes

Figure 4.4: The structure of shape 1 (top view).
For clarity the drawing is not scaled.

technology), which could maximally increase the effective area between two electrodes. The overall size is restricted to 1500 μm×1000 μm due to the constraint imposed by the chip size. Assume the capacitance of one unit is C_{01} which is aligned perpendicular to the long side of the rectangle area as shown in the Figure, the value of C_{01} is derived in equation (4.3).

$$C_{01} = \frac{\varepsilon_0 \varepsilon_r (1000-6) \times 1.875}{1.5} + \frac{\varepsilon_0 \varepsilon_r 1.5 \times 1.875}{1.5} \approx 1.24 \times 10^{-3} C_0 \qquad (4.3)$$

The structure of shape 1 consists of 499 units (C_{01}). Therefore the capacitance of shape 1, C_1 is equal to 499 times of unit capacitance C_{01} which is about 62% of the reference capacitance C_0, as shown in equation (4.4).

$$C_1 = 0.62 C_o \qquad (4.4)$$

In the case that the electrodes are oriented perpendicular to the smaller side of rectangle area, the overall capacitance will be smaller by 0.05% only.

- **Shape 2**

Shape 1 leads to the possibility of adding extra surface (bars) between two electrodes. Therefore, the second considered structure (as shown in Figure 4.5), which is comb-like electrodes with bar-shape prominence, is proposed. "Bar1" is defined as the bar-shape prominence on one electrode, while "bar2" is defined as the bar-shape prominence on the other electrode. Figure 4.5 shows that there is no relative area between "bar1" and "bar2", since "bar1" and "bar2" are not interdigited. Due to the limitation of overall size, the number of parts (consist of two electrodes, as shown in Figure 4.5) must be reduced in order to

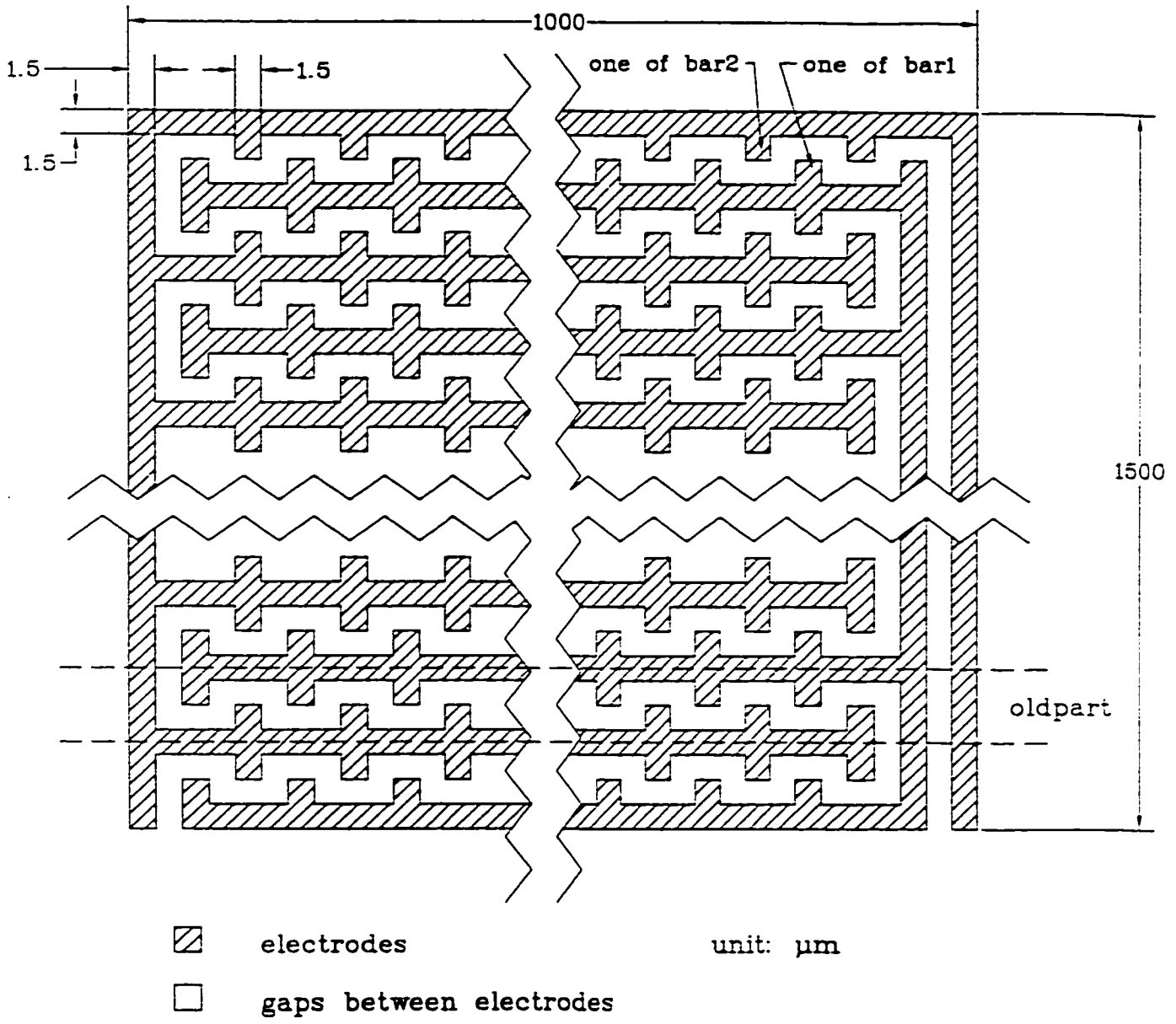

Figure 4.5: The structure of shape 2 (top view).
The prominent part on the electrodes is called bar. Bar1 and bar2 are on the different electrodes.

increase the length of "bar1" and "bar2", further to increase the relative area between "bar1" and "bar2". One part of new structure which increases the length of "bar1" and "bar2" is illustrated in Figure 4.6. Because the relative area between "bar1" and "bar2" yields extra capacitance, one part of the new structure yields larger capacitance than the old part as shown in Figure 4.5. However, the new structure also results less numbers of new parts in the same area compared to the number of the parts in old structure. The calculation shows that the maximum capacitance can only be achieved in new structure when approaches one part, which is exactly the same structure as shape 1. Therefore, the resultant value of capacitance for shape 2 would not exceed the capacitance accomplished by shape 1.

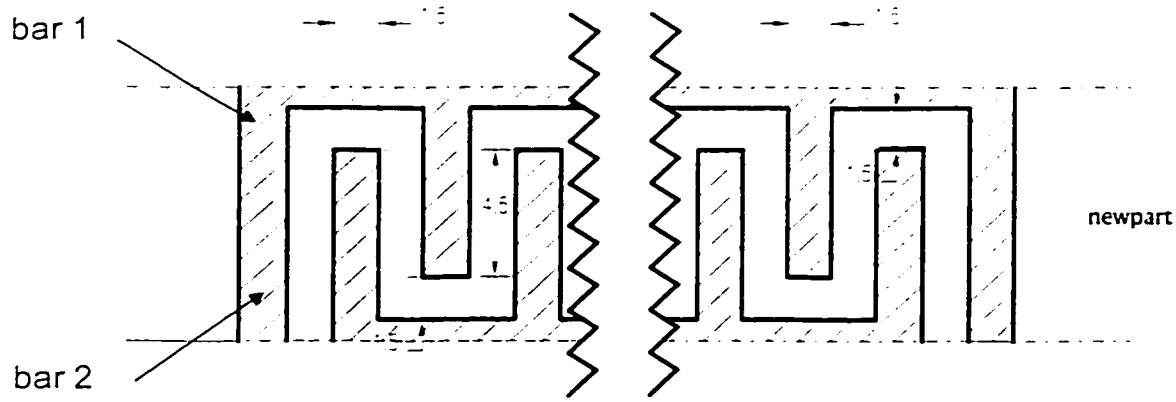

Figure 4.6: The structure of new part.

- **Shape 3**

Other electrode shape such as the structure with zigzag-shape electrode (as shown in Figure 4.7) is also considered. The 1.5 μm wide zigzag-shape electrodes are arranged with 1.5 μm spacing. The structure is designed to achieve maximum capacitance in 1000 μm×1500 μm, which is the same area as considered in the previous two designs. One branch of the electrode is illustrated in Figure 4.8. The capacitance of this structure can be derived as equation (4.5).

$$C = \frac{\varepsilon_0 \varepsilon_r A_r}{d_r} = \frac{\varepsilon_0 \varepsilon_r \dfrac{1500}{4.5} \times \dfrac{1000-6}{1.5} \times \dfrac{\chi + \dfrac{1.5}{\sin\alpha}}{\cos\alpha} \times 1.875}{\dfrac{4.5}{\sin\alpha} + \chi \quad (\chi + \dfrac{1.5}{\sin\alpha})\mathrm{tg}\alpha \quad 1.5}$$

$$= \text{constant} \times \frac{1}{4.5 + \chi \sin\alpha} \qquad (4.5)$$

when $\sin\alpha$ is equal to -1, equation (3.5) achieves its maximum value, which yields derives α as the following value: $\alpha = 270°$; $2\alpha = 540° = 180° + 2\pi$. When $2\alpha = 180°$, the zigzag electrodes of Figure 4.7 become straight lines, which points again to shape 1. So the maximum value of shape 3 has the same capacitance value as shape 1. Therefore, the zigzag electrode shape could not yield the maximum capacitance output. Besides, the effect due to the sharp edges may reduce the performances of the structure of capacitor.

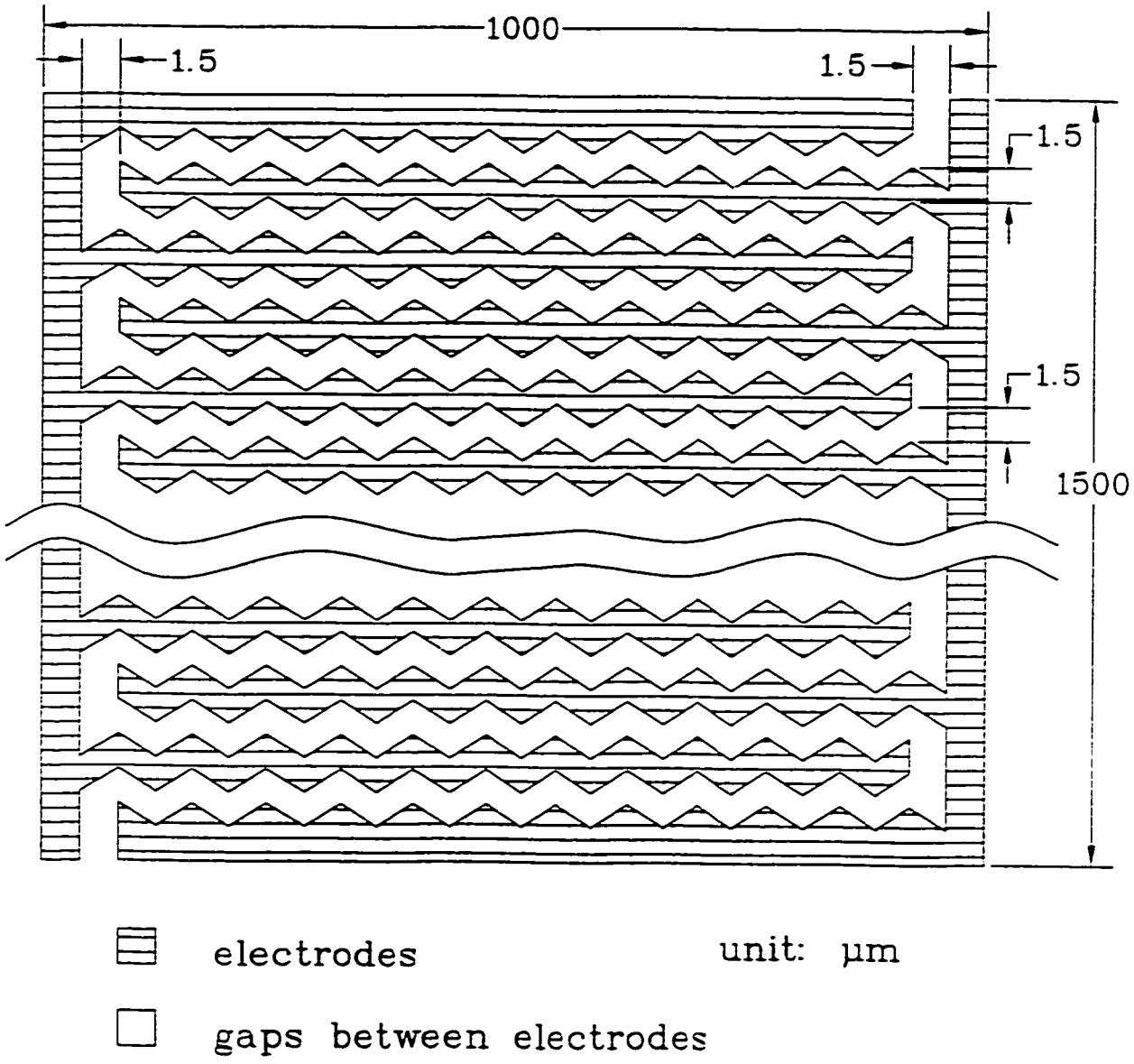

Figure 4.7: The structure of shape 3 (top view).

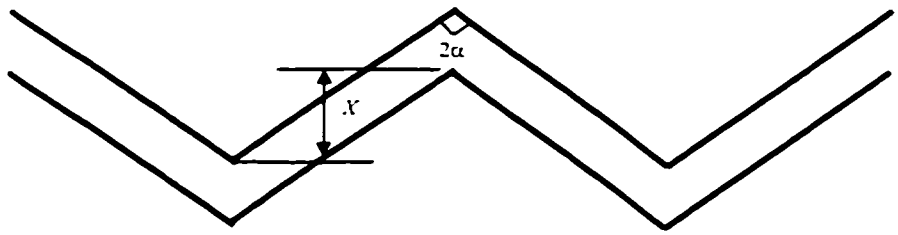

Figure 4.8: The branch of one electrode.

Through the comparison of the above three shapes, shape 1 (shown in Figure 4.4) is the optimal design configuration which could yield maximum capacitance in limited area. The electrodes are comb-like shapes which would ease the processing and post-processing.

4.4.3 Analytical Model Development

Humidity measurement using capacitive sensors is usually based on the variation in the relative dielectric permittivity of an active material with moisture absorption properties. In order to accurately predict the output of capacitive transducers, it is very important to develop a reliable analytical model of relative dielectric coefficient in transducer simulation. In this section, a steady and a transient analytical model of humidity transducer with thin film are developed. The performance characteristics of capacitive humidity transducer, which can be

categorized as steady characteristics and transient characteristics are investigated.

4.4.3.1 Sensitive material selection

In order to effectively evaluate response of capacitive humidity transducer, a humidity sensing material must satisfy the following desired characteristics. The sensing material must change its dielectric characteristics when absorbing water. The sensing material must exhibit low hysteresis, good stability in time and low sensitivity to variation in temperature or to gases or other volatile chemicals in surrounding air. Polyimide seems to satisfy most of these desired characteristics due its hydrophobic nature and rigid structure. Thus polyimide was used to prepare a capacitive-type humidity sensor. In this study, the capacitive sensor, based on the dielectric properties of polyimide is investigated.

The principle of measurement is based on the change in properties of a heterogeneous dielectric. Such a material is defined as a composite of two or more immiscible dielectrics in the same system. The system of concern here is water in polyimide. A large range of theoretical and empirical formulas have been extensively reviewed and compared with experiments [52,53]. No mixture formulas have been found which could represent all or most of the experimental data. Theoretical formulas are often applicable to a specific geometry of one dielectric or another, while empirical formulas generally apply to larger, but still limited, class of data.

When the water vapor is absorbed by the active material, the dielectric constant of the original dried polymer changes. Looyenga [4] proposed a semi-empirical relationship to determine the equivalent dielectric constant of the combined active material (polymer and water) which is illustrated in equation (4.6).

$$\varepsilon_r = (\nu(\varepsilon_{2r}^{1/3} - \varepsilon_{1r}^{1/3}) + \varepsilon_{1r}^{1/3})^3 \qquad (4.6)$$

where $\varepsilon_{1r} = 2.93$ and $\varepsilon_{2r} = 80.0$ are the relative dielectric constants of the polymer and water, respectively. ν represents the fractional volume of water absorbed.

However, the relationship given in equation (4.6) requires the function about the fractional volume of absorbed water. Although Fick's model was proposed in Chapter 2 as the absorption analytical model, extensive work is needed to estimate the above coefficient. Thus, the semi-empirical relationship proposed by Dubinin [54] that describes the absorption of water into the bulk of a material was considered. Equation (4.7) describes the function of fractional volume of absorbed water.

$$\nu = \nu_m^0 \exp[-(RT \ln x / E)^n - \alpha(T - T_0)] \qquad (4.7)$$

where ν_m^0 is the maximum fractional volume of absorption at the temperature T_0; R is universal gas constant; T is absolute temperature; α is thermal coefficient of limiting absorption; E is free energy of absorption; n is an empirical factor determined through experiment. This formula is semi-empirical in nature, requiring three empirical fitting parameters (α, E and n), which are derived from a specific physical model and includes standard thermodynamic functions. A

matching linearized graph indicating the absorbed volume of water versus the relative humidity according to Dubinin's equation is shown in Figure 4.9.

The Dubinin's equation can be simplified to yield an approximate linear relationship between ν and relative humidity RH, assuming negligible thermal expansion of the dielectric:

$$\nu = 0.043RH \tag{4.8}$$

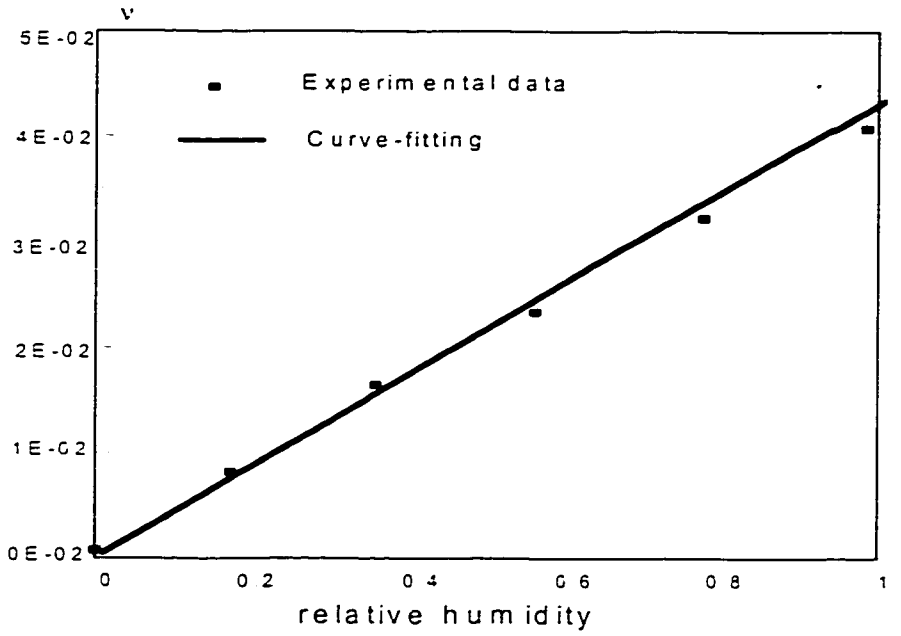

Figure 4.9: Volume of absorbed water vs. relative humidity according to Dubinin's model.

4.4.3.2 Steady response of transducer

The capacitance C_s of the capacitive transducer of the proposed shape 1 can be computed using the relative dielectric constant derived from Looyenga's equation, substituting for ν from equation (4.8) will further yield:

$$C_s = \frac{\varepsilon_0 \varepsilon_r A_r}{d_r} = \frac{\varepsilon_0 \left[v\left(\varepsilon_{2r}^{1/3} - \varepsilon_{1r}^{1/3}\right) + \varepsilon_{1r}^{1/3} \right]^3 A_r}{d_r} \qquad (4.9)$$

$$= (0.2187RH + 2.5274)^3 \, pF$$

where ε_0 = 8.854187817*10^{-12} is basic dielectric constant; ε_{1r} and ε_{2r} are the relative dielectric constants of the polymer and water, respectively; v is the fractional volume of water absorbed; A_r is relative area between electrodes; d_r is distance between two electrodes. Figure 4.10 illustrates the capacitance of transducer as a function of relative humidity. It is concluded from Figure 4.10 that capacitance of transducer increases with the increase of relative humidity. The figure also shows the relationship between capacitance of transducer and relative humidity exhibits good linearity. The capacitance ranges from about 16pF to 21 pF.

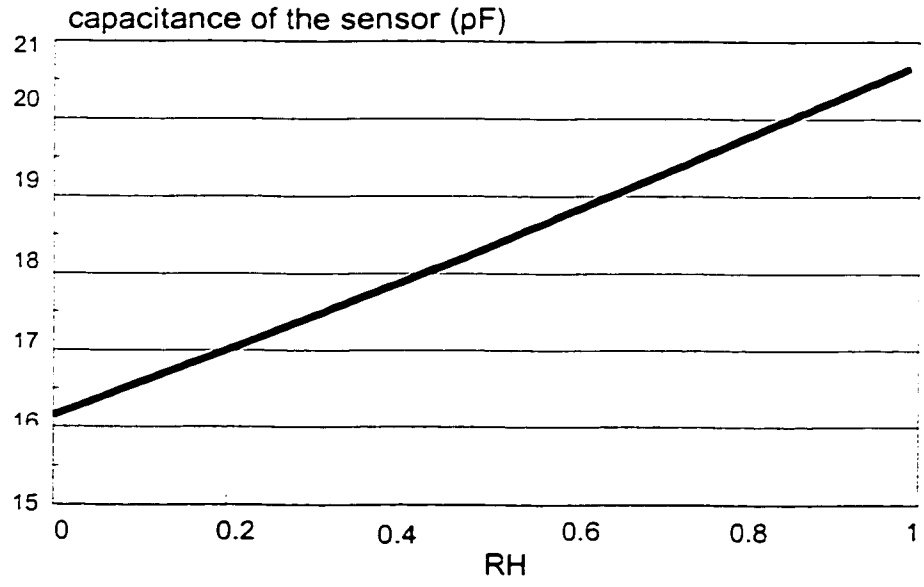

Figure 4.10: The capacitance C_S of the humidity polyimide sensor as a function of relative humidity.

4.4.3.3 Sensitivity of transducer

Sensitivity of transducer is given as the ratio of variation of output capacitance of the transducer and variation of input relative humidity, as shown in equation (4.10).

$$\frac{\Delta(\text{output})}{\Delta(\text{input})} = \frac{dC_S}{dRH} = \frac{d(0.2187RH + 2.5274)^3}{dRH} = 0.6561 * (0.2187RH + 2.5274)^2 \quad (4.10)$$

where C_S is output capacitance, RH is relative humidity level. The sensitivity curve for the transducer is shown in Figure 4.11. Sensitivity of the transducer establishes the slope of the calibration curve which is shown in Figure 4.10. It is concluded that the sensitivity of the transducer is dependent on the relative humidity. The sensitivity of the capacitive transducer ranges from 4.2 to 4.9(pF/RH). The sensitivity of the transducer remains at 4.4±0.1(pF/RH), when the relative humidity is in 20%-60% band. In this range, it is concluded that the capacitive transducer exhibits good sensitivity and linearity.

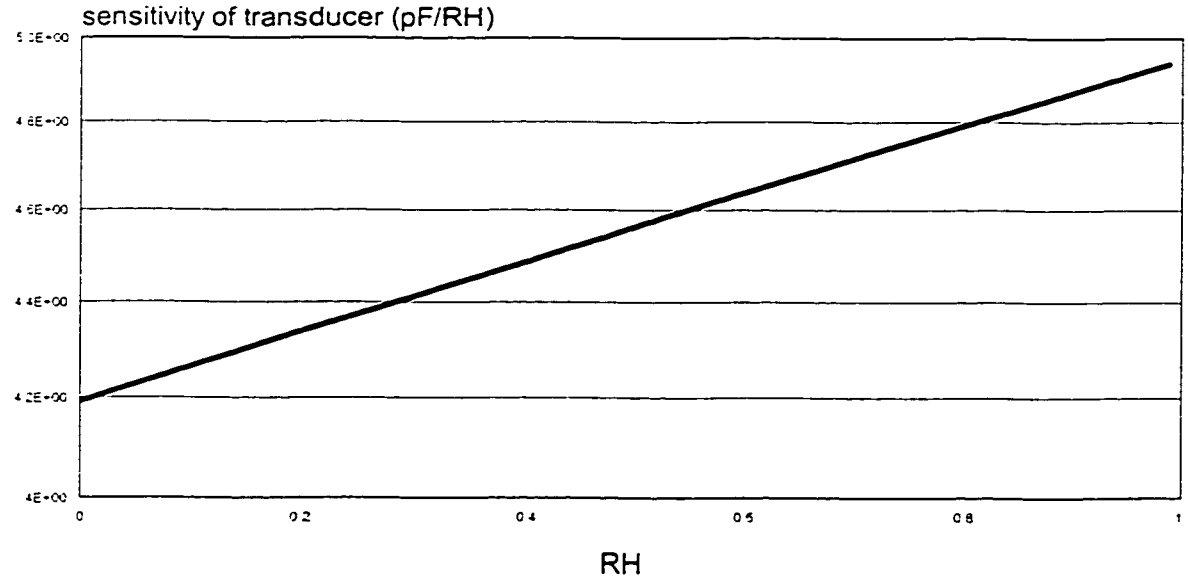

Figure 4.11: The sensitivity of the capacitive polyimide transducer.

4.4.3.4 Diffusion model of sensitive material

The empirical models proposed by Dubinin and Looyenga to estimate the variation of capacitance due to the variation in the input RH will not work in assessing the dynamic response of the transducers. Thus, the available Fick's time-dependent model is again used to evaluate the absorption coefficient of polyimide from the reported time response [4].

In this study, polyimide is used as the sensitive material in capacitive sensor. The response time of polyimide is reported to be 6 seconds, when The thickness is 5μm [4]. The function of the ratio of transient relative humidity and steady state of relative humidity RA(t) can be obtained from equation (3.22), for a specific time (as shown in equation 4.11).

$$RA(d,t) = \frac{U(d,t)}{U_s} = \frac{U_s \operatorname{erfc}\left(\frac{d}{2\sqrt{Dt}}\right)}{U_s} = \operatorname{erfc}\left(\frac{d}{2\sqrt{Dt}}\right) \qquad (4.11)$$

where d is the current depth at which the amount of water vapour into the humidity sensitive material is assessed; t is time; U_S is the surface moisture content; D is diffusion coefficient for polyimide.

Similar to the derivation of Figure 3.16, the relationship between the response time and diffusion coefficient at film thickness 5μm can be obtained, as shown in Figure 4.12. From Figure 4.12, It is concluded that the diffusion coefficient is directly related to response time. The large response time is, the smaller is diffusion coefficient. Since the response time reported in literature for

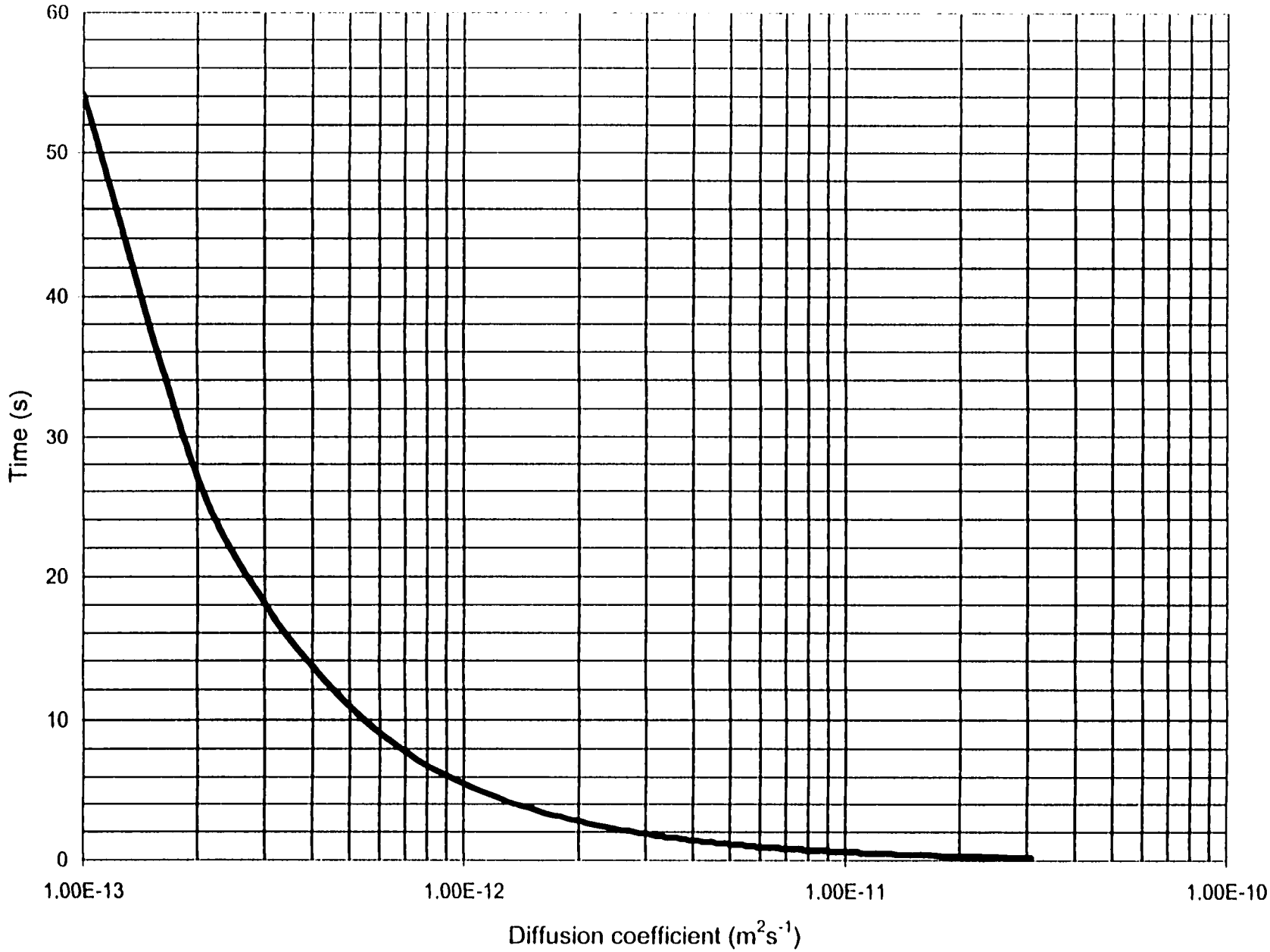

Figure 4.12: The response time vs.diffusion coefficient at film thickness 5μm

polyimide is around 6 seconds at film thickness 5μm, it can be derived from Figure 4.12 that the diffusion coefficient of polyimide is about 9×10^{-13} m^2 s^{-1}.

4.4.3.5 Transient response of transducer

Transient response is an important element to evaluate the transducer's performance. The response of the transducer to a step input is evaluated. For capacitive humidity sensor, the transient response reveals that the relationship between the variation of output capacitance with step input is dependent on the relative humidity level of the input. The transient response is strongly related on water absorption properties of the material.

For the capacitive transducer, the steady response (the relationship between the relative humidity and the output resistance) is shown in equation (3.9). The transient response of the transducer can be derived by multiplying the steady response C_S with the ratio of the transient relative humidity and steady state of relative humidity RA(t), which is shown in Figure 4.13. For different step input (relative humidity level), all the curves exhibit the same trend, which is the capacitance of transducer increasing with time increasing. With humidity level increasing, the capacitance is increasing, which displays the same characteristics as steady response. The results also show that it takes longer to detect higher humidity levels. When time is less than around 40 seconds, the capacitance changes more dramatic than the time after 40 seconds, which attributes to the short response time of the transducer with polyimide as sensitive material. In addition, after 40 seconds the active material becomes almost

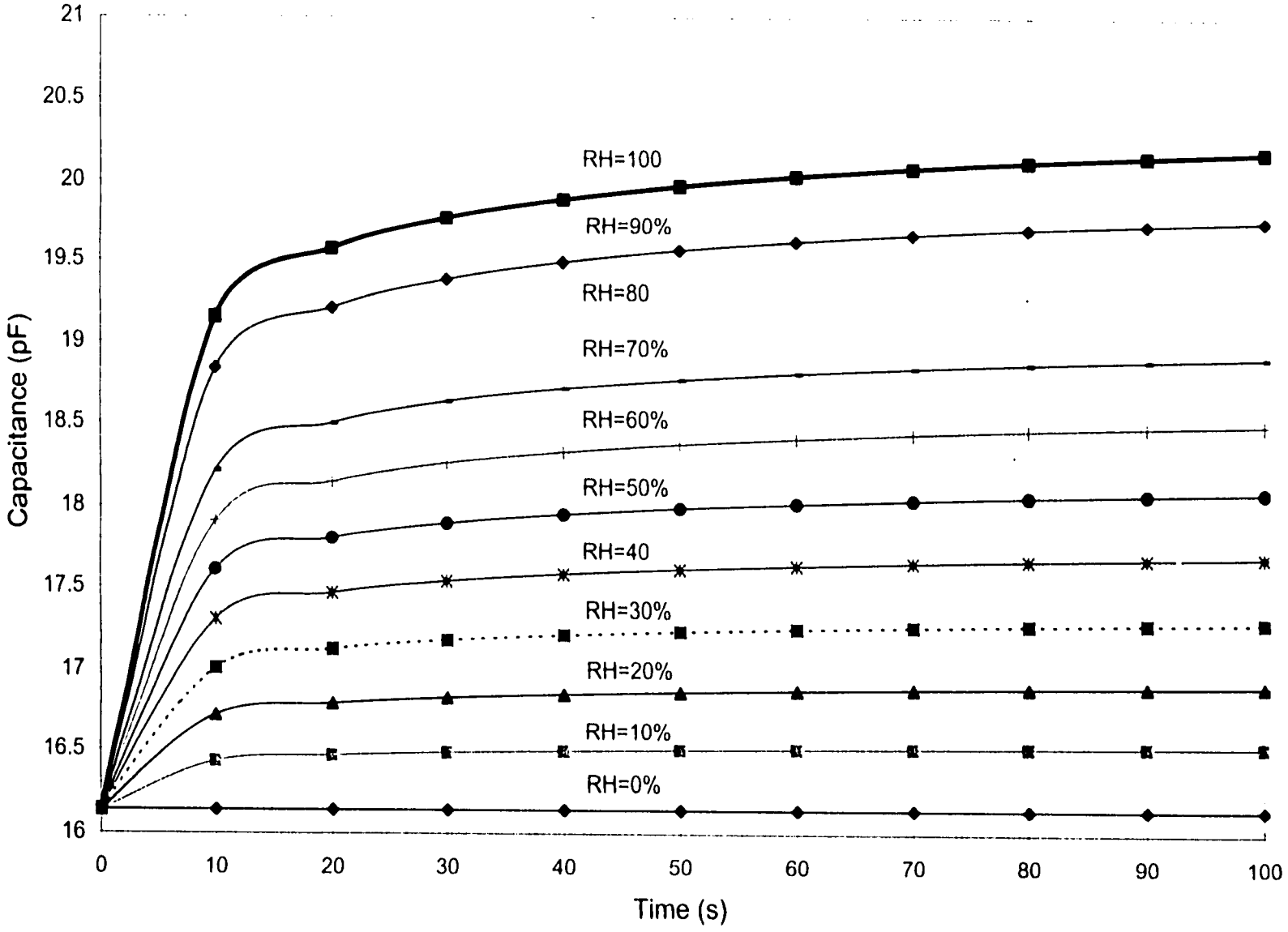

Figure 4.13: The transient reponse of the capacitive sensor at specific RH.

saturated with water molecules. It is also shown that the limit value which the output capacitance of transducer approaches in time is the steady capacitance of the transducer.

4.5 POST-PROCESSING

Post-processing is an important step in fabrication of the micro-sensors. The micro-sensors must be deposited with the active sensitive layers, after received from Si foundry. Out of the diversity of humidity sensitive materials available on the market, polymer is the most attractive material for humidity capacitive sensing. This material is convenient for micro-electronics applications and it exhibits humidity sensitivity. It is supplied as a highly viscous solution ideally suited for either spin or roller coating application.

Solvent evaporation techniques are common simple post-processing employed with polymeric materials, and include casting, painting, dip coating, and spin coating. This technique can be used in conjunction with a mask to define the chemically selective area of the device. Dilute solutions of the coating are prepared in volatile solvents such as methanol, chloroform, acetone, or toluene and coated onto the device surface.

Langmuir-Blodgett (LB) film technology is another simple post-processing method which allows the deposition of molecular structures onto flat substrates. It has been widely used for producing polar thin films on a variety of substrates [35]. Materials capable of forming monolayer films are characterized by having

distinct hydrophilic and hydrophobic regions. Typically, a small quantity of the material is dissolved in a nonpolar solvent and allowed to spread across a water surface. A moving barrier can then be used to compress the film until a close-packed ordering of the molecules is obtained. Transfer of the film to a substrate is achieved by passing the solvent perpendicularly through the substrate. The barrier is normally moved simultaneously during transfer to ensure constant film pressure. The efficiency of the process is then measured by the transfer ratio, defined as the monolayer area removed from the water surface divided by the area of the coated substrate. The layers may collapse or undergo reorientation as entrained water evaporates from the transferred film. Mixed monolayers can also be employed, in which transfer of the desired material is aided by the addition of a second material which promotes film formation and deposition.

Among all these post-processings, spin-coating offers the greatest prospects for the low-cost, controlled and reproducible processing of humidity sensitive films. The thickness of the film is determined by the spin speed and the viscosity of the solution. Baking step is usually necessary after spin coating. Other forms of baking such as convection may be used for equivalent effect where necessary. The baking step in polyimide deposition produces imidization process of original polyamic acid. It is usually done at elevated temperatures in excess of 325 °C. Slow ramping and cooling in air sometimes is recommended to minimize substrate deformation.

4.6 MEASUREMENT CIRCUITRY

For the measurement of the capacitive sensors, a basic measurement circuitry, comprising these opamps and a number of passive elements, is as shown in Figure 4.14. The sensor capacitance can be conveniently measured by comparing the charge time of the sensor capacitor C_s and the reference capacitor C_r. The circuit design can be easily realized on the sensor chip using the cadence software design library for opamps in the Mitel15 design kit. This circuitry can provide a reasonably accurate measure of capacitance as low as 1.5 fF. The overall accuracy of the circuit capacitance, however, relies on the accuracy of the reference capacitor.

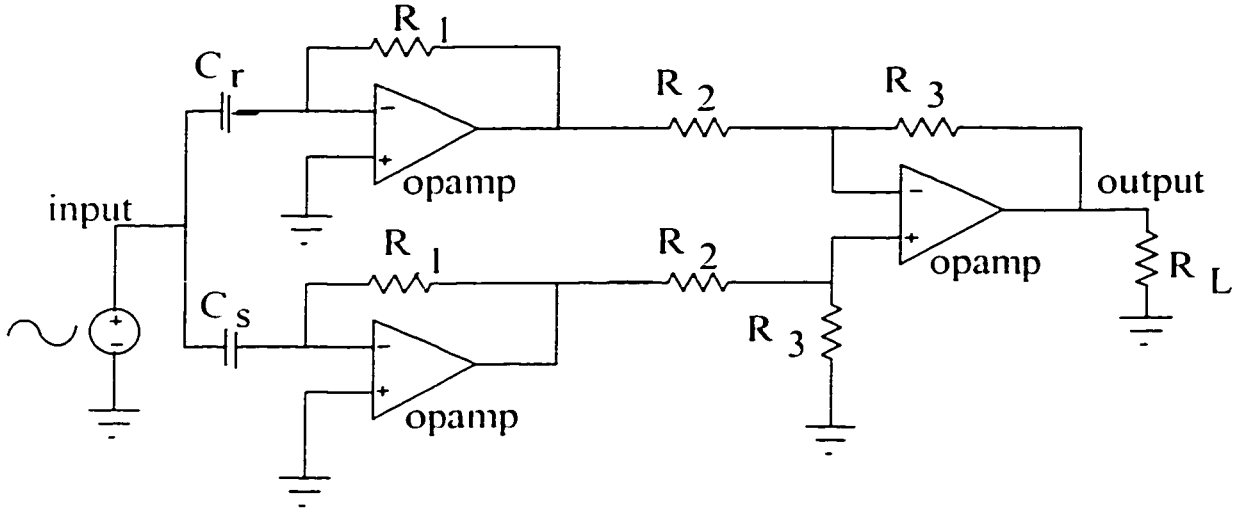

Figure 4.14: The conditioning circuitry of the humidity sensor. C_s represents the capacitance of the sensor, C_r represents the reference capacitance.

Another solution [50] is to include the sensor capacitance as the input branch of a switched capacitor amplifier as illustrated in Figure 4.15. While switch ϕ_1 is on and ϕ_2 is off, the capacitor C_s is charged by the reference voltage V_{ref}. While switch ϕ_1 is off and ϕ_2 is on, the capacitor C_s is discharged through C_1. This is a very convenient circuitry since it directly produces a voltage output. However, it gives a measure of the capacitance ratio against a reference capacitor and therefore is also limited in accuracy. In addition, the physical accomplishment of fast switches is a challenging task in Mitel15 technology.

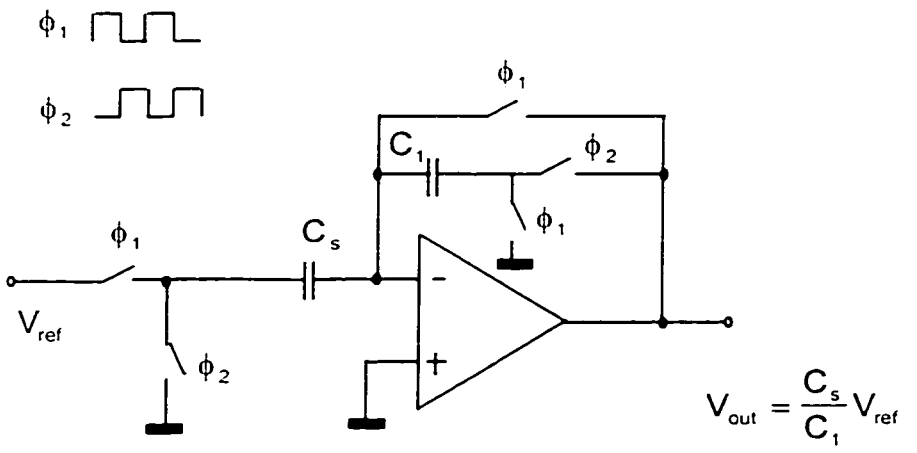

Figure 4.15: Capacitance measurement circuitry with sensitive capacitor C_s in the input branch.

Instead of taking the amplifier output voltage as output, the measurements of charging or discharging currents can provide an effective measure of the sensor capacitance, while eliminating the dependence on the availability of a reference capacitance. This idea is illustrated in Figure 4.16,

which illustrates the charging (discharging) current flows through the VSS (VDD) supply line of the amplifier output stage. It seems straightforward to implement this solution by using an amplifier with zero quiescent current on the output stage. However, the frequency compensation of such amplifier is very difficult, which may lead to an oscillating behavior. This effect cannot be tolerated since it introduces additional terms in the supply current and generates a non-negligible error.

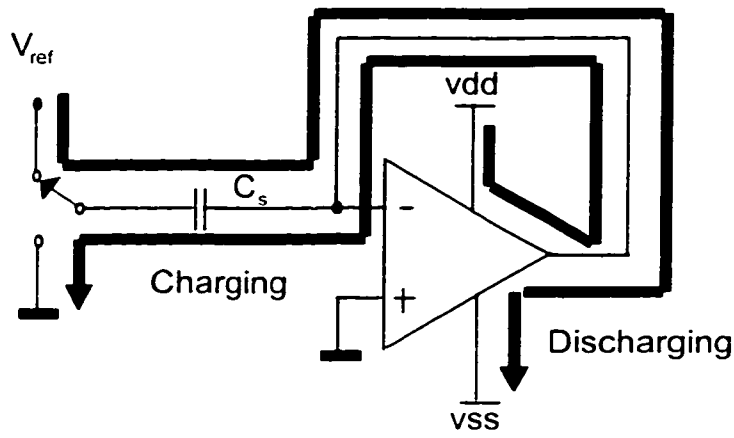

Figure 4.16: Operation principle of the absolute value capacitance meter [58].

An improved design of the previous circuit is shown in Figure 4.17, where a comparator followed by a zero quiescent current buffer is employed in place of an amplifier. When the input switch is commuted to V_{ref}, the voltage at node A rises from ground to V_{ref} (assuming no parasitic capacitance to ground on this node). The comparator output, node B, then saturates at VSS and drives M_2 into

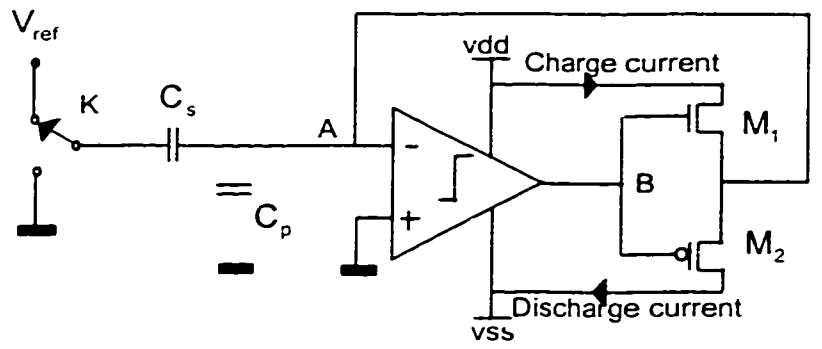

Figure 4.17: Schematic diagram of the circuit [57].

conduction. The sensor capacitor, C_s, thus charges until the voltage at node A approaches zero. This will make the comparator go out of saturation with its output voltage increasing from VSS until the transistor M_2 is driven into cut-off. At this point, the voltage at node A is close to zero and both transistors in the output buffer remain cut-off until the next discharge phase. If the comparator is sufficiently fast and has high gain, the complete charge of the capacitance of sensor is completed in a non-oscillatory manner. By driving the input switch at a frequency F_s, the supply current of M_1 or M_2 is related to C_S through the expression

$$I_S = F_S V_{ref} C_S \tag{4.13}$$

where both the externally applied reference voltage V_{ref}, and clock frequency, F_S, are precisely known. The amplifier offset voltage, the parasitic capacitances to ground, and charge injection from the input switches do not affect the supply current I_S. The above approximate analysis, however, assumes a very high gain and fast response of the comparator. This circuitry provides a new approach for on-chip evaluation of floating, and allows for precise circuitry measurement of the

absolute value of the capacitance. This circuitry, however, requires additional design efforts to achieve expected results in the Mitel 1.5μm technology.

4.7 SUMMARY (CONTRIBUTIONS INDICATED AS UNDERLINE)

In this chapter, the design of a fully integrated surface micromachined humidity capacitive sensor is proposed and the fabrication and post processing is described.

- Capacitive sensing presents certain advantages versus the resistive measurement. Low power consumption associated with improved thermal characteristics are the most important advantages of capacitive measurement.
- Two principal aspects are followed in the design of capactitive humidity transducer. One is selection and/or design a material, the other is optimization of the sensor configuration and measurement method.
- Humidity measurement of capacitive sensors is usually based on the modification of the relative dielectric permititivity of the active material.
- Ceramics and polymers are widely used in capacitive sensor design due to the larger change of their characteristics with water absorption.
- A new electrode configuration which can be manufactured using CMOS MITEL 1.5μm technology is proposed. The electrodes consist of three layers: Poly 2, Metal 1 and Metal 2. The advantage of this structure is related to the position of the electrodes in the same plane, which provide high sensitivity, and low cost through simple post-processing. The parallel

electrodes also enable an easy access of water vapor absorption into humidity sensitive material due to the humidity sensing material exposure to the surrounding environment.

- Three different electrode shapes are proposed and their characteristics are discussed in view of output capacitance and issued related to fabrication. The comb-like shape could yield maximum capacitance output in limited area of the three proposed. This shape would ease the processing and post-processing.
- An analytical model of the humidity transducer with thin film is developed to study its steady-state and transient response characteristics.
- The semi-empirical relationship (Looyenga equation) provides the equivalent dielectric constant of the combined active material.
- The static response and the sensitivity of the transducer illustrate that the proposed capacitive transducer exhibits good sensitivity and linearity.
- Fick's equation is used to derive transient model of humidity sensitive material, which is the relationship between the response time and diffusion coefficient.
- Solvent evaporation techniques and Langmuir-Blodgett (LB) film technology are discussed and compared.
- The measurement circuitry with no reference capacitor is investigated.

CHAPTER 5

TEST AND VALIDATION

5.1 INTRODUCTION

Developments in micro sensors involve design, fabrication, post-processing and extensive experimental assessments. The experimental assessments form an integral part of the development process, which yield most important informations related to performance characteristics of the sensors. These include static sensitivity, linearity, hysteresis, range, resolution, dynamic range, etc. The development process may necessitate redesign and variations in fabrication and post-processing techniques, depending upon the experimental assessments. The experimental evaluations of a prototype sensor are thus extremely vital for enhancement of its performance.

In this dissertation, laboratory experiments are performed on a prototype resistive micromachined humidity sensor. Such experiments are considered more vital for humidity sensor, since their performance relies heavily on the properties of the humidity sensitive materials. Although thin film deposition of a humidity sensitive material on the surface of sensor electrodes is relatively simple and a low cost process, the sensor performance may depend upon the film thickness and the deposition process. The measured data may thus be used to assess the sensor characteristics as related to the material properties and deposition process. The measured data can be further used to examine the validity of the analytical model developed in Chapter 3.

The low cost deposition is associated with a deposition process that involves simple equipment and well established techniques. Spin coating represents an excellent candidate for such low cost deposition processes. It requires the deposition material to be in a fluid state exhibiting a constant viscosity. Such materials are either nanometer particulates dispersed in a fluid mass or viscous solutions. Polymers exhibit tremendous advantages in humidity sensing application against other materials, due to the low curing point and the low cost of deposition.

Polyaniline is a polymer which is explored in this dissertation as a resistive humidity sensitive material. Polyaniline exhibits humidity sensitive potential due to its good water absorption properties [4]. Dispersions of polyaniline, which are heterogeneous on a microscopic scale, are used in the experiment in order to simplify the deposition process. Nanometer scale particulate dispersions behave as solutions when the particles are not clustered [47]. The role of the solvent in dispersion is to reduce the high surface tension of the materials, which further reduce the viscosity of the materials. In this study, a conductive polyaniline that exhibits resistance variations with change in relative humidity is conveniently used to develop a prototype sensor. The advantages of this dispersion include that the thickness of deposited film can be controlled through spin speed and viscosity, the low cost of the deposition method, simple curing process and relatively good adhesion of the film to the electrodes. Dispersion of 10nm polyaniline particles in volatile liquid mass was used in experiments. Such dispersion is commercially available from ORMECON GmbH - Germany under

the commercial name of CORRPASSIV primer 900226/19. The destination of this material is not related to humidity sensing such that the capability of polyaniline to be used as humidity active material must be assessed.

The experiments are performed to derive an input-output relationship and the response time. The response time data is further utilized to derive certain properties of polyaniline. The diffusion coefficient of the film is evaluated by matching the response time with that derived from Fick's equation as a function of the deposited film thickness.

5.2 EXPERIMENTAL WORK

The first set of tests conceived to evaluate the humidity sensitive properties of polymer dispersion were carried out on samples of 22mm×22mm flat glass substrates. During the experiments, dispersions of polymer were spin-coated at various speeds. As a consequence, different values of thickness of the deposited films were attained. In order to examine the influence of material properties on the performance, two different compositions of dispersion were considered for deposition using spin coating. These include: (i) polyanilne compound, as obtained from the supplier; and (ii) a 3:2 proportion of the polyaniline compound in 1-methoxy-2-propanol.98% ($CH_3CH(OH)CH_2OCH_3$) derived from experimental experience.

The initial depositions and measurements were performed to examine the feasibility of the compound and the deposition process. A second series of tests were further performed on the prototype micro-machined sensor structure

designed by the candidate and fabricated through CMC using the proposed design. The properties of the polyaniline dispersion, which are relevant to the application, are summarized in Table 5.1.

Table 5.1: Properties of Polyaniline Dispersion [47].

Delivery form	Lacquer for instant application
Viscosity	40 - 50 s
Solids dispersion content	42%
Solvents	xylene/2-methoxypropan/propan/butan
Drying time	Approx. 12h (at room temperature)

5.2.1 Objectives of the Experiments

The primary objectives of the proposed experiments are two-folded: (i) to study the feasibility of the material considered for application in micro relative humidity sensors; and (ii) to examine the validity of analytical relationships, specifically relevant to the response time and the diffusion coefficient as derived from the Fick's law. The experiments are further expected to yield significant knowledge on the feasibility of the sensitive material and on the proposed micro-sensor design. More specifically, details on the following items are aimed:

- Relationship between the film thickness and the spin-coating speed for a specific ratio of polymer and volatile liquid phase.
- The conductive properties of cured polyaniline films.
- A relationship between the film resistance and the relative humidity level as a function of the film thickness.

- Time constant or response time of the film with variations in the humidity response to a step variation.
- An assessment of hysteresis of the material as a function of the film thickness.
- The influence of film thickness to the value of the diffusion coefficient.
- A preliminary assessment of repeatability in resistance and variation in film resistance with continued humidity exposure of the film.

5.2.2 Sample Preparation and Test Methodology

A standard spin-coating machine was used to deposit polymer on the glass substrates. The glass samples were used as delivered by the supplier (cleaned and sterile) and handled with tweezers. After spin-coating, the samples were left to dry in the clean room at room temperature (approximately 20°C) and ambient relative humidity (approximately 30% RH) for more than 12 hours.

5.2.2.1 Spin-coating theory

Spin-coating presents considerable advantages against other deposition methods. Although such polymers may also be deposited by dipping, sponging, printing or spraying, such methods pose considerable difficulties in controlling the film thickness. The spin-coating deposition technique is quite simple and low cost, and can yield nearly uniform thickness that can be well controlled by the spin speed, the viscosity of the deposited fluid and the duration of the spin.

The spin coating technique has been extensively used and reported in many studies [5,7,12,17,40]. Majority of these studies, however, have been limited to homogenous viscous fluids, while the deposition of dispersions has

been addressed in only few studies. In the spin coating process, the large particle dispersions are centrifuged towards the periphery. The smaller particles may also accumulate near the periphery, when they cluster to form relatively large size particles. A uniform deposition of small size particles, however, can be attained through selection of appropriate spin speed. The spin speed thus plays the role of a filter, which removes the large size particles above a specific diameter from the deposition surface of interest. At an optimal speed, the two dominant forces acting on the particles of dispersion (viscosity forces and centrifugal forces, as shown in Figure 5.1) are balanced. The particles of size within certain diameter would rest within the surface of interest with adequate distribution of dispersion even at lower speeds, resulting in minimal film thickness. Although interested in achieving a specific film thickness, the conductivity of film can be accomplished only when the configuration of polymer

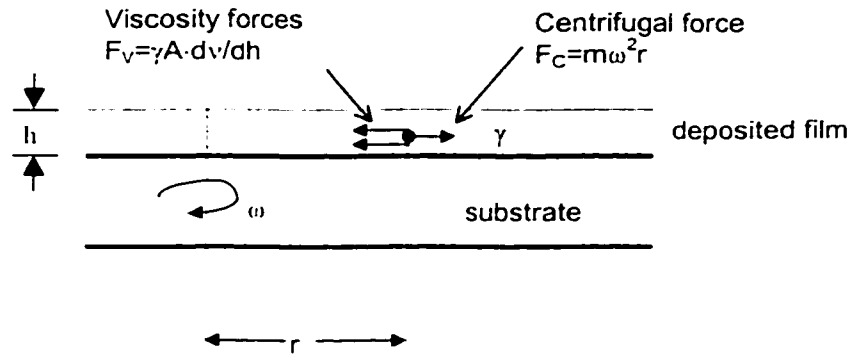

Figure 5.1: Schematic of particles in thin film.

particles is of a minimum compactness. This could be achieved by spinning a thicker film of a specific mass density in the liquid solvent. Such requirements point towards the existence of an optimal speed. Beyond the optimal speed, the particles in suspension will be pushed away beyond the critical radius (R) so that the remaining smaller particles may not constitute in a conductive film. This phenomenon was observed during experiments. The duration of the spin is also an important factor. A controlled spin coating process of dispersions may yield high quality films of dispersions. The process can be effectively used to remove the large clustered particles. The centrifugal force acting on a particle can be expressed as:

$$F_C = m\omega^2 r = \rho(3/4\pi\Re^3)h\cdot\omega^2\cdot r \qquad (5.1)$$

where m is mass of the particle of dispersion, ω is the angular velocity; r is the distance between the rotation center and the center of the particle, ρ is resistivity of the material, $\Re$ is radius of the particulate in dispersion, h is the thickness of spun film. The viscous force developed at the particle can be expressed as:

$$F_V = \gamma A\cdot dv/dh = \gamma(\pi\Re^2)(dv/dh) \qquad (5.2)$$

where γ is viscosity coefficient which is determined from properties of the material; v is the speed of the particle; and A is surface area of the particle exposed to drag while moving. The specific radius R mentioned before can be derived as following. At this specific radius R, the centrifugal force shall be equal to the viscosity force on the particles, as shown in equation (5.3), assuming a linear variation of the speed of the fluid within the thickness of the fluid.

$$F_C = F_V \qquad \text{or} \qquad \frac{dR}{dt} - \frac{2\pi\rho h\omega^2}{3\gamma} R = 0 \tag{5.3}$$

The specific radius R is illustrated in equation (5.4) which is derived from equations (5.1), (5.2) and (5.3).

$$R = e^{\frac{2\pi\rho h\omega^2}{3\gamma}t} \tag{5.4}$$

The specific radius depends on rotating speed, area of particle exposed to viscous friction while moving, mass of the particle, viscosity of fluid material and the spinning time. Few studies have investigated the influence of spin time on the spin coating process [49].

5.2.2.2 Experimental results of film thickness versus spin-coating speed

In the experiments, results have shown that initial deposition is performed for a duration of 30 seconds at 500 rpm to wet the surface. The spin is then continued for additional 30 seconds at different spin speeds to thin film thickness, as illustrated in Table 5.2 and Table 5.3. The magnitude of centrifugal force increases with the spin speed. The particle is centrifuged to the periphery beyond the area of deposition, when the centrifugal force acting on the particle exceeds the viscous force. It can be further noted that low viscosity materials can yield finer deposition areas with thin film. Same viscosity materials will yield relatively thicker films at low rpm, while thin film can be achieved at higher rpm.

Upon drying of the samples, the thickness of deposited films was measured using an optical microscope (OLYMPUS BX 60M). The film on the substrate was scratched in a few spots after fully drying of the samples, to

facilitate the measurements. With maximum magnification (X1000), the field of microscope was focused at the surface of thin film layer, and then at the surface of substrate. At ×1000 magnification, the depth of focus field is quite reduced, which is less than 1μm. The difference between two indications on the focusing hub of the microscope represents the thickness of the spin-coated film in μm.

The film resistance is measured by pointing two spots of silver conductive paste on each sample, to enhance the repeatability of measurement between the same two points on the film. Assuming negligible resistance due to the silver paste, the measurement is considered to provide resistance of the conductive polymer on the same sample. Figure 5.2 shows the top view and the cross section of specimen.

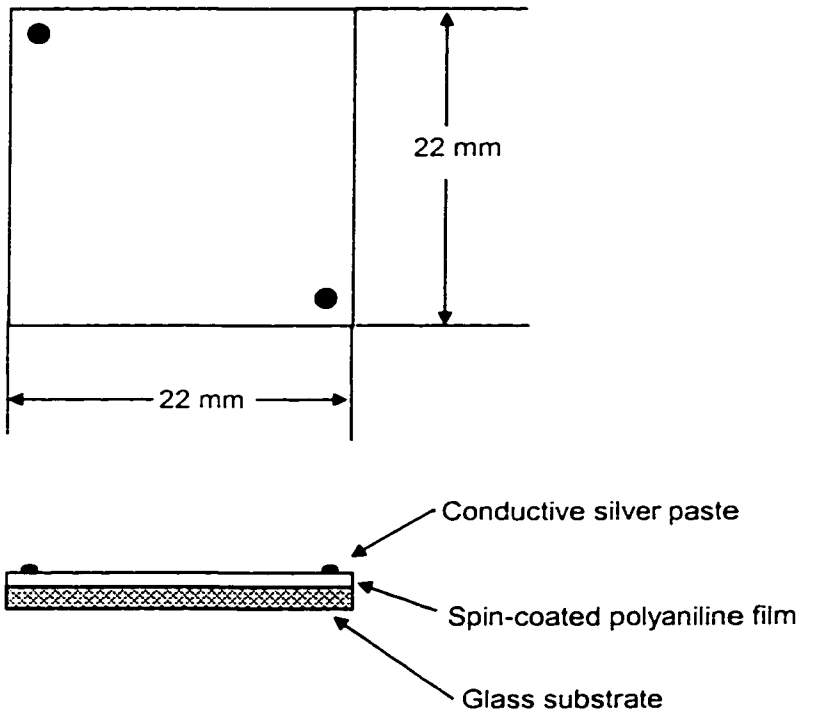

Figure 5.2: Schematic representation of the glass substrate with spin-coated film and conductive silver points.

The samples were arranged into a sealed box with electrical connection drawn outside. The relative humidity and the temperature inside the box were carefully monitored. The resistance of samples was measured through the electrical connections of the box through direct resistance measurement.

A number of samples were prepared by performing spin coating at different speeds: 500, 1500, 2000, 2500, 3000, 3500 and 3750 rpm. Several samples were prepared for each speed. Each sample group was spun with the same solution of polyaniline of same viscosity at specific different speeds. The samples were allowed to cure at room temperature for more than 12 hours. This resulted in seven different average thickness of polyaniline film, as outlined in Table 5.2. The film thickness of the specimens varied from a low of 42 μm attained at high speed of 3750 rpm to a maximum of 164 μm attained at low speed of 500 rpm.

The resistance measurement studies revealed that the deposited films approach non-conductive characteristics at higher spin speeds. At high speeds, the deposited films exhibit non-conductive characteristics. Although the spin speed can be increased considerably for non-dilluted polymer to achieve a very thin layer, the resistance of the film increased beyond the range of the resistance meter used in the laboratory. This condition for a specific specimen was considered to yield non-conductive layers on specimen. It is experimentally found that the viscosity of the commercial product would hardly allow to attain deposition thickness below 20 μm.

Table 5.2: Spin-coating conditions employed for sample preparation and resulting film thickness.

Speed (rpm)	Spinning-Time (seconds)	Average thickness after drying (μm)
500	30 seconds at 500 rpm	164
1500	30 seconds at 500 rpm and 30 seconds at the indicated speed	133
2000		106
2500		67
3000		58
3500		46
3750		42

By reducing the viscosity of the dispersion, it is expected that a lower film thickness can be achieved at the same spin-coating speed for the same spin duration. The viscous forces acting on the particle of dispersion would decrease with reducing the viscosity of dispersion, and thus result in lower film thickness. Reduction in the viscosity of polyaniline dispersion was thus considered in this study. A diluted polyaniline dispersion was prepared to achieve lower viscosity. The spin coating was performed with different proportions of polyaniline and the thinner (1-methoxy-2-propanol.98%). It was concluded that the volume proportion 3:2 between polyaniline and thinner is most suitable to achieve thin and conductive films. Different sample groups were thus prepared, where each

group was spun with solution of polyaniline prepared in the same lot at same viscosity at four different speeds, as outlined in Table 5.3. This resulted in four different average thickness of polyaniline film, ranging from 6.7μm to 14.9 μm. The maximum speed that could yield conductive films for diluted polyaniline was found to be in the order of 3000 rpm. Table 5.3 illustrates the test conditions employed for sample preparation with low viscosity dispersion.

Table 5.3: Spin-coating conditions employed for sample preparation (3 parts polyaniline and 2 parts thinner) and resulting film thickness.

Speed (rpm)	Spinning-Time (seconds)	Average thickness after drying (μm)
500	30 seconds at 500 rpm	14.9
1000	30 seconds at 500 rpm and 30 seconds at the indicated speed	10.5
2000		8.4
3000		6.7

A comparison of the resulting film thickness of the deposited layers attained from the commercial and low viscosity dispersions, presented in Tables 5.2 and 5.3, clearly illustrates that low viscosity dispersion permits lower thickness depositions. The measured values of average film thickness are further examined as a function of the spin speed and viscosity of the dispersion. Figure 5.3 illustrates the relationship between spin-coating speed and the film thickness for two viscosities of the dispersion: a) as provided by manufacturer;

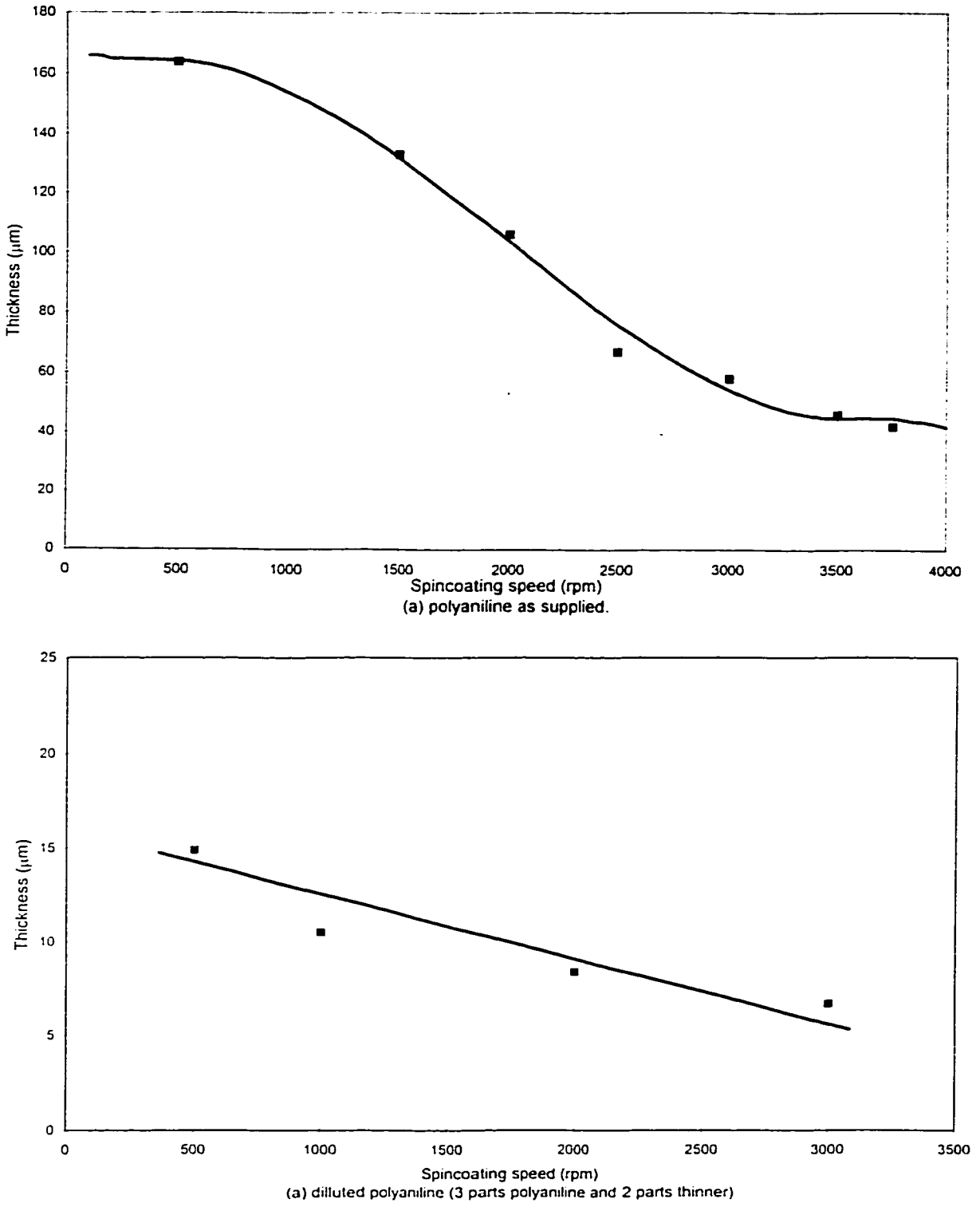

Figure 5.3: The relationship between measured values of average film thickness and spin coating speed.
a) as supplied; b) diluted polyaniline.

and b) 3:2 diluted as described earlier. The results show that the thickness of films decreases with the increase in the spin speed for both cases. The film thickness of the commercial compound can be considered to decrease in a linear manner with increase in spin speed in the 1500-3000 rpm range. The film thickness in case of the diluted compound varies nonlinearly with the spin speed. The change in film thickness is observed to be considerably small at speeds exceeding 1000 rpm.

5.2.3 Test Results

A series of tests were carried out on the prepared samples to assess the humidity sensitive properties of polyaniline for both precursor solutions: as supplied and 3:2 diluted polyaniline. Both steady state and transient response characteristics of the samples were acquired under different test conditions. The test procedures and the results are described below.

5.2.3.1 Steady state resistance characteristics

The resistance characteristics of film of different samples were measured under controlled values of relative humidity to derive a steady-state relationship for the samples. A sealed transparent box was fabricated to create specific relative humidity levels, which served as the input. A sponge soaked in water was placed in the box to serve as a source of moisture. The humidity level inside the laboratory was measured on a daily basis during the experiments and it was

found to vary slightly about a mean value of 30% RH. This value of 30% RH was thus used as a reference for all the measurements.

The humidity level in the box was systematically increased and measurements were taken corresponding to different discrete values of RH such as 40%, 50%, 60%, 70%, 80% and 90%. The sponge was removed from the box after a specific value of RH was attained. The resistance of the test sample was recorded, when the resistance value approached its steady state. The time for stabilization of the resistance was found to depend on a number of variables, such as relative humidity level, thickness of the film and the uniformity of the film surface.

The variations in film resistance with variations in RH were recorded for different samples of varying film thickness. The measured data can thus provide the resistance - RH relationships as a function of the film thickness. The measurements were also performed after aging of the film for 1 day, 8 days, 20 days and 100 days to study the effects of aging and the exposure cycles on the sample resistance. Figure 5.4 illustrates the measured resistance of the sample with variations in RH, film thickness and aging period. The results also show the resistance variations for both polyaniline compound, commercial and diluted.

The results show that the film resistance under a specific RH level decreases with the increase in the film thickness. For a given film thickness, the resistance increases with the decrease in relative humidity level. Under low RH levels, the film resistance varies considerably with the film thickness for both compounds. Under high RH level, the diluted compound yields relatively small

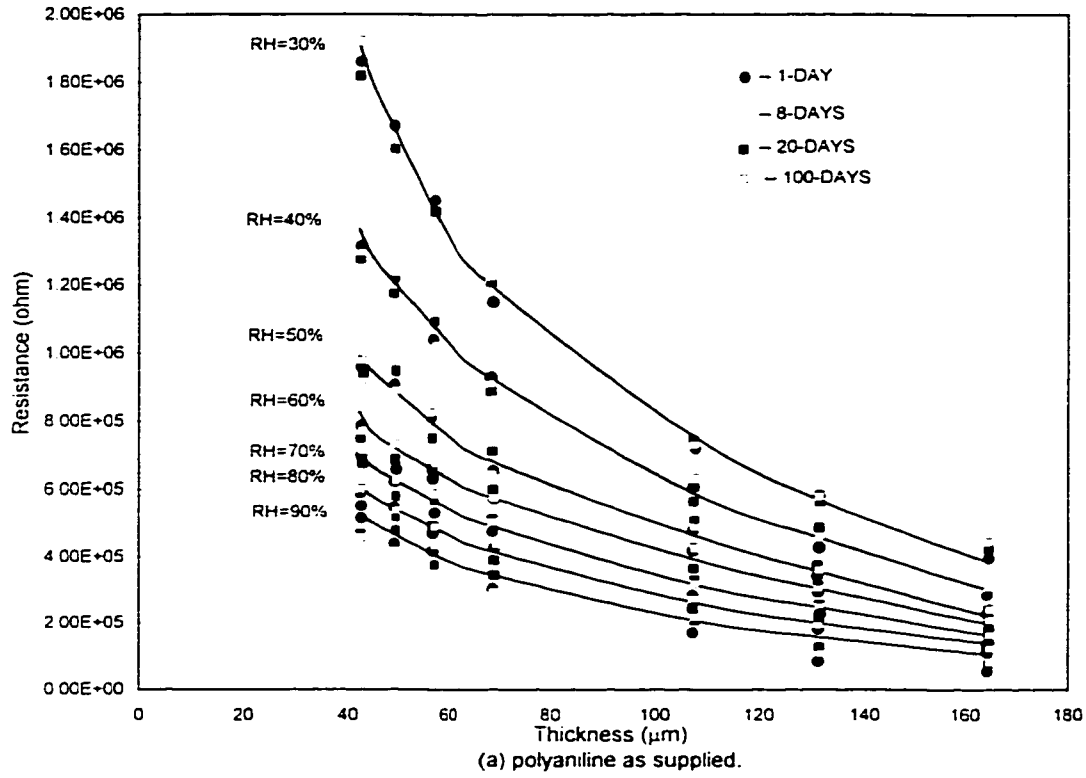

(a) polyaniline as supplied.

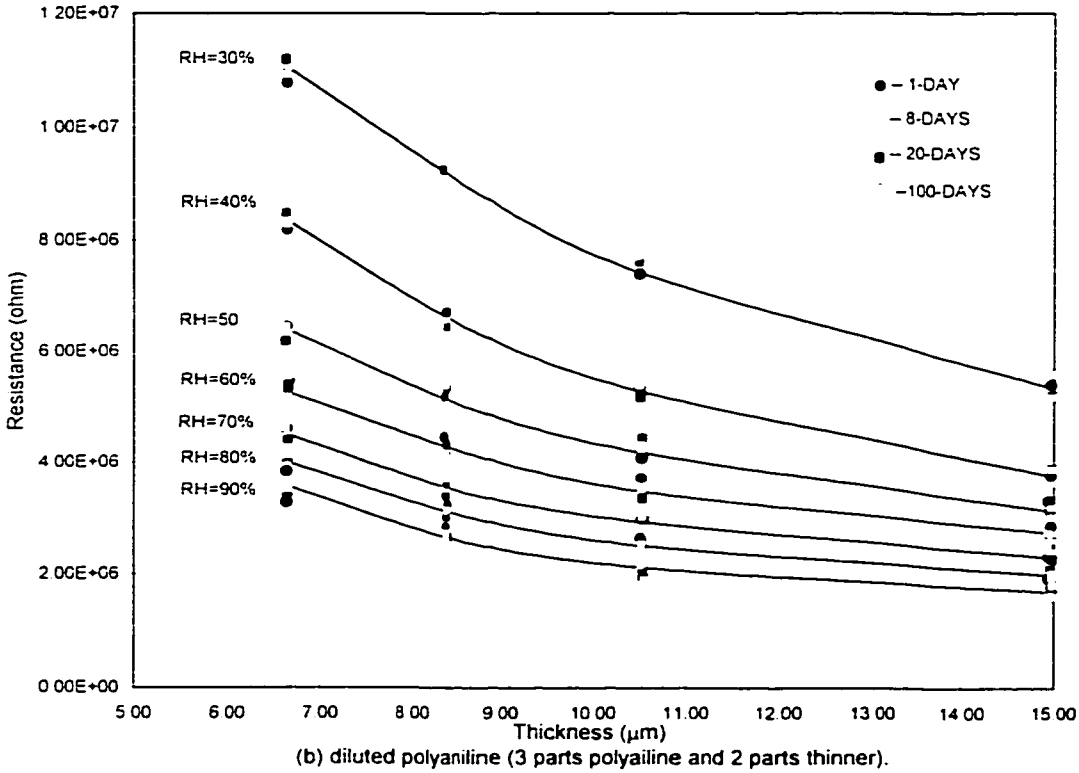

(b) diluted polyaniline (3 parts polyailine and 2 parts thinner).

Figure 5.4: The relationship between film resistance and film thickness for RH ranging from 30% to 90%, and the effect of aging.
a) polyaniline as supplied; b) polyaniline diluted.

variations in the film resistance. The results further show that a thin film yields considerably larger variation in the film resistance with variations in the RH level. This variation is relatively small for films of higher thickness. The film resistance variations are observed to be considerably larger for the commercial compound when compared with those obtained for the diluted compound.

The resistance measurements on the samples were performed over certain interval (after 1 day, 8 days, 20 days and 100 days) and the data was analyzed to study the effect of aging. The results presented in Figure 5.4 reflect only insignificant variations in resistance over the 100 days aging period. The peak variation in resistance due to aging was obtained in the order of 4%. The measurements performed on different days, however, did not reveal a particular trend. It is thus believed that the variations in measured resistance are most likely attributed to the precision and repeatability errors of the resistance meter and the commercial humidity sensors, and precision error of the samples.

The measured data was further analyzed to study the effect of dilution performed on the polyaniline compound. The results presented in Figure 5.4 clearly show that deposition using diluted compound yields overall higher resistance but considerably lower film thickness. While the compound dilution allows for deposition of more uniform and thin films, it also yields relatively larger variations in film resistance. The distribution density of polymer particles in the deposited film depends on the density of particles in the volatile solution. The lower the concentration of particles is, the higher the film resistance is expected. The rate of change of resistance with humidity is higher at lower humidity levels

than that attained at higher RH levels. This may be attributed to the saturation of the polymer in water vapors at high RH and does not allow further penetration of water molecules within the depth of the film. This conclusion is also further supported by the Fick's law and the absorption model.

The film resistance of the samples is further measured under decreasing values of RH to study the absorption and desorption properties of the polymer. A sponge soaked in water was kept inside the sealed box until the RH approached 90%. Then, the sponge was removed. After data were recorded for the specific RH level, the box was opened to release excess of water vapor until the next desired value humidity level was attained in the box, and the resistance measurement was repeated. These measurements were continued until the RH reached a value of 30%. It should be noted that thicker films require more time to release water vapor than the thinner films. Since the measurments were initiated at 90% RH, one single measurement was taken for 90% RH.

Figure 5.5 illustrates the variations in film resistance measured under increasing and decreasing RH for samples of varying film thickness. The results show relatively larger hysteresis for the films deposited using undiluted polymer, while the diluted polymer yields considerably lower hysteresis. For diluted compound, the magnitude of hysteresis tends to increase with the film thickness. This trend, however, could not be established for the undiluted compound. The hysteresis curves obtained for 6.7 μm, 10.5 μm and 14.9 μm films exhibit crossover in the 30% to 35% RH range. This is most likely attributed to the

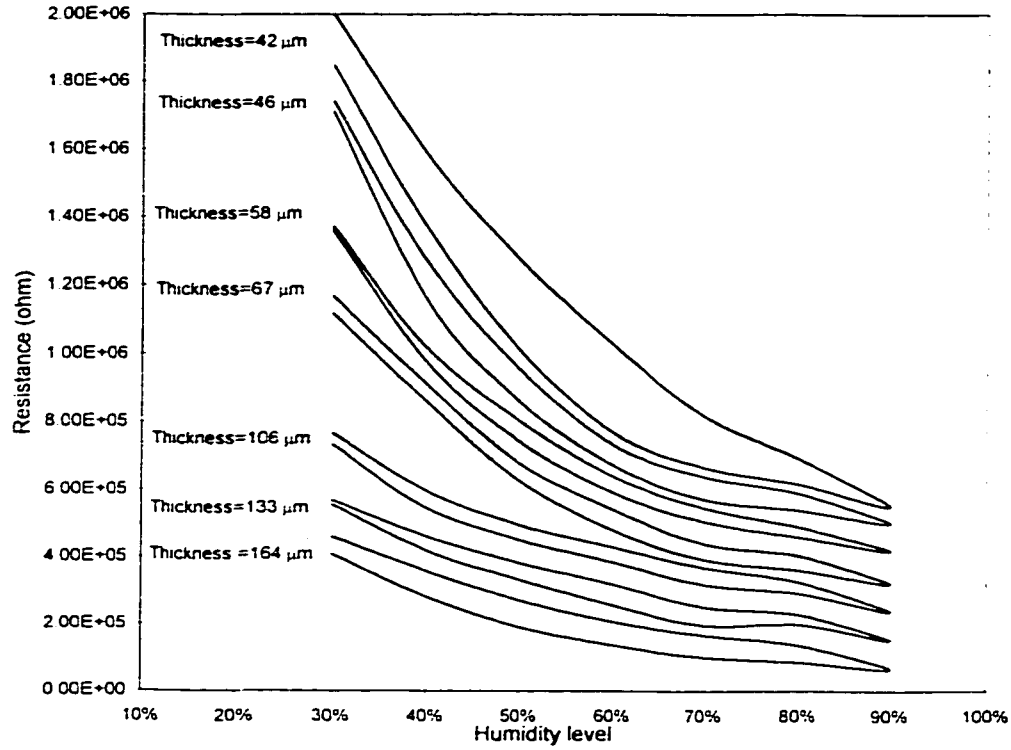

(a) polyaniline as supplied.

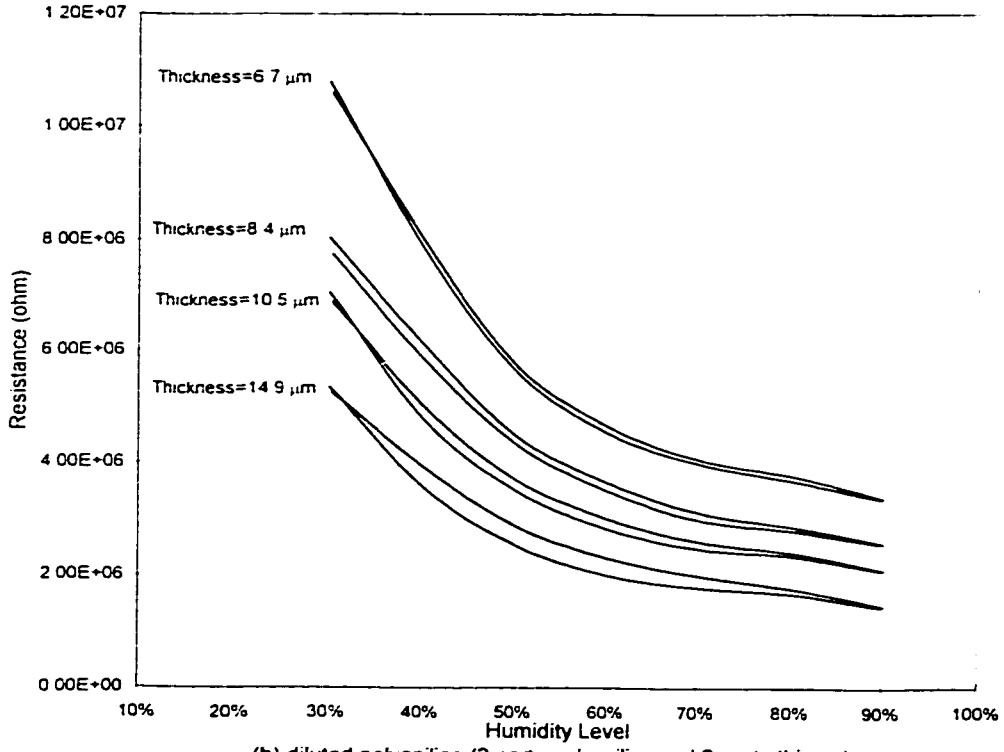

(b) diluted polyaniline (3 parts polyaniline and 2 parts thinner).

Figure 5.5: Variations in film resistance measured under increasing and decreasing relative humidity.
a) as supplied; b) diluted polyanline.
(Result data are measured two hours after applying inputs.)

gradient of the humidity level in the measured environment or experimental errors due to manual collection of data. For polyaniline as supplied, the film with lowest thickness exhibits the largest hysteresis between 30% and 60% RH which is the most common humidity level. For higher thickness of polyaniline, the hysteresis is lower but remains almost the same for most cases, which may be due to the fact that water vapor cannot fully penetrate through a thicker film.

Hysteresis represents the difference of water vapor absorption into the film and water vapor desorption from the film. The value of the difference between the resistance when humidity is increased and decreased divided by the maximum value yields the relative hysteresis of the material at specific humidity level in relative units [55]. The relationship between hysteresis and thickness of the films is further illustrated in Figure 5.6 for both dispersion.

The results show considerably larger hysteresis of the films attained using commercial polymer, specifically for film thickness below 45 μm and above 110 μm. The lowest hysteresis of approximately 8% is obtained for film thickness of 60 μm. The maximum hysteresis of films realized from the diluted polymer ranges from 2.3% to 10.6% for different values of thickness ranging from 6μm to 15μm. The difference in the hysteresis of the two polymers is due to the film thickness and porosity of the film. The porosity of the film is created by the particle size clustering of the particles, air cavities and compactness of the particles within the layer. Thin films are thus expected to yield higher porosity and lower hysteresis. It is also noted from Figure 5.6 that hysteresis of the

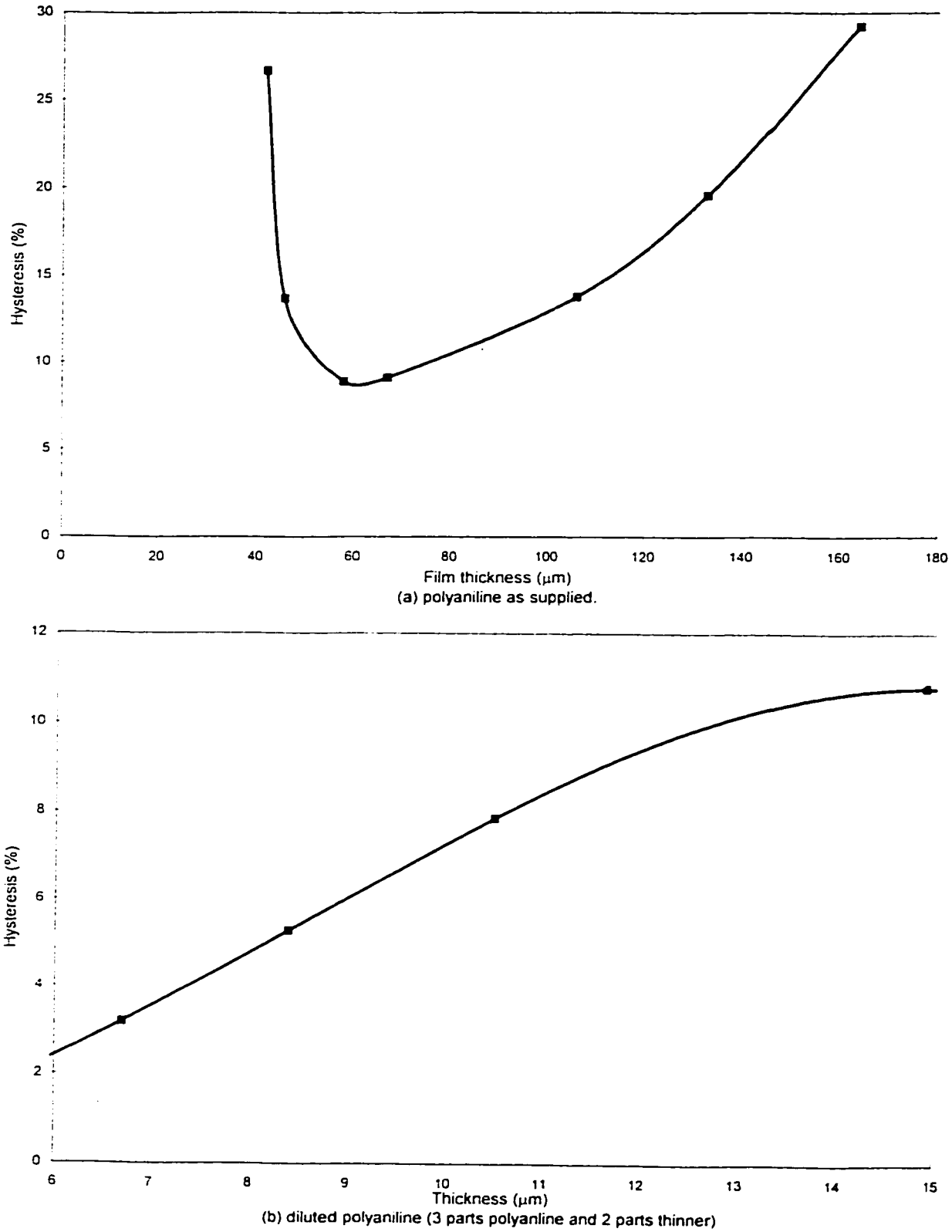

Figure 5.6: Measured hysteresis of the samples.
(a) polyaniline as supplied; b) diluted polyaniline)

sample with approx. 60 μm thick film is much lower than those with different thickness in the range of 40 μm and above 80 μm. This may be due to the structure of the particles in the film which is the most convenient for diffusion of water vapor at about 60μm thickness.

5.2.3.2 Transient state R-RH% measurements

The steady state response of a system characterizes only its partial behavior to static inputs. The steady-state response of the humidity sensitive active material yields only steady state variations in resistance with RH, as described in the previous section. The development of an effective humidity sensor requires study of its transient response, specifically the response time, which is related to the absorption and desorption properties of the film.

The response time of the humidity sensitive material film could be further used to evaluate the diffusion coefficient of water vapor in polyaniline film using the Fick's model of diffusion. The diffusion coefficient can effectively describe the distribution of water vapors within the film, and thus directly affects the transient response of the film to water absorption. A larger value of the diffusion coefficient of a material in general yields rapid transient response of the sensing element.

Different specimens of the humidity sensitive material film are evaluated in the laboratory for their transient response behavior under a step change in RH. The experiments were performed using the setup described in the previous section. The humidity level was initially increased within the sealed box to 90% RH. A sample initially exposed to 30% RH of ambient air was inserted the box,

while the water soaked sponge was removed. The sample was thus exposed to a sudden change in RH from 30% to 90%. The sample resistance was measured at regular equi-spaced time intervals over a time span. The time span was taken as the settling time of the sensors, when resistance reached its steady state value. The settling time for different samples varied due to different film thickness. The experiments with each individual sample was repeated four times to assess the repeatability of measurement and reliability of the methodology. Different trials resulted in nearly identical transient response characteristics.

The transient response of the sample is considered to represent the transient behavior of sensitive film, while the contributions due to connectors and wires assumed negligible. This assumption is justified by the fact that humidity absorption of the film is the slowest process within the entire system. The response time of the sample was then estimated using the 63.2% method, as the time when output approaches a value which is 63.2% of the difference between the final and initial values. The above experiments are repeated with different samples and the results are examined to study the effect of film thickness and the dilution of polyaniline on the transient response.

Figure 5.7 illustrates the response time derived from the transient response of different samples. The results clearly show that the response time of the samples realized from deposition of polyaniline and the thinner is considerably lower when compared to those realized with polyaniline deposition. This is attributed to lower film thickness and hence the increased capability of

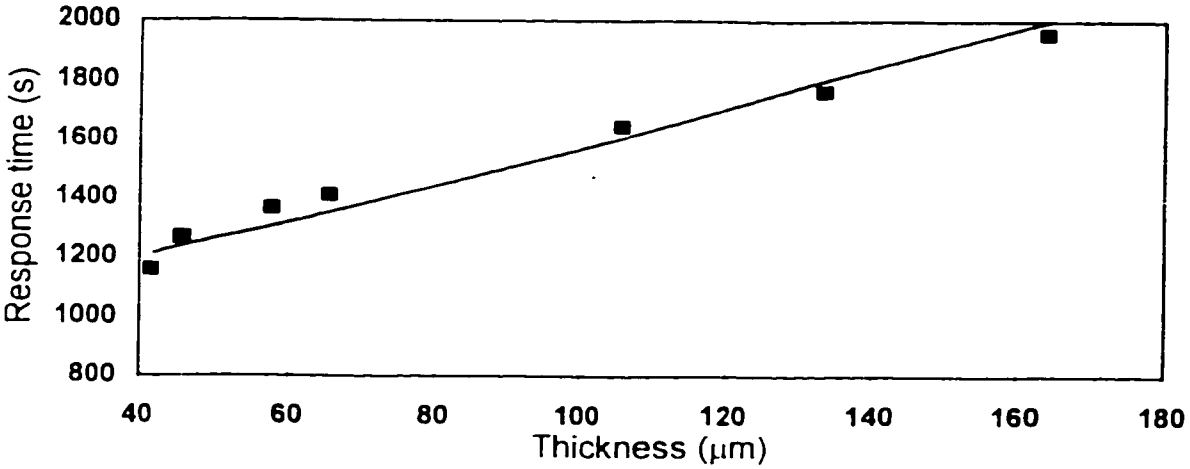

(a) polyaniline as supplied.

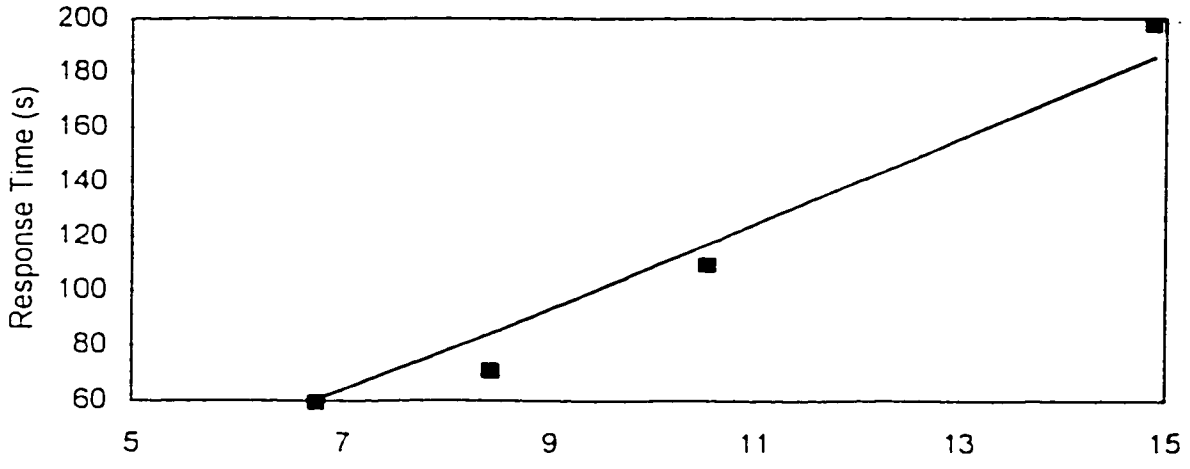

(b) diluted polyaniline (3 parts polyaniline and 2 parts thinner)

Figure 5.7: Response time of different samples derived from the transient response.
(a) as supplied; (b) diluted polyanilline.

the film to become saturated. The samples developed using polyaniline and the thinner with film thickness of 6.7 μm, 8.4 μm, 10.5 μm and 14.9 μm, exhibit the response time of a comparable order. The response time, however, increases with increasing film thickness. For these samples, the increase in the response time appears to be nearly linear with the thickness.

The samples realized using polyaniline deposition exhibit considerably higher response time due to the poor absorption properties of relatively thick films. The response time of these samples also tends to increase with increase in film thickness in a nearly linear manner, specifically for film thickness values exceeding 45 μm.

5.2.4 Analysis and Discussion of Experimental Results

The steady-state and transient response data acquired for different samples are analyzed to study the effects of film thickness and spin coating speed on the response behavior, such as hysteresis, variations in resistance with change in RH and the response time. The response time in this study refers to the time constant of the sample. The data are further analyzed in an attempt to understand relationships between film thickness and spin coating speed, response time and film thickness, and hysteresis and film thickness. The effects of dilution of the polyaniline are further analyzed in terms of the response parameters. The observations made from the analyses of the measured data are summarized below:

- From the results presented in Figure 5.3 on the influence of spin coating speed and thinner on sensitive film thickness, it can be concluded that the film thickness decreases with the increase in spin coating speed. The film thickness also decreases considerably with the addition of the thinner to the polyaniline. The results clearly show that spin coating speed and viscosity are two main elements affecting the spin coating process when the spin time is held constant. The thinner reduces the viscosity of material, while higher spin coating speed increases the centrifugal force acting on the material particles, which results in finer distribution of the dispersion on the substrate.
- The variations in the film resistance under a given RH for the two compounds used in the study (Figure 5.4) are observed to be nearly linear with the film thickness. This trend supports the basic resistance law. For the same film thickness, the film resistance decreases with the increase in the relative humidity level, which directly relates to the sensing characteristics of the material. The variations in resistance reveal similar trends for both the diluted and nominal polyaniline. The addition of the thinner thus does not vary the sensing characteristics of the material, although it enhances the bulk resistance and ability to achieve finer film thickness. The film resistance spun out of diluted polyaniline is much higher than that realized from the nominal polyaniline. The variations in resistance of the sensing film were quite significant in the 30% RH to 50% RH range, which is the most common range of humidity level encountered

in the indoor air. From the measurements performed over a prolonged exposure period, it can be further concluded that the material properties remain stable within 100 days.

- The thin film deposition realized using diluted polyaniline forms a more uniform film of relatively smaller particles with enhanced porosity. Such films yield considerably lower hysteresis, as illustrated in Figure 5.5. The hysteresis of the sensing film increased with increase in thickness when using the nominal polyaniline. The hysteresis approaches minimum value for a film thickness of 58μm spun at 3000rpm for the nominal polyaniline. Based upon the factors considered in this study and experimental measurements, it may be deduced that 3000rpm (58μm) corresponds to an optimal spin-coating speed for the sensing material. For the nominal polyaniline, the hysteresis increases when spin-coating speed exceeds 3000rpm. The hysteresis also tends to increase with decrease in the spin-coating speed below 3000rpm. For diluted polyaniline, the hysteresis decreases with decrease in the film thickness. An examination of two curves shown in Figure 5.6 also reveals that addition of the thinner alters the film hysteresis characteristics significantly. The polyaniline and thinner spun on the substrate exhibit significantly reduced film hysteresis.
- The response time increases with the increase of the humidity sensitive layer thickness. The absorption of water molecule becomes longer in thicker film. The Fick's equation (3.9), presented in Chapter 3, describes this absorption process. Thick sensing films thus yield slower response

and the response time increases nearly linearly with the film thickness as shown in Figure 5.7. Thin sensing films realized through deposition of diluted polyaniline yield considerably faster response when compared to that of the films realized from nominal polyaniline.

- From the above analysis, the thickness of humidity sensitive layer is mainly dependent on spin coating process. There are two elements which affect this process: the spin-coating speed and the viscosity of the deposited material. Higher spin coating speed results in increased centrifugal forces. The viscosity of material can be decreased by using the appropriate thinner. The thickness of the film can be controlled by controlling the spin coating speed and viscosity of the material to be deposited. In chemical sensors, the thickness of active material is often the main element affecting the response time of the sensor. The hysteresis of the sample also depends on the film thickness and film structure. If the film is very compact, the hysteresis is expected to be lower than that attained with thick films, which tend to trap the molecules of water in micro-pores. The spin time may also influence the spin coating process. The spin time, however, was maintained constant in this study, which was chosen out of the experience gathered during the initial trial depositions.
- The consistent results obtained from the experimental data indicate that the simple post-processing technique considered in this study is appropriate for achieving uniform active material layers. The correlation

between thickness and spin speed reveals that a specific thickness corresponds to a specific spin coating speed at a given viscosity. The above methodology can be applied to assess the humidity sensing characteristics of other resistive films.

5.2.5 Post-processing of Micromachined Sensor

The laboratory experiments are further performed on the resistive microsensor. The prototype sensors were fabricated using Mitel 1.5 CMOS technology. The die (humidity sensitive sensor structure- without the sensitive layer) was attached to a 40-pin dip header. The chip was fully packaged and the top lid on the header was not attached. Figure 5.8 illustrates a pictorial view of the microsensor prior to post-processing .

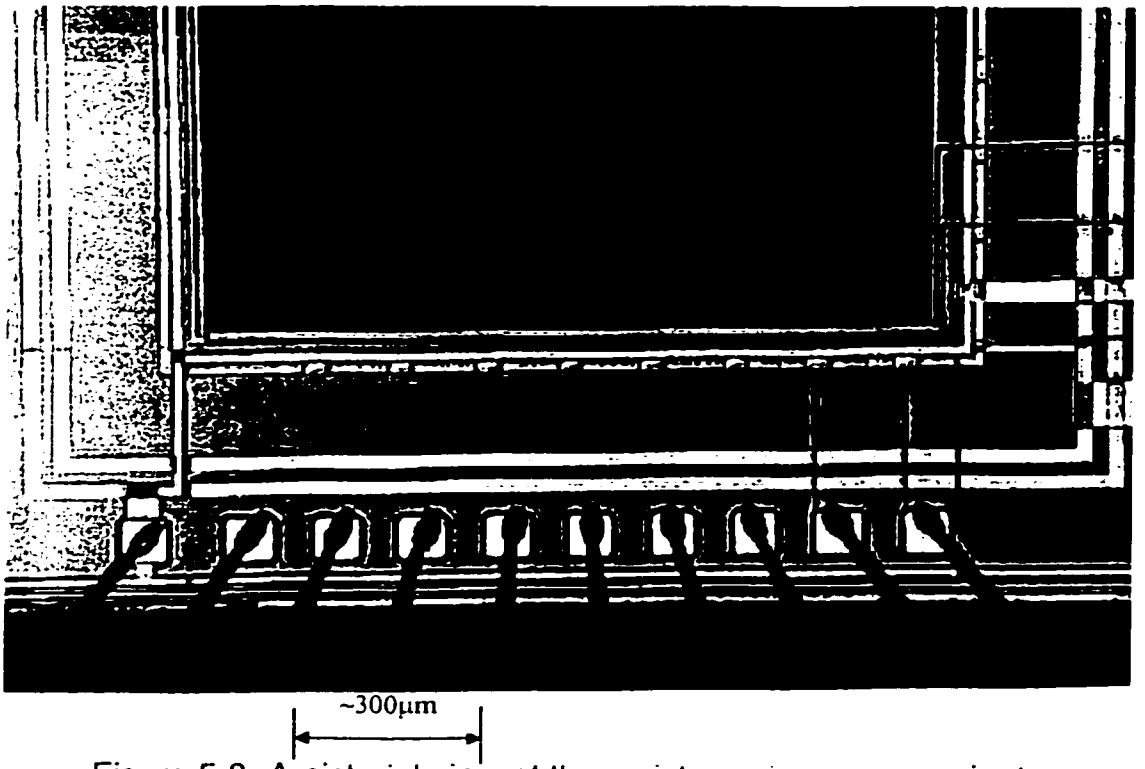

Figure 5.8: A pictorial view of the resistive microsensor prior to post-processing.

The scope of the present work is to analyze and design humidity micro-sensors that require low cost post-processing. Simple post-processing was used to spin-coat humidity sensitive material in thin layers on the active area of the micromachined sensor. The material was spun over packaged chips, the pads as well as the electrodes were thus covered by the polymer (as shown in Figure 5.9). The effect of clothing of polymer between wires was minimized by judiciously choosing the amount of dispersed polymer. The sample measurements, described earlier, revealed that a rapid response time and low hysteresis could be accomplished with relatively thin films realized using the thinner. Thinner films could be achieved at high spin-coating speed and lower viscosity of the deposition materials. The polyaniline with thinner (3:2) at spin-coating speed 3000 rpm was therefore used to achieve thinner deposited film on the electrodes. The spin coating was performed using the procedures described in the previous section, while the amount of material was reduced to 1 drop to minimize the spill over the connecting wires. After deposition, the microsensor chips were left at room temperature to cure for at least 12 hours. Some of the sensors did not perform successfully, as expected, due to shifting of the metal1 mask during the fabrication process. The deposition of polymer on the chips further required number of trials. The first batch of chips revealed poor quality of deposited film, specially the poor uniformity and inadequate thickness. However, an identical post-processing would be performed on full wafers, which is followed by dicing and packaging.

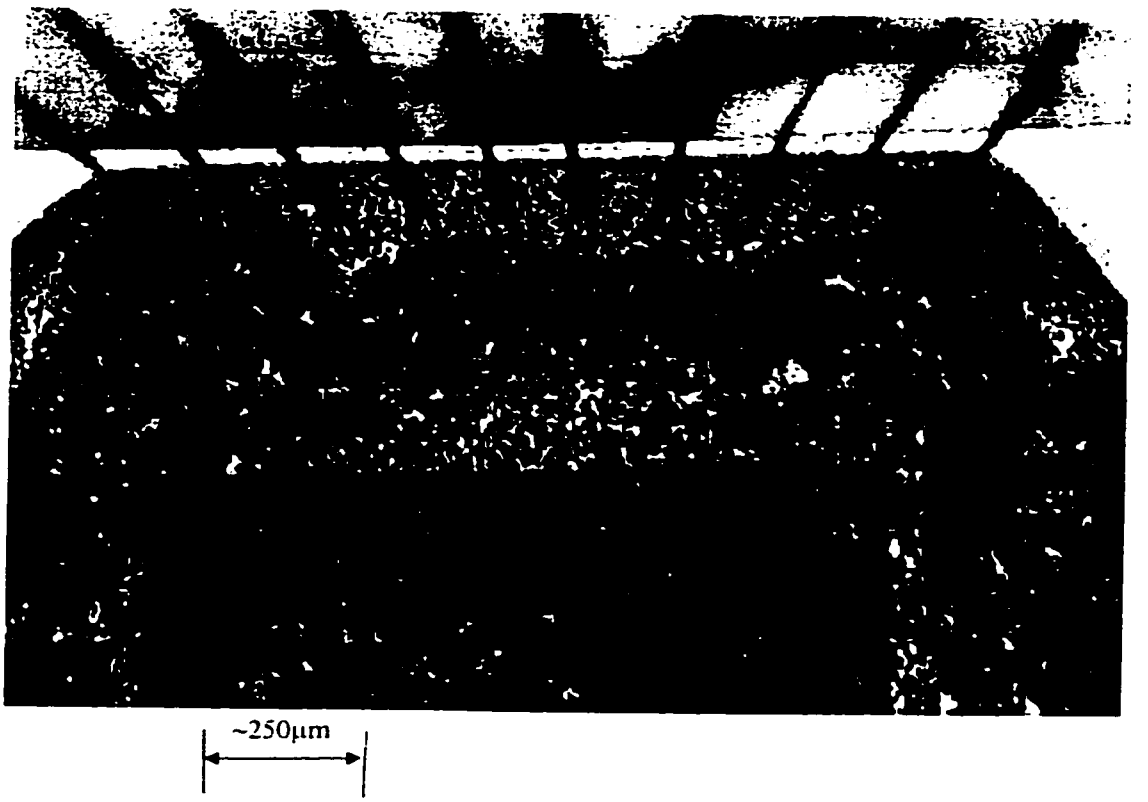

Figure 5.9: A micrograph of a microsensor after post-processing.

The quality of deposition for each sensor was evaluated through observations under a microscope. The observations revealed inconsistent deposition on some of the samples, specifically when thin layers were attempted. The film revealed considerable discontinuities in the deposition of thin films as illustrated in Figure 5.10. The figure shows two regions between the clusters of material particles, marked as A and B, where discontinuity in the thin film can be observed. Further measurements performed on the prototypes indicated that discontinuous films were not always conductive. A relatively thicker layer spun at 3000 rpm was therefore realized for the prototype microsensors. Figure 5.11 illustrates two magnified views of the coating polymer film, which shows the

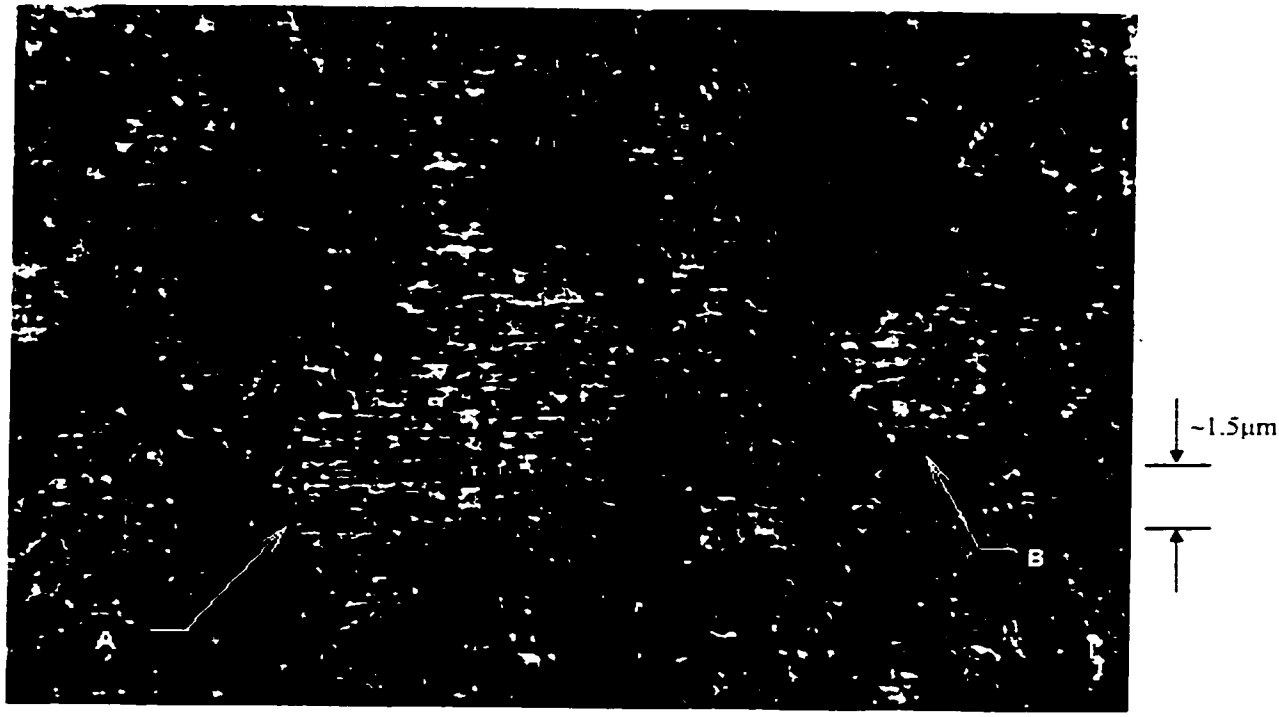

Figure 5.10: A pictorial view of the sensing film showing discontinuities in deposited film.
The space between cluster of material particles is shown by light gray area, and cluster of materials is shown by dark area.

central and peripheral regions of the sensitive film on sensor electrodes. The film in both regions comprises of particles of different sizes clustered together. A comparison of two micrographs illustrated the two different regions reveals that the particles clusters of thin film in the central region are much larger than those in the peripheral regions. This may be attributed to large centrifugal forces acting on the particles in the peripheral region. The average thickness of the film was measured as 19 μm.

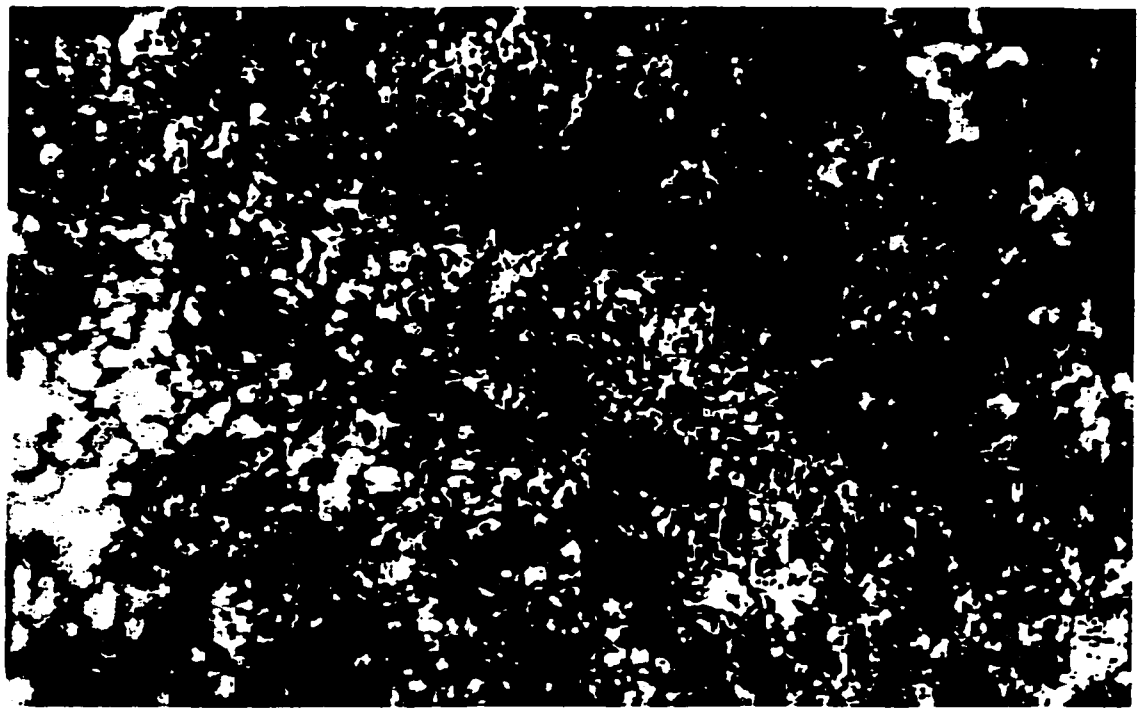

(a) center area of thin film on microsensor

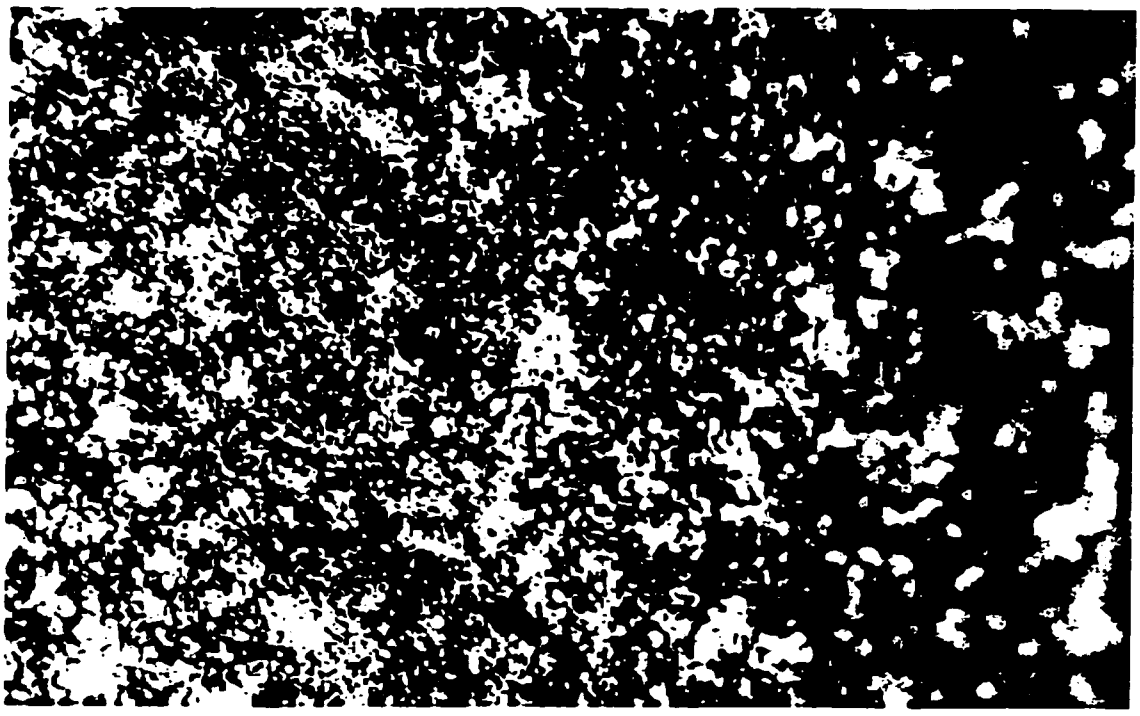

(b) corner area of thin film on microsensor

Figure 5.11: Magnified view of the central and peripheral regions of the film deposited on the microsensor.

5.2.6 Measurement of Sensor Characteristics

Measurements are performed on the prototype sensors to study their steady-state and transient response behavior. The steady-state variations in the sensor resistance are measured as a function of RH to examine the sensitivity of the prototype sensors. The resistance measurements were performed 1, 8, 20 and 100 days after the deposition and curing to examine the effect of aging on the resistance output. Figure 5.12 illustrates the variations in steady-state resistance of prototype sensor in the 30% to 90% RH range. It can be seen that the resistance decreases with increase in relative humidity in a nonlinear manner. The variations in resistance with respect to change in RH (dR/dRH) is observed to be larger at low RH levels, which tends to decrease considerably at higher RH levels. The figure further illustrates the measured resistance values after 1, 8, 20 and 100 days. The results do not exhibit significant change in resistance with aging. Slight variations among the different measurements of sensor resistance, however, are observed. Figure 5.13 illustrates the relative error of measured resistance with reference to the average resistance. The relative error is defined as the difference between measured data and average data divided by average data [10]. The results show peak variation in measurement performed after 100 day of approximately 4.2% occurring at 60% RH. The variation in resistance, however, do not exhibit a define pattern with aging of the polymer. Such variations are thus most likely attributed to the precision of measurement systems and methodology.

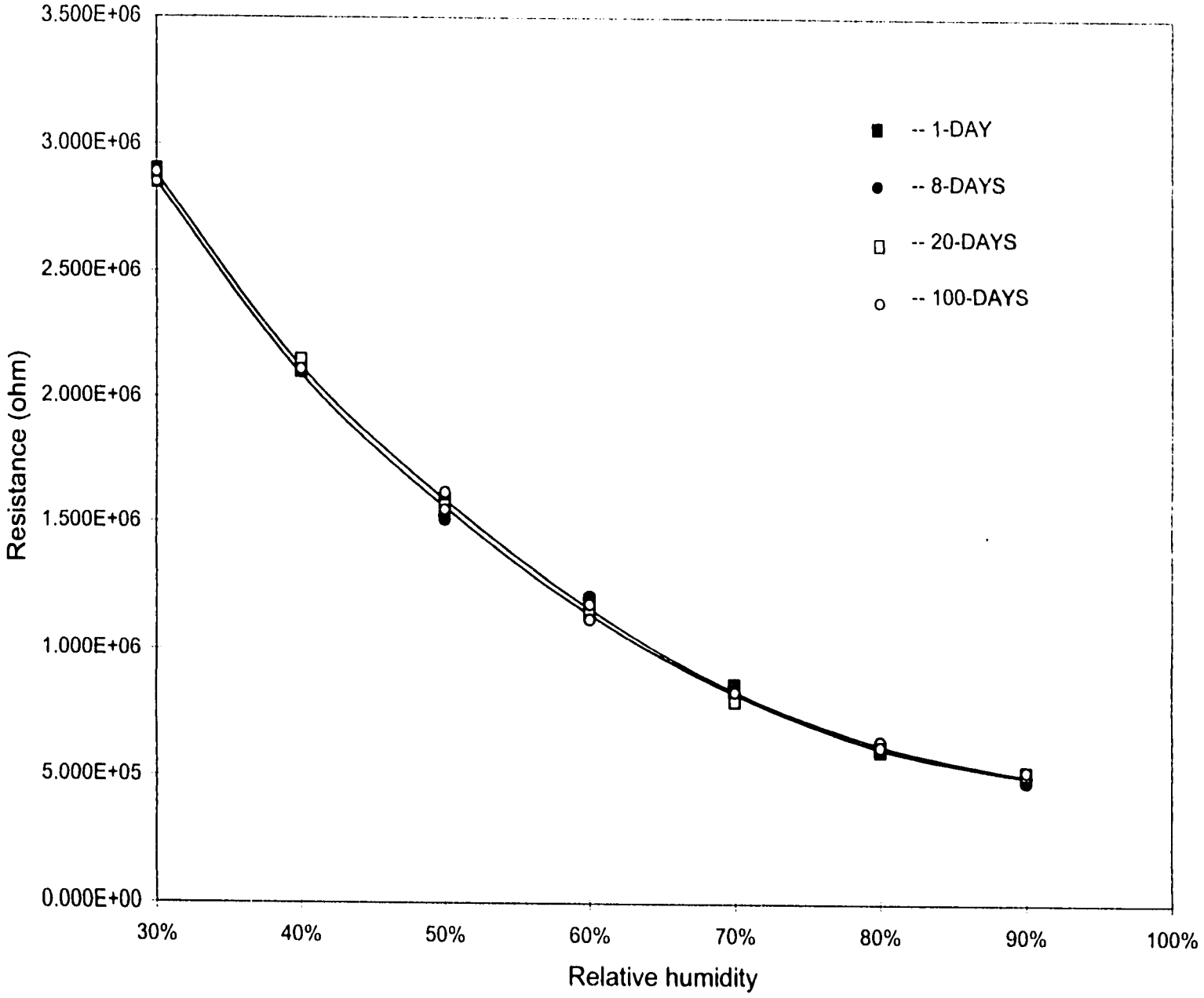

Figure 5.12: Steady-state change in sensor resistance with variances in the RH.

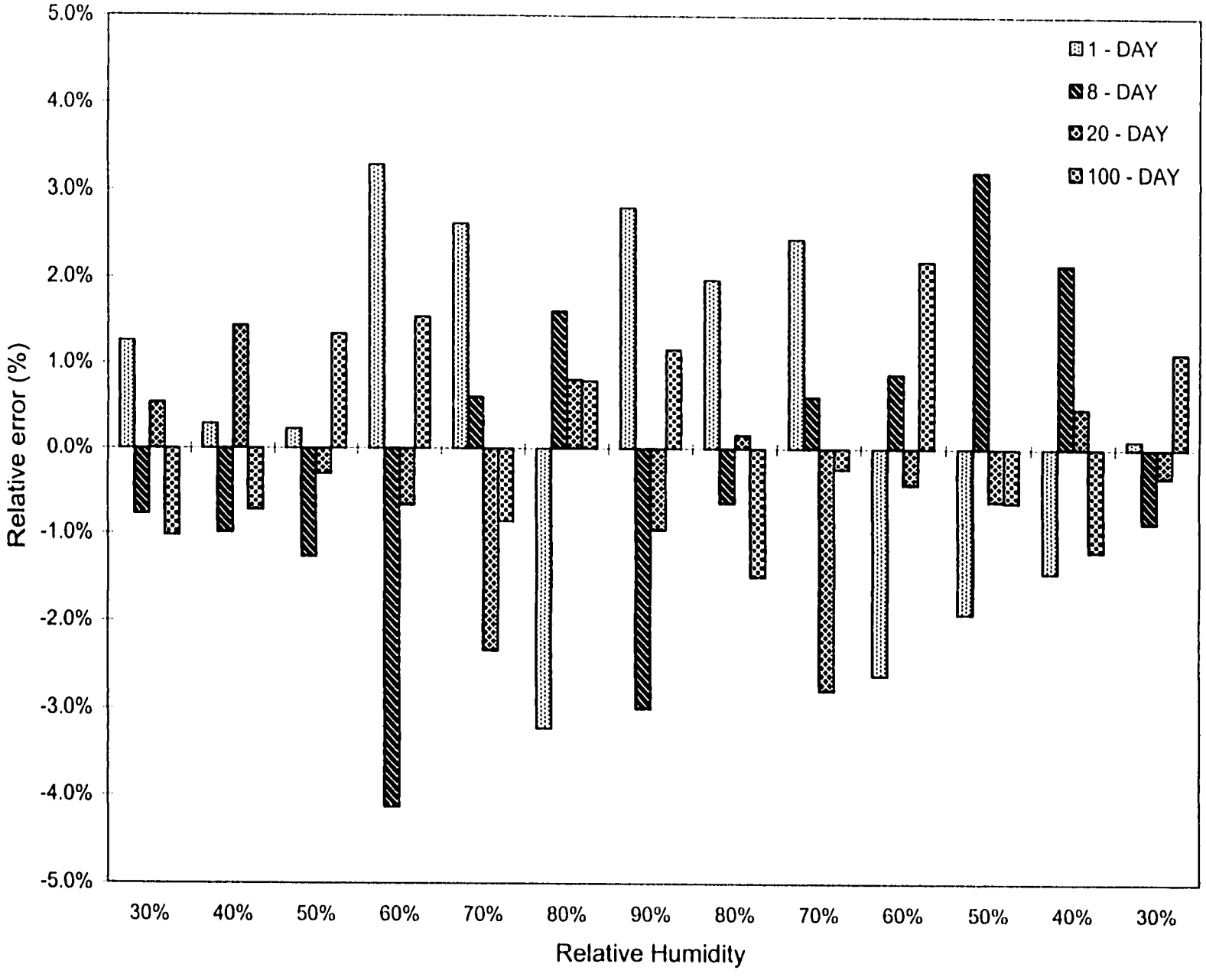

Figure 5.13: Relative error of variations in senor resistance with polymer aging.

The transient response characteristics of the sensor are measured by subjecting the sensor to a step change in RH from 30% to 90%, as described earlier in transient state R-RH% measurement of section 5.2.3. The variations in sensor resistance are recorded in frequent interval during the absorption process, until a steady value of resistance is attained. The sensor is then subjected to step change in RH in the opposite direction, from 90% to 30%, as shown in Figure 5.14. The transient variations in sensor resistance were recorded during the desorption process. The transient response tests were performed after 1, 8, 20 and 100 days of deposition and curing in order to study the effect of polymer aging. Figure 5.14 illustrates the measured transient variation in the sensor resistance. The results show nearly symmetric variations in resistance under absorption and desorption cycles and negligible aging effects. The transient response data is further analyzed to determine the hysteresis associated with absorption and desorption cycles. The peak hysteresis was obtained in the order of 3.2%, while the response time was observed as 1600s.

The steady-state resistance data is further analyzed to estimate the static sensitivity of the sensing element in terms of resistance variation. Curve fitting performed on the measured data resulted in following nonlinear relationship between the steady-state resistance and RH:

$$R = \frac{a}{RH} + b \qquad (5.5)$$

where $a = 11.6 \times 10^6\ \Omega \cdot RH$ and $b = -0.76 \times 10^6\ \Omega$

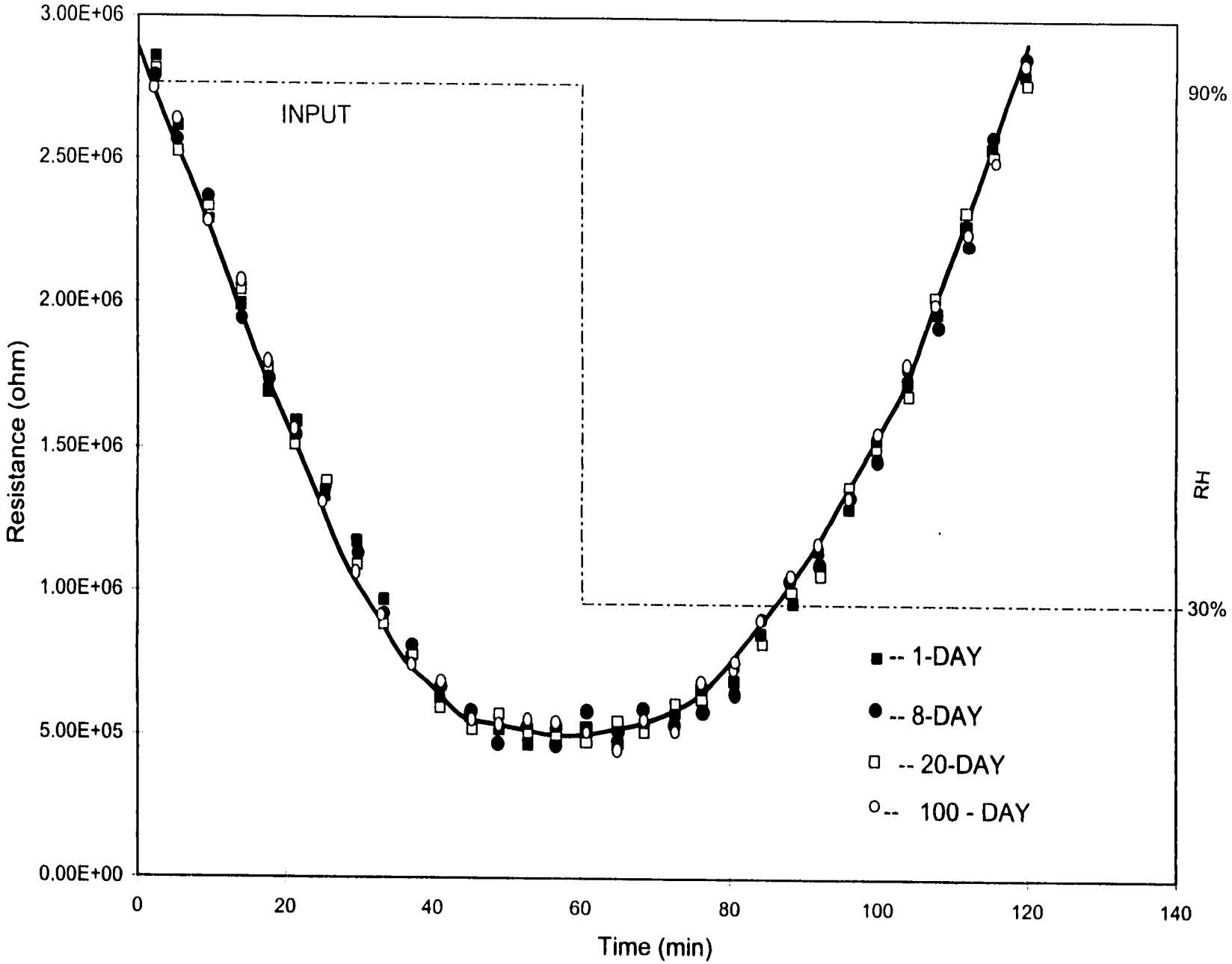

Figure 5.14: Transient response of humidity microsensor.

The static sensitivity of the prototype sensor is then derived as:

$$K = \left|\frac{dR}{dRH}\right| = \frac{a}{RH^2} \tag{5.6}$$

where K is the static sensitivity of the prototype sensor expressed in Ω/RH, which is inversely proportional to the square of RH. The prototype sensor thus yields higher sensitivity at low RH levels and lower sensitivity at high RH levels.

5.3 VALIDATION OF RESISTIVE MODEL MICROSENSOR

The experimental data acquired for the different samples and the prototype sensor are analyzed to examine the validity of the analytical model developed in Chapter 3. The Fick's diffusion equation (3.21) is solved to derive a relationship between the response time and the diffusion coefficient D. This relationship has been presented in Figure 3.16 for a film thickness of 3.4μm, which is usually attained through oxidation of Si in standard IC processing corresponding to the designed microsensor. In this dissertation research, the measured data is acquired for various samples with film thickness ranging from 6.7μm to 164μm. The transient response data measured for these samples provided a measure of the time constant for various values of film thickness h. The transient response data is analyzed to determine the diffusion coefficients for different thickness values of the deposited polyaniline.

In chapter 3, the water molecules absorption within the film of active material was assumed to follow the Fick's law. This assumption provides an analytical model for the diffusion. Thus, plugging in the various deposited films

such as those employed in characterization, a family of plots describing the response time versus diffusion coefficient can be risen, as shown in Figure 5.15. Since the diffusion coefficient is of very high importance in further modeling of humidity sensors based on the resistive principle, the estimation of the effective value for polyaniline is carried out. The experiments described in transient state R-RH% measurements in section 5.2.3 showed the response time for each humidiity level and film thickness. The response time obtained by experiment is searched on the corresponding plot which is drawn against the diffusion coefficient, which is thus found. Although theoretically, the response time should be distributed such that the diffusion coefficient is found as a constant number. The experiments yield different coefficient values such that the range of variation for D is quite large for the polymer deposited as is. However, the polymer diluted with thinner exhibits much lower variation range.

The thickness of sensitive layer on humidity sensitive sensor was measured as 19 μm. It is shown that the diffusion coefficient D corresponding to 19 μm is around 0.35E-12 (m^2/s) in Figure 5.16. Using this value in Fick's diffusion law to obtain the theoretical transient response of humidity sensor. The comparison between theoretical data derived from equation (3.17) and test data is shown in Figure 5.17. The relative error can be derived by using the difference of theoretical data and test data dividing by theoretical data. The comparison of the theoretical response and test response reveals reasonably good correlation, although the maximum error is 12%. The relative error is shown in Figure 5.18.

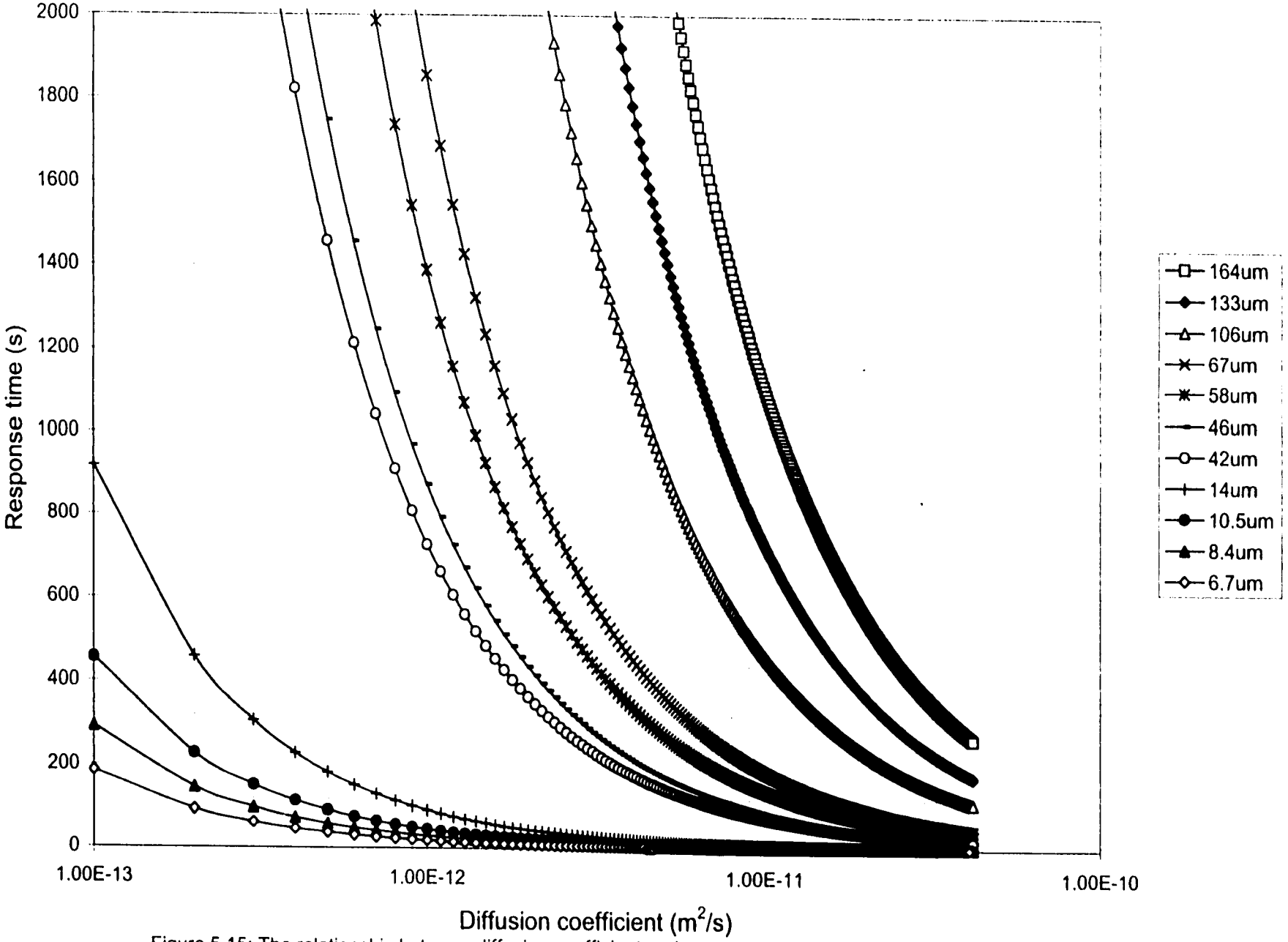

Figure 5.15: The relationship between diffusion coefficient and response time corresponding to different thickness.

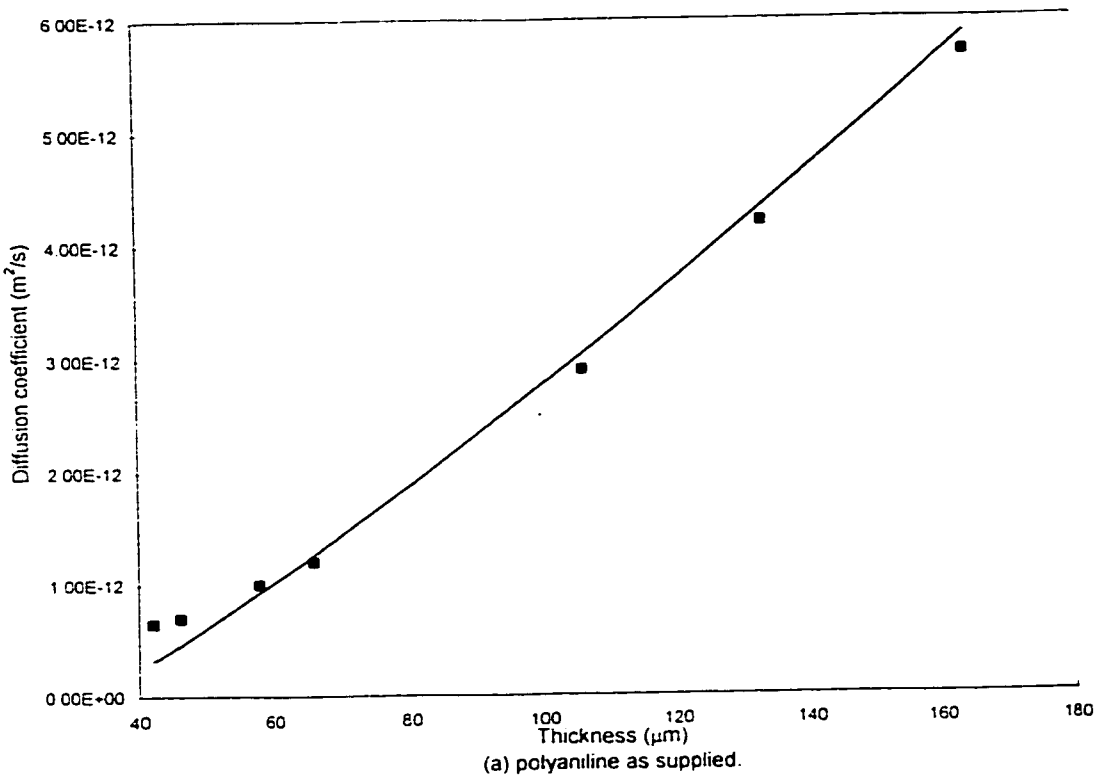

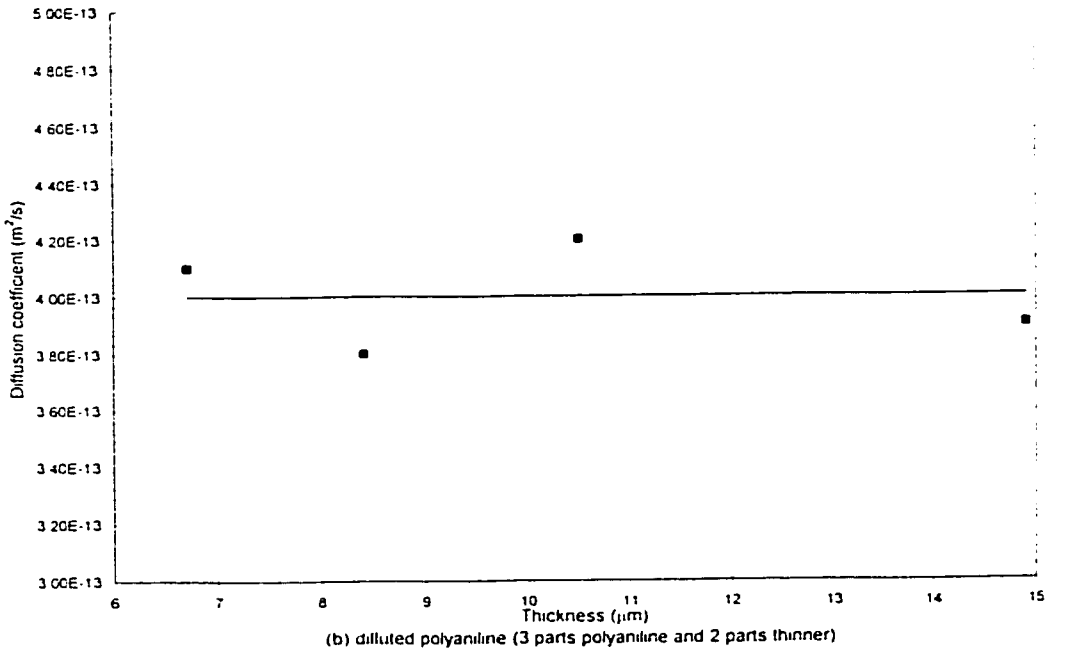

Figure 5.16: The relationship between diffusion coefficient D and thickness of sensitive layer.
(a) polyaniline as supplied; (b) diluted polyaniline.

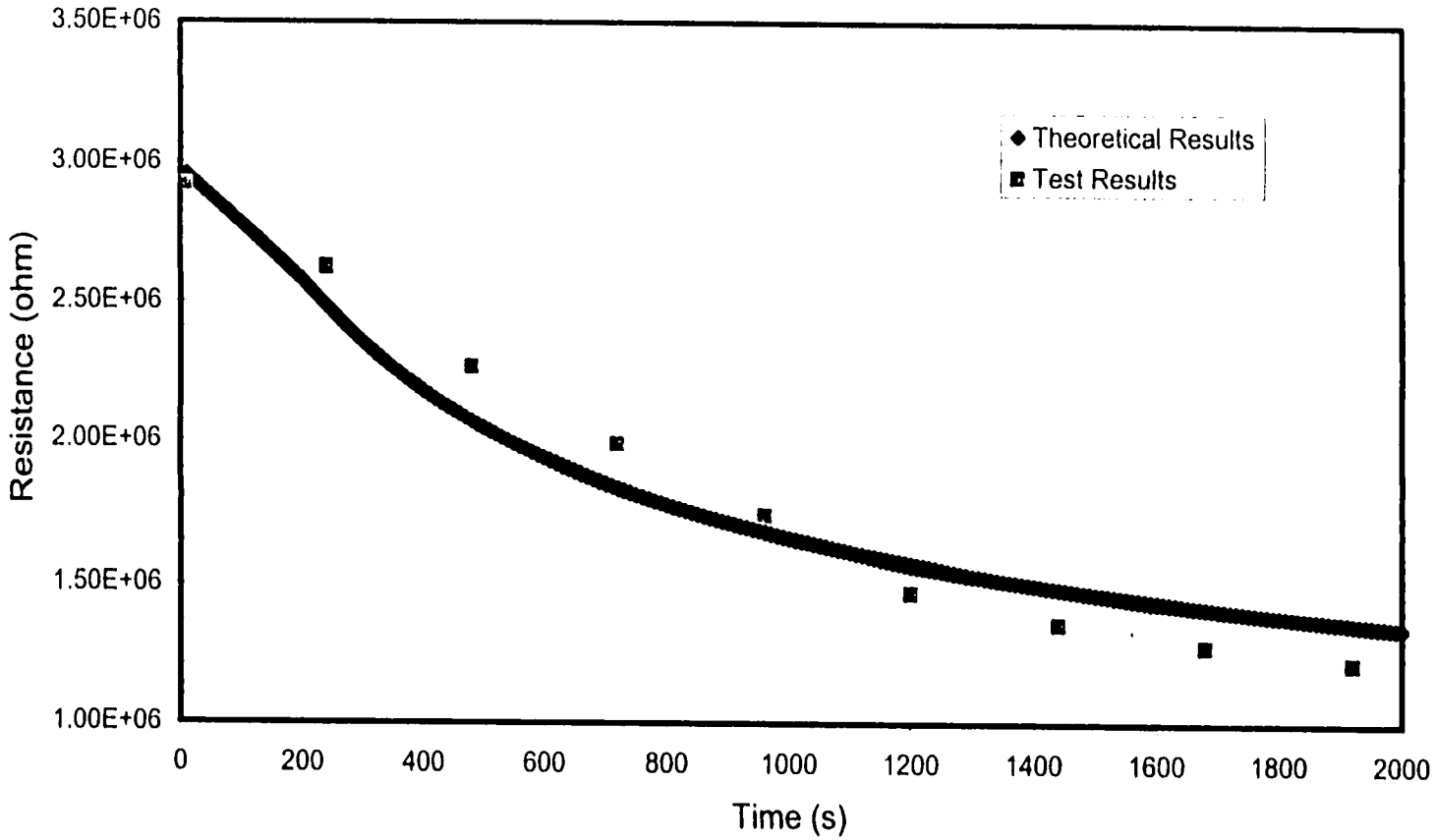

Figure 5.17: The comparison between theoretical response and test response.

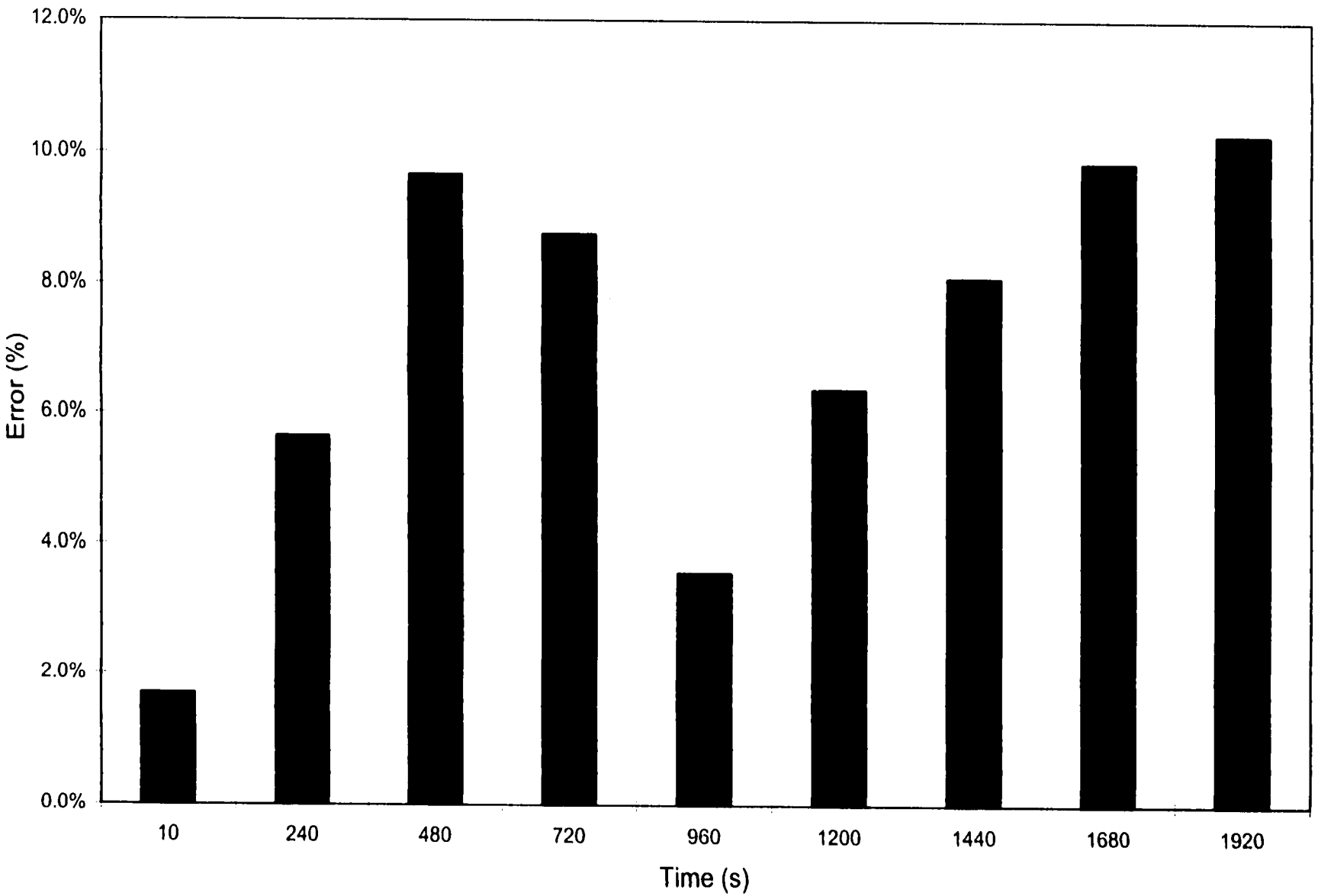

Figure 5.18: The relative error of theoretical data and test data.

The analysis and design process carried out and described in Chapter 3 yield solutions for the configurations of the electrodes of the resistive microsensor that could be fabricated in Mitel 1.5μm technology and post-processed using minimized resources. Since very limited information on the humidity absorption properties of active materials are available, the characteristics of the resistance versus humidity of a polyaniline dispersion was carried out and presented in this study. Since both components of the microsensor are either known through analytical investigations or experiments, the coupling of the two could be somehow predicted. Thus, the predicted performances of the sensor are compared with measurements carried out on the microsensor. Abatement from the analytical model is to some extend expected due to the large variance of the configurations of the dispersion particles in the deposited film.

The major conclusions drawn from the above analysis are:

- Standard CMOS technology enables the fabrication of microsensors which requires minimum low cost post-processing.
- The accomplishment of humidity microsensor based on resistive humidity sensitive thin film has proved its feasibility and its realization.
- Testing results also show that the sensor has consistent properties.
- Simple model of Fick's diffusion law can be used to estimate response time and diffusion coefficient for future use.

5.4 SUMMARY (CONTRIBUTIONS INDICATED AS UNDERLINE)

The properties of a humidity sensitive material, polyaniline, are investigated through a series of laboratory tests. A simple post processing technique for deposition of polyaniline and its diluted compound is proposed to realize humidity sensitivity films. An array of samples are fabricated at different spin coating speeds to achieve different film thickness. Experiments are performed to study the steady-state and transient variations in the film resistance of the nominal and diluted polyaniline. The spin-coating performed at different speeds resulted in film thickness ranging from 6.7 μm to 164 μm. A prototype resistive humidity sensor is further realized by depositing the diluted compound. A film thickness of 19 μm was obtained to ensure uniform distribution of particles within the exposed film area. The steady-state and transient response characteristics of the prototype sensors are measured under varying levels of RH, and step changes in RH from 30% to 90%, and 90% to 30%. The transient response data is further analyzed to derive the diffusion coefficients, as a function of the film thickness. The analytical model of the resistive sensor is solved using the diffusion coefficients identified from the data. The analytical results are compared with those derived from the experiments. The comparison revealed that the peak difference between the analytical and experimental results does not exceed 12%. The results of experimental study performed on samples and the humidity microsensor are summarized below:

- High spin coating speed and low viscosity yield thin humidity sensitive film. The addition of a thinner can reduce the viscosity of sensitivity

material and thus yield thinner deposition films. Thick films result in lower film resistance, and the sensor response time increases with increase in film thickness.

- The sensor yields relatively high sensitivity over the entire range of relative humidity. The range of static sensitivity of the sensor exceeds 9.40E+05 Ω/RH.
- The variations in microsensor resistance caused by aging over a period of 100 days was measured to be less than 4.2%, which is most likely attributed to the precision of the measurement systems.
- The peak relative error between the experimental results and analytical results is less than 12%.
- The methodology using Fick's law on deriving diffusion coefficient and response time of sensitive material is validated, which extends the possibility of its application on other sensitive materials.

CHAPTER 6

CONCLUSIONS AND SUGGESTIONS FOR FUTURE WORK

6.1 INTRODUCTION

The design and fabrication of resistive and capacitive sensors for measurement of relative humidity of air in confined spaces is investigated in this dissertation. A design and fabrication methodology based upon silicon surface micromachining technology is formulated. Various electrode configurations are proposed to achieve optimal bulk resistance and high capacitance of the sensing element. Optimal design configurations are proposed that can be applied to realize effective sensor design with minimal post-processing. The properties of various humidity sensitive materials are reviewed to identify most suitable active materials for applications in micro-humidity sensors. Analytical models of the electrodes and diffusion behavior of the sensing materials are derived. The analytical models are analyzed to examine the adequacy of the sensitivity of the proposed designs to variations in relative humidity. The designs of conditioning circuitry, which can be investigated within the sensor chip are further proposed.

Simple and low cost post-processing techniques comprising only deposition through spin-coating is proposed to realize the micro-humidity sensor. The effectiveness of the post processing technique is thoroughly investigated through preparation of various samples, which involved depositions of polyaniline polymer at different spin speeds. It is further proposed that thin film deposition can be realized by addition of thinner to the polyaniline compound. A prototype

resistive sensor design was realized through fabrication of the proposed design through the CMC, and deposition of diluted polyaniline in the laboratory. A series of experiments were performed on the prototype samples in the laboratory to study the effects of spin-coating speed, film thickness, dilution of the polymer on the steady-state and transient response, and hysteresis of the film.

The steady-state and transient response characteristics of the prototype sensor were measured in the laboratory. The measured data is used to derive the diffusion coefficients for the active material film, and to examine the validity of the analytical model. The major conclusions drawn from the dissertation research are summarized in the following section.

6.2 CONCLUSIONS (CONTRIBUTIONS INDICATED AS UNDERLINE)

The primary objective of this dissertation research is to contribute to the field of Micro-Electro-Mechanical System (MEMS) through systematic investigations leading to the design, fabrication and efficient post-processing of resistive and capacitive humidity microsensors. In an attempt to enhance the bulk resistance and capacitance of the sensing element, various configurations of the sensing structure were conceived and analyzed to characterize their bulk resistance and capacitance. Different post-processing techniques were reviewed to identify a simple and efficient technique, based upon spin coating alone. Spin coating was selected as post-processing due to its simplicity and low-cost. Post-processing was performed on a resistive sensor, which was fabricated through the CMC using Mitel15 technology. The electrode configuration was obtained by

judiciously patterning Metal1, Metal2, SiO_2 and passive films. The properties of a polymer material, polyaniline were investigated to examine its application as a humidity sensitive material. The characteristics of supplied polyaniline and diluted polyaniline were derived through a series of tests performed on the prototype samples realized in the laboratory. Laboratory experiments were performed at different spin coating speeds and the results were evaluated to identify a near optimal spin speed. The results obtained through experiments were compared with those obtained from simulation to examine the validity of the proposed analytical models.

The following conclusions are drawn from the studies performed in this dissertation research.

- Design of humidity sensors was realized by using standard layout and simulation software, such as CADENCE, which, however, does not include MEMS simulation modules. Therefore, in Chapter 3 and Chapter 4, the models for the resistive and capacitive humidity sensors were proposed. The proposed models are in good agreement with the measured data.
- The 1.5μm resolution of the CMOS technology is satisfactory for the structures considered in this dissertation. 75% yield out of 6 was achieved through all delivered chips, although within the same lot, inconsistent results were found. The inconsistency of results is mainly due to the systematic violation in design rules that are set for electronic circuitry and

not for MEMS. Besides, the removal of the passivation layers at concave corners is performed mostly incompletely.

- The results of the simulation for the two types of sensors reveal that the slight changes in the shape and geometrical parameters of the sensors introduce large variations in the output of the device. Therefore, precision design and machining of Micro-Electro-Mechanical Systems (MEMS) play an important role in realizing high accuracy measurement devices.
- The resistive humidity sensors with electrodes configured in array, yield better output. The circle cut shapes further enable a less-defect processing due to the absence of sharp corners.
- The capacitive humidity sensors with interdigital comb-like electrodes can be realized using a one-step low cost post processing. The design of interdigital comb-like electrodes can thus be considered as a near optimal design when compared with other proposed shapes of electrodes.
- The electrodes in the proposed capacitive sensors are parallel bars patterned from polysilicon and two metal layers. The parallel electrodes could be easily embedded in humidity sensitive material, which permit the access to water vapors into the sensing film to alter its dielectric properties.
- Spin coating post-processing is a very effective method to deposit thin films of polymers or dispersions. The film thickness could be controlled by three parameters: spin speed, viscosity of the deposition material and spin

time. An analytical relationship that relates all three factors was proposed in the thesis.

- Polyaniline in dispersion can be used as an effective resistive humidity sensitive material. Polyaniline in dispersion can be easily deposited in controlled uniform films. The resulting films revealed good sensitivity to variations in relative humidity variation. Although the dispersed particle is 10nm, the clustering of polyaniline, in larger grains could yield non-uniform and discontinuous films on the electrodes. A thin and uniformly conductive film can be realized through coating at appropriate spin speed.
- Diluted polyaniline reduces the viscosity of material, while high spin speed increases the centrifugal forces on the particles of material in dispersion when spinning. Low viscosity and high centrifugal force can yield thinner films, which yield relative short response time for the sensor. However, spin speeds beyond a threshold value yield nonconductive layers.
- The film thickness results as a compromise between thin layer, required by the short absorption time and the thick layer, required by the resistance properties of the film. A spin speed of 3000rpm was found to be the most suitable for the polyaniline dispersion.
- Humidity resistive properties of polymers were evaluated based on the absorption model of Fick's law. The diffusion coefficient that stands for the absorption constant could be evaluated based upon the response time for the film.

- Transient response of the sensor was modeled using Fick's diffusion model. The proposed model is validated within 12% of the experimental results.
- The influence of aging to the resistive humidity dependent properties of the polymer were assessed. No trend in dependency was found.
- The results of the laboratory tests performed on a prototype resistive micro-sensor revealed that the sensor is very sensitive to variations in relative humidity. The results also revealed reasonably good repeatability, within 4.2%.
- The results of testing on resistive micro-sensor show that the micro-sensor is very sensitive to relative humidity level change. The results are also repeatable. This proved that the design of the sensor was conceptually correct and viable.

6.3 RECOMMENDATIONS FOR FUTURE WORK

The present dissertation research has explored the properties of polyaniline compound, while the properties of many other potential humidity sensitive materials have been discussed. Although polymer film humidity sensors still remain modest in practical applications, their potential applications have been steadily growing. Polymer films are well suited for standard IC processing techniques to fabricate miniature and low cost sensors. In this thesis, only polyaniline was discussed and investigated. Preliminary tests were also carried out for capacitive microsensors using pyraline as humidity sensitive material. It is

recommended that other polymers should also be investigated, specifically in view of their transient response characteristics and sensitivity.

Ceramic materials are also known to exhibit adequate properties for humidity sensors, specifically high mechanical strength, high temperature capability and high resistance to chemical attack. It is also known that most ceramics are hard to deposit as sensitive layers and require high temperature post-processing. Further studies may thus explore methods to deposit ceramic materials on the sensor structure.

It is suggested that further experimental and analytical studies be performed on the micro humidity sensors with on-chip circuitry. The analytical model for the integrated sensor can thus provide direct input-output relations, and static and dynamic characteristics.

REFERENCES

1. K.Otsuka, S.Kinoki and T.Usui, "Organic Polymer Humidity Sensor." *Denshi-zairyo*, (Sept. 1980) 68-73.
2. Senturia, M.G. Huberman, B. Vanderkloot, "Moisture Sensing With Charge Flow Transistor", NBS Spe. Publ. US, 40069, pp. 108-114 (1981).
3. G. Huyberechts and J. Roggen, "Planar Humidity Sensors", Journal A, 32 (1991) 38-42.
4. Peter J. Schubert, Joseph H. Nevin, "A Polyimide-Based Capacitance Humidity Sensor," in *IEEE transactions on electron devices*, Vol. ED-32, No.7, July, 1985.
5. Yamauchi, "Chemical Sensor Technology", National Rehabilitation Center for the Disabled, Tokorozawa, Japan.
6. Nakaasa Instrument Co.Ltd., Catalogue, C911-84001-15K-2D (1984) pp.78.
7. E. Salasmaa and P. Kostamo, "New Thin Film Humidity Sensor", *Vaisala News*, No.66 (1975).
8. Wise, K.D. 1991 "Integrated Microelectromechanical Systems: A Perspective On MEMS in the 90s." In *Proc.IEEE MicroElectroMechanical Systems Workshop*. pp. 33-38.

9. Wood, R.A., C.J. Han, and P.W. Kruse. 1992. "Integrated Uncooled Infrared Detector Imaging Arrays." In *Digest IEEE Solid-Stated Sensor and Actuator Workshop*. pp. 132-135.

10. Fujimasa, Iwao, "Micromachines — A New Erain In Mechanical Engineering", Oxford University Press, 1996.

11. Yuhua Ma, Shuangyu Ma, Tieliu Wang, Weiling Fang, "Air-flow Sensor And Humidity Sensor Application To Neonatal Infant Respiration Monitoring", *Sensor and Actuators A 49* (1995) 47-50.

12. T. Boltshauser, H. Baltes, " Capacitive Humidity Sensors in SACMOS Technology With Moisture Absorbing Photosensitive Polyimide", *Sensors and Actuators A*, 25-27 (1991) 509-512.

13. G. Gusmano, G. Montesperelli and E. Traversa, "Magnesium Aluminium Spinel Thin Film As A Humidity Sensor", *Sensors and Actuators* B, 7 (1992).

14. G.M.Ohalloran, P.M.Sarro, J.Groeneweg, P.J.Trimp, and P.J.Frence, "A Bulk Micromachined Humidity Sensor Based On Porous Silicon", *TRANSDUCERS' 97*, Chicago, June 16-19, 1997.

15. J. E. Moneyron, A. De Roy and J.P.Besse, "Realization Of A Humidity Sensor", *Sensors and Actuators B*, 4 (1991) 189-194.

16. Yamazoe, N., Shimizu, Y., "Humidity Sensors: Principles And Applications", *Sensors and Actuators*, 10 (1986), pp. 379 - 398.

17. M. Hoummady, D. Hauden, "Acoustic Wave Thermal Sensitivity: Temperature Sensor And Temperature Compensation In Microsensors", *Sensors and Actuators, A* 44 (1994) pp. 177 - 182.

18. D.W. Galipeau, J. F. Veltelino and R. Lec, "The Study Of Polyimide Films And Adhesion Using A Surface Acoustic Wave Sensor", *Sensors and Actuators B*, 5 (1991) 59-65.

19. Dunmore, "An Electrometer And Its Application To Radio Meteorography", *J. Res. Nat.Bur.Std.*, 20 (1938) 723-744.

20. Radeva, K.Bobev and L.Spassov, "Study And Application Of Glow Discharge Polymer Layers As Humidity Sensors", *Sensors and Actuators B*,8 (1992) 21-25.

21. T.Nitta, J.Terada, and F.Fukushima, "Multifunctional Ceramic Sensors: Humidity-Gas Sensor And Temperature-Humidity Sensor", in *IEEE trans. on electron devices*, VOL. ED-29, No.1, January 1982, 95-102.

22. T.Nitta, Z.Terade and S.Hayakawa, "Humidity-Sensitive Electrical Conduction Of $MgCr_2O_4 - TiO_2$ Porous Ceramics, *J.Am.Ceram.Soc*, 63(1980) 296-300.

23. T. Nitta, Z.Terada and T.Kanazawa, "Ceramic Humidity Sensor 'Humiceram'". *Nat. Tech. Rep.*, 24 (1978) 422-435.

24. K.Katayama and T.Akiba, Rutil "Humidity Sensor", *Proc. Int. Meet. On Chemical Sensor*, Kodansha, 1983, pp. 433-438.

25. Y. Shimizu, H. Ichinose, H. Arai and T. Seiyama, "Ceramic Humidity Sensors - Microstructure And Simulation Of Humidity Sensitive Characteristics", *Nippon Kagaku Kaishi* (1985) 1270 - 1277.

26. T. Suzuki and N. Matsui, "Properties of Humidity Sensitive Oxides With Alkali Additive", *Proc. Int. Meet. On Chemical Sensors, Kodansha*, 1983, pp. 381-386.

27. Uchikawa, K. Miyao, K.Shimamoto and K. Nakanishi, "Surface OH Concentration And Electrical Resistance Of Hymidity-Sensitive Silicon Composite Films", *Ceram. Bull.*, 63 (1984) 1043 - 1046.

28. F. Uchikawa, K. Miyao, K.Shimamoto, "Time Variability Of Surface Ionic Conduction On Humidity Sensitive SiO_2 Films", *Am. Ceram.Soc.Bull.*, 64 (1985) 1137-1141.

29. Y. Yokomizo, S. Uno, M. Harata and H. Hiraki, "Microstructure And Humidity-Sensitive Properties Of $ZnCr_2O_4 - LiZnVO_4$ Ceramic Sensors", *Sensors And Actuators*, 4 (1983) 599-606.

30. Y.Yamada, "Lithium Chloride Humidity Sensor", *Denshi-gijutsum* 21(9) (1979) 26-30.

31. H. A C Tilmans, K. Baert, A. Verbist and R. Puers "CMOS Foundry-Based Micromachining", 1996.

32. H. Seidel "Silicon Micromechanical Devices And Their Manufacturing Technology", *Micromechenics*, Report 309 (1996), 29-30.

33 D. Banks, "Microsystems, Microsensors & Microactuators: An Introduction To Microengineering", 1996.

34 D. Moser, "CMOS Flow Sensors", *Physical Electronics Labratory*, 1993, 77-87.

35 N. F. De Rooij, "Technology And Applications of Microsystems", *Proceeding Of The Second Micro Structure Workshop*, 1996.

36. Cichocki, R. Unbehauen, "Application Of Switched-Capacitor Self-Oscillating Circuits To The Conversion Of RLC Parameters Into Frequency Or Digital Signal", *Sensors and Actuators A*, 24 (1990) 129-137.

37. Patranabis, S. Ghosh, and D.K.Ghosh, "Circuit for Linear Frequency-Independence Output From A Differential-Capacitance Displacement Transducer", *IEEE,1985* Vol. IM-34, No.1.

38. Wen H. Ko, "Solid-State Capacitive Pressure Transducer", *Sensors And Actuators*, 10 (1986) 302-320.

39. EDWARDS, A. Inst. P., F.B.I.S., "Electronic Measurement Techniques", London.

40. J. Hal, "Recent Trends in Silicon Micromachining Technology", *EG&G IC Sensors*, 1995.

41. R. T. Howe, "Polysilicon Integrated Microsystems: Technology And Applications", *Proceedings of the 8th International Conference On Solid State Sensors And Actuators*, Stockholm, June, 1995, 43 - 46.

42. C. Read, V. M. Bright, and J. H. Comtois, "Mechanical And Optical Characterization Of Microactuators Fabricated In A CMOS Process", *Air Force Institute of Technology*, 1995.

43. H. Huang, "Electrical And Thermodynamic Characterization Of Water Vapour/Polymetric Film System For Humidity Sensing", *Digest of Technical Papers, 3rd Int. Conf. On Solid-State Sensors and Actuators (Transducers' '85)*, 1985, 206-208.

44. S. Tsuchitani, T. Sugawara, H. Kinjo and S. Ohara, "Humidity Sensor Using Ionic Copolymer", *Digest Of Technical Papers, 3rd Int. Conf. On Solid-State Sensors and Actuators (Transducers' '85)*, 1985, 210-212.

45. Y. Sakai, Y. Sadaoka and K. Ikeuchi, "Humidity Sensors Composed Of Graft Copolymers", *Digest Of Technical Papers, 3rd Int. Conf. On Solid-State Sensors and Actuators (Transducers' '85)*, 1985, 213-216.

46. G.Sberveglieri, G.Faglia and R.Ricci, "Selective And Sensitive Humidity Sensor Based On Barium Chloride Dihydrate", Sensors And Actuators B, 13-14 (1993) 615-616.

47. M. Pelino, C. Colella, C. cantalini, M. Faccio, G. Ferri and A. D'Amico, "Microstructure And Electrical Properties Of Humidity Sensors", *Sensors and Actuators B*, 7 (1992) 464-469.

48. Lars-Goran Mansson, Sven A.Svennberg, "Demand Controlled Ventilating System" Energy Conservation In Buildings And Community Systems Program Annex 18, August 1992.

49. I.Stiharu, S.Rakheja and L. Wang, "Humidity Microsensor in CMOS Mitel15 Technology" *Proceeding of 1999 IEEE Canadian Conference on Electrical and Computer Engineering Shaw Conference Center*, Edmonton, Alberta, Canada May 9-12 1999.

50. D.L. Bartley and D.D.Dominguez, *Anal.Chem*, 1990,62,1649.

51. M. C. Glenn and J. A. Schuetz, "An IC Compatable Polymer Humidity Sensor", *Digest of Technical Papers, 3rd Int. Conf. on Solid-State Sensors And Actuators*, June 11-14, 1985, 217-220.

52. Lin Wang, I. Stiharu, S. Rekheja, "Humidity Capacitive Sensor By Silicon Surface Micromachining", *16th Canadian Congress of Applied Mechanics (CANCAM 97)*, June 1997.

53. G. Delapierre, H. Grange, B. Chambaz and L. Destannes, "Polymer-Based Capacitive Humidity Sensor: Characteristics And Experimental Results", *Sensors and Actuators*, 4 (1983) 97-104.

54. Boltshauser, C. Azeredoleme and H. Baltes, "High Sensitivity CMOS Humidity Sensors With On-Chip Absolute Capacitance Measurement System", *Sensors And Actuators B*, 15 -16 (1993) 75-80.

55. K, Kondo, K. Watanabe, "A Switched-Capacitor Interface For Capacitive Sensors With Wide Dynamic Range", *IEEE transactions on instrumentation and measurement*, Vol. 38, No. 3, June 1989.

56. L. K. H. van Beck, "Dielectric Behavior Of Heterogeneous Systems," in *Progress in Dielectrics 7*, J. B. Birks, ED. Brooklyn, NY: Heywood Books, 1967, pp.69.

57. S.Kisdnassamy and P.S. Neelakantaswamy, "Complex Permittivity Of A Dielectric Mixture: Modified Fricke's Formula Based On Logarithimic Law Of Mixing," *Electron. Lett.*, vol.20, no.7, pp.281, 1984.

58. M. M. Dubinin and V.A. Astakhov, "Description Of Absorption Equilibria Of Vapors On Zeolites Over Wide Ranges Of Temperature And Pressure," in *Molecular Sieve Zeolites*, vol. II, R.F. Gould, Ed., in Adv. in Chemistry Series, no. 102. New York: Amer. Chem.Soc., 1971.

59. W. Kidwell, "Electrical Instruments And Measurements," McGRAW-HILL book company, New York, 1989.